2.12.4 Finite Element Analysis

This appendix provides supporting drop simulation data for the certification testing performed on the 435-B package. This material summarizes the information presented in the drop analysis [1].

2.12.4.1 Introduction

The primary method of demonstration of the 435-B is certification test. Finite element analysis is used to:

- Demonstrate that the bounding drop orientations were chosen for the certification testing.
- Calculate the maximum closure bolt stress (not generated by any certification tests).
- Calculate the maximum warm case crush (since the warm foam used in the certification test was not bounding).

The Finite Element Analysis (FEA) simulations performed in this appendix are for supporting the selection of worst-case orientations tested, and to determine the performance in orientations not tested. The FEA simulations include benchmark orientations that are compared directly to the certification test results. Free drop impact deformation and acceleration results are used to benchmark the finite element analysis model for use in non-tested orientations and conditions. The non-tested orientations are slapdown free drops with both the base impact limiter primary and the bell (lid) torispherical head primary in a wide range of angles. The slapdown free drops are considered drop orientations where a primary impact occurs with the drop pad inducing significant rotation of the package such that a secondary and potentially bounding impact occurs. Most drops for which the center of gravity was over the impact were physically tested as documented in Appendix 2.13.3, *Certification Test Results*.

The simulations must demonstrate the bounding certification test orientations were performed and the simulations should also corroborate the certification test results. Simulations are performed using the explicit finite element software LS-DYNA [6], version ls971s R4.2.1, 53450 from Livermore Software Technology Corporation (LSTC).

2.12.4.2 Design Input

2.12.4.2.1 Conditions

The certification test conditions are defined by Appendix 2.12.2, *Certification Test Plan*, and are documented by Appendix 2.12.3, *Certification Test Results*. The benchmarked free drops include the end drop, D1 series on CTU #1, side drop, D2 series on CTU #1, and the cg-over-top knuckle, D3 series on CTU #2. These orientations are chosen for benchmarking because they encompass the maximum axial impact (end drop), maximum transverse impact (side drop), and maximum containment boundary deformation (cg-over-top knuckle).

Numerous slapdown free drop orientations, which are not included in certification testing, are simulated with the benchmarked finite element model. The slapdown free drop simulation results are compared with certification test simulation results to demonstrate the bounding attributes of the certification test orientations.

2.12.4.2.2 Geometry

The 435-B Certification Test Unit (CTU) packaging is defined by the drawings in Appendix 1.3.3, *Packaging General Arrangement Drawings*, except as discussed in Section 2.12.3.3, *Certification Test Unit Configuration.* The finite element model is based on the test unit drawings and as-tested configuration. The inner container (IC) is not included in these simulations because the packaging deformations observed in certification testing with the IC are less than those observed when tested with the lodgment and LTSS. Therefore, certification testing and simulations performed with the lodgment and LTSS are bounding with respect to packaging deformations and payload accelerations.

2.12.4.2.3 Material Properties

The benchmarking and other simulations are performed at cold temperatures. Properties at elevated temperatures are not needed except as discussed in following paragraphs for the polyurethane foam crush strength.

The 435-B base, thermal shield(s), miscellaneous components, and LTSS are designed utilizing Type 304 stainless steel, predominately ASTM A240, A276, and A479. The minimum material yield strength is 30,000 psi and the minimum material ultimate strength is 75,000 psi from Table 2.2-1. The Modulus of Elasticity is 28.3×10^6 psi per Table 2.2-1, and Poisson's ratio is 0.31 from Section 2.2.1, *Material Properties and Specifications.*

The cylindrical side shell of the bell, including the torispherical head and welded hoist ring boss, are designed with Type 304 stainless steel and specified to have a minimum material yield strength of 40 ksi and minimum material ultimate strength of 80 ksi, which is above the minimum material specifications for ASTM Type 304 stainless steel.

The closure bolts are ASTM A320 Grade L43 where the minimum material yield strength is 105,000 psi and the minimum material ultimate strength is 125,000 psi from Table 2.2-3. The Modulus of Elasticity is 27.8×10^6 psi per Table 2.2-3, and Poisson's ratio is 0.30 from Section 2.2.1, *Material Properties and Specifications.*

The base weldment is filled with General Plastics FR-3700 series polyurethane foam. The prototypic foam density is 15 pounds per cubic foot (pcf). The certification test units had 16 pcf (Units 1 & 3) and 14 pcf (Unit 2).

The lodgment is designed with aluminum material, 6061-T6 or T651, predominantly ASTM B209, B221, and B308. The material yield strength is 35,000 psi for B209, B221, and B308 for 6061-T6 or T651 aluminum per Table 2.2-4. The material ultimate strength is 42,000 psi for 6061-T651 per Table 2.2-4. The Modulus of Elasticity is 10.0×10^6 psi per Table 2.2-4, and Poisson's ratio is 0.33 from Section 2.2.1, *Material Properties and Specifications.* The bolts used to secure the upper and lower halves of the lodgment together are ASTM A193 Grade B8 that has a yield strength of 30,000 psi and ultimate strength of 75,000 psi.

The material models used in the simulations are described in the following sub-sections.

2.12.4.2.3.1 Type 304 Stainless Steel (*mat_plastic_kinematic)

The base flange and lower torispherical head weldment, upper flange, internal impact limiter stabilizer (dome) sheets, and lower center tube are modeled with a Type 304 stainless steel

plastic kinematic material for all simulations. This is LS-DYNA material model 3. The following properties are discussed above and converted to true stress-strain. The elongation below is taken as ultimate elongation from ASME Section II, Part A.

- Stainless Steel SA-240 Type 304 at -20 to 100F
- E = 28,300 ksi, Sy = 30.0 ksi, Su = 75.0 ksi, elongation = 0.40, density = 0.290 lb/in^3
- True Yield Stress: Syt = Sy(1+(Sy/E+0.002)) = 30.1 ksi
- True Ultimate Stress: Sut = Su(1+eu) = 105.0 ksi
- True Yield Strain: eyt = ln(1+ey) = 0.00306
- True Ultimate Strain: eut = ln(1+eu) = 0.336
- True Tangent Modulus: Etant = (Sut-Syt)/(eut-eyt) = 225.0 ksi

Where ey is the engineering yield strain (Sy/E+0.002), and eu is the engineering ultimate strain (elongation = 0.40).

2.12.4.2.3.2 Type 304 Stainless Steel (*mat_piecewise_linear plasticity)

The outer shell and upper torispherical head (bell), thermal shields, bell skin (enclosing the bolt tubes and foam blocks), bolt tubes, base skin (external impact limiter shell), internal impact limiter clips (base blocks), and internal impact limiter tubes are modeled with a Type 304 stainless steel elastic-plastic material. This is LS-DYNA material model 24. The material properties of Type 304 stainless steel are obtained from Section 2.2, *Materials* as shown above, and actual Certified Material Test Reports (CMTRs) from the certification test units.

The true stress-strain behavior of Type 304 stainless steel is presented in Table 2.12.4-1. From [5], stainless steel is modeled using a power-law hardening material model. This model treats the material as elastic up to the limit of proportionality and captures the plasticity by the equation:

$$\sigma = \sigma_p + A\left\langle \varepsilon_p - \varepsilon_l \right\rangle^n$$

Where σ is the true stress, σ_p is the stress at the limit of proportionality (taken as the true yield strength), A is the hardening constant, ε_p is the true equivalent plastic strain, ε_l is the Luder's strain (zero for stainless steel), $\langle\ \rangle$ indicates the Heaviside function where the expression enclosed in the brackets is unchanged when positive and equal to zero when negative and n is the hardening exponent. Note that the values from the above equation correspond to room temperature. From [5], the parameters for 304L stainless steel are σ_p = 28 ksi, A = 192.746 ksi, ε_l = 0 and n = 0.74819.

To use this equation for Type 304 at temperature, a conversion is necessary and is performed as follows. The mechanical and chemical properties of Type 304 and Type 304L are similar, so it is assumed that the stress-strain values obtained for Type 304L from [5] can be scaled to obtain Type 304 stress values at temperature. The stress values are scaled based on the scaling equation:

$$\sigma_{304} = \sigma_{304L} \frac{\sigma_{ty\text{-}304}}{\sigma_p}$$

where σ_{304} is the true stress for Type 304 stainless steel, σ_{304L} is the result of the power law equation above using the parameters from [5], σ_p equals 28,000, and $\sigma_{ty\text{-}304}$ is the true yield stress for Type 304 at temperature. Engineering stresses and elastic moduli at temperature are taken from Section 2.2, *Materials* and CMTRs from the certification test units. Three material curves are generated using this method, material identities 15, 16, and 17.

Material ID 15 uses a yield strength of 40.0 ksi that comes from a minimum strength note on the drawings in Appendix 1.3.3, *Packaging General Arrangement Drawings*, for the bell outer shell and upper torispherical head. Material ID 15 is used for the bell skin (enclosing the bolt tubes and foam blocks), bolt tubes, base skin (external impact limiter shell), and internal impact limiter clips (base blocks) for all simulations. Material ID 15 is also used for the outer shell and upper torispherical head (bell), and shell side thermal shield for all the slapdown simulations. The shell side thermal shield also uses Material ID 15 for the D3 benchmark simulation.

Material ID 16 uses a yield strength of 51.5 ksi that comes from the average CMTR value of the internal impact limiter crush tubes. Material ID 16 is used for the internal impact limiter tubes and upper torispherical head thermal shield in all simulations.

Material ID 17 uses a yield strength of 45.0 ksi from the CMTR for the bell outer shell and upper torispherical head on CTUs 1 and 2. Material ID 17 is used exclusively for the outer shell and upper torispherical head (bell) in the benchmark simulations.

2.12.4.2.3.3 6061-T6 Aluminum (*mat_plastic_kinematic)

The flat plates of the internal impact limiters and the lodgment are modeled with a 6061-T651 aluminum plastic kinematic material. This is LS-DYNA material model 3. The following properties are from Section 2.2, *Materials* and converted to true stress-strain. This material model was used for all non-benchmark simulations. The elongation below is taken as ultimate elongation from ASME Section II, Part B.

- 6061-T651 Aluminum at -20 to 100F
- E = 10,000 ksi, Sy = 35.0 ksi, Su = 42.0 ksi, elongation = 0.10, density = 0.098 lb/in^3
- True Yield Stress: Syt = Sy(1+(Sy/E+0.002)) = 35.2 ksi *
- True Ultimate Stress: Sut = Su(1+eu) = 46.2 ksi
- True Yield Strain: eyt = ln(1+ey) = 0.00548
- True Ultimate Strain: eut = ln(1+eu) = 0.0953
- True Tangent Modulus: Etant = (Sut-Syt)/(eut-eyt) = 122.5 ksi

Where ey is the engineering yield strain (Sy/E+0.002), and eu is the engineering ultimate strain (elongation = 0.10). * Note, 38.7 ksi was used in all non-benchmark simulations based on performance of the benchmarked CMTR value below, instead of 35.2 ksi.

The aluminum properties shown below for the benchmark simulations are from the CTU-1 CMTR.

- 6061-T651 Aluminum at -20 to 100F
- E = 10,000 ksi, Sy = 38.7 ksi, Su = 43.7 ksi, elongation = 0.16, density = 0.098 lb/in^3
- True Yield Stress: Syt = Sy(1+(Sy/E+0.002)) = 38.9 ksi
- True Ultimate Stress: Sut = Su(1+eu) = 50.7 ksi
- True Yield Strain: eyt = ln(1+ey) = 0.00585
- True Ultimate Strain: eut = ln(1+eu) = 0.148
- True Tangent Modulus: Etant = (Sut-Syt)/(eut-eyt) = 83.0 ksi

Where ey is the engineering yield strain (Sy/E+0.002), and eu is the engineering ultimate strain (elongation = 0.16, from the CMTR).

2.12.4.2.3.4 Polyurethane Foam (*mat_crushable_foam)

The 435-B external impact limiter contains General Plastics FR-3700 series polyurethane foam that is modeled with a crushable foam material. This is LS-DYNA material model 63. The foam functions as an impact limiter around the bolted bell-to-base joint and as a thermal barrier reducing the heat input to the butyl rubber containment O-rings from the HAC fire case. The prototypic foam density is 15 pounds per cubic foot (pcf). Certification testing was performed with 16 pcf foam in CTU-1 and CTU-3, and 14 pcf foam in CTU-2. The minimum temperature requirement from TS-R-1 [3] is -40 °F, and the maximum bulk average NCT temperature of the foam is bounded by 150 °F. Performing full scale certification testing at -40 °F and 150 °F is extremely challenging, therefore cold impact testing was performed at -10 °F with a harder density 16 pcf foam and the warm maximum crush testing was performed at 117 °F with a softer density 14 pcf foam. These two foam densities have very comparable crush strength properties to the prototypic 15 pcf foam at the respective -40 °F and 150 °F temperatures as shown in Figure 2.12.4-1. This method of testing equivalency is also discussed in the test plan, Section 2.12.2.2.1, *Temperature and Pressure* and test results, Section 2.12.3.3, *Certification Test Unit Configuration.* The crush strength properties are developed in the paragraphs below.

The foam has specific crush strength properties that are dependent on the foam density, temperature, orientation (parallel or perpendicular to foam rise), and dynamic factors. The foam design guide [7] has detailed descriptions and data for compensating the foam crush strength curve for these variables. The material property inputs required for performing the drop simulations are the foam crush strength curves. Four separate foam crush strength curves are generated for this purpose and are presented in Table 2.12.4-4. These four curves represent the bounding properties for the certification test units and prototypic packaging cases.

The actual static foam crush strength data at room temperature (~75 °F) for CTU-1 and CTU-2 is included in Table 2.12.4-2 from supplier test records. The static prototypic foam crush strength data is also included in Table 2.12.4-2. The prototypic 15 pcf foam, CTU-1 16 pcf foam, and CTU-2 14 pcf foam are adjusted for applicable test temperatures using the method and data from the foam design guide [7]. This includes multiplying the foam crush strength by the appropriate temperature correction factor, C_T, given in [7]. Crush strength curves at -20 °F, 100 °F, and 140 °F are created in a spreadsheet and then the values are interpolated or extrapolated to populate the crush strengths at the desired temperatures of -40 °F, 0 °F, 117 °F, and 150 °F. The prototypic (or production) foam is also conservatively compensated for a manufacturing

tolerance of ± 10%. The foam at cold temperature is toleranced to be stronger by 10% and the foam at warm temperature is toleranced to be weaker by 10%. The foam curves are then averaged between their orientation properties (parallel or perpendicular to foam rise) and listed in Table 2.12.4-3.

Lastly, the crush strengths are compensated for dynamic effects per the foam design guide [7] using the formula:

$$\sigma_{Dynamic} = Y_{int}(\sigma_{Static})^S$$

where Y_{int} and S are dynamic factors from Table 9 of [7], and σ_{Static} is the averaged and temperature adjusted static crush strength from Table 2.12.4-3. All the crush strength values above 70% strain are extrapolated in a spreadsheet, and shaded grey in Table 2.12.4-2 through Table 2.12.4-4.

The final foam crush strength curves are shown in Table 2.12.4-4 and Figure 2.12.4-1. The crush strength of 16 pcf at -10 °F is slightly harder than the crush strength of 15 pcf at -40 °F, and is therefore bounding with respect to the cold impacts. The crush strength of 15 pcf at 150 °F is slightly softer than the as-tested crush strength of 14 pcf at 117 °F. Therefore, the warm prototypic foam is not bounded by the as-tested warm CTU-2 foam and a relation must be developed to bound the maximum crush deformation for thermal performance consideration. See Section 2.7.1.5.2, *Maximum Impact Limiter Crush Deformation.*

For an example of how the foam crush strengths are calculated the following demonstration for 16 pcf foam at 40% strain is provided.

From Table 2.12.4-2 the actual static crush strength of 16 pcf foam at 40% strain and 75 °F is 930 psi parallel to rise, and 934 psi perpendicular to rise. From the foam design guide [7] the temperature correction factor, C_T, for -20 °F is 1.31 parallel to rise and 1.33 perpendicular to rise.

Parallel to Rise

Crush strength of 16 pcf at 40% strain and -20 °F = C_T x Actual Static at 75 °F

= 1.31 x 930 = 1,218 psi

Perpendicular to Rise

Crush strength of 16 pcf at 40% strain and -20 °F = C_T x Actual Static at 75 °F

= 1.33 x 934 = 1,242 psi

Then the crush strength values at 75 °F and -20 °F are used to linearly interpolate the crush strength at -10 °F, which for 16 pcf at 40% strain is 1,189 psi parallel to rise and 1,210 psi perpendicular to rise. These values are then averaged providing the 1,200 psi shown in Table 2.12.4-3. At this point, prototypic 15 pcf foam would be adjusted by a factor of 1.1 to account for manufacturing tolerance. It is not done in this example since it is for the actual foam test data from the CTU.

The dynamic factor is then applied per the equation discussed above.

$$\sigma_{Dynamic} = Y_{int}(\sigma_{Static})^S = 1.3887(1{,}200)^{1.0028} = 1{,}700 \text{ psi}$$

Where Y_{int} = 1.3887 and S = 1.0028 from [7]. This is the final crush strength value used in the simulations, and represented in Table 2.12.4-4 and Figure 2.12.4-1.

2.12.4.2.3.5 A320 Grade L43 (*mat_spotweld)

The closure bolts are 1 1/4 – 7UNC socket head bolts manufactured from ASTM A320 GR L43, LS-DYNA material model 100 is used with an elastic yield strength of 105 ksi.

2.12.4.2.3.6 Rigid LTSS and Drop Pad (*mat_rigid)

The LTSS and drop pad are modeled with LS-DYNA rigid material model 20. This material does not absorb energy and no stresses or strains are calculated. The density of the LTSS is controlled to model the gross weight of the prototypic LTSS and the as-tested LTSS. The elastic modulus and Poisson's ratio of steel are used, but only relevant to the contact algorithms.

2.12.4.3 Methodology

2.12.4.3.1 435-B FEA Model

2.12.4.3.1.1 Benchmark Model

The first phase of work in this calculation is to develop a FEA model and benchmark the simulation performance to the full-scale certification test results. The certification testing to be benchmarked includes three different free drop orientations and two CTUs. The results from Appendix 2.12.3, *Certification Test Results* to be used for benchmarking include: CTU #1 in test series D1 including bottom-down 4-ft NCT and 30-ft HAC free drops, CTU #1 in test series D2 including the side orientation (where the impact limiter corner and the knuckle contacted simultaneously) 4-ft NCT and 30-ft HAC free drops, and CTU #2 in test series D3 that consisted of 4-ft NCT and 30-ft HAC free drops in the c.g.-over-top knuckle orientation. There are two primary differences between CTU #1 and CTU #2. CTU #1 has cold 16 pcf foam, while CTU #2 has warm 14 pcf foam and a thermal shield on the upper torisperical head. CTU #3, which has 16 pcf foam and is loaded with an inner container was not benchmarked.

The benchmark model consists of four components; the 435-B packaging, the lodgment, the LTSS, and the impact surface. A total of 45 parts are defined in LS-DYNA for the benchmark, which includes approximately 800,000 nodes and 700,000 elements. The 435-B packaging is comprised of numerous parts utilizing solid, shell, and beam elements. The structural parts of the containment boundary including the upper and lower flanges, bell shell, upper and lower torispherical heads, and impact limiter clips (base blocks) are modeled with solid type 2, fully integrated selectively reduced elements. The shell, upper and lower torispherical heads are 1/2 inch thick type 304 stainless steel and have three elements through their thickness. The lower torispherical head, lower and upper flange use the plastic kinematic material in Section 2.12.4.2.3.1, *Type 304 Stainless Steel (*mat_plastic_kinematic)*. The bell shell, upper torispherical head, and impact limiter clips (base blocks) use the elastic-plastic material from Section 2.12.4.2.3.2, *Type 304 Stainless Steel (*mat_piecewise_linear plasticity)*. The benchmark simulations use the 45 ksi yield strength, material ID 17 from Table 2.12.4-1 for bell shell and upper torispherical head. The internal impact limiter clips (base blocks) use the 40 ksi yield strength, material ID 15 from Table 2.12.4-1.

The polyurethane foam in the base is modeled with the default, solid type 1 constant stress elements with type 5 Flanagan-Belytschko hourglass control, which is a stiffness form with exact

volume integration for solid elements. The foam blocks in the bell that are between the closure bolt access tubes are modeled with the same element type and material as the base external impact limiter foam. The design calls for these foam blocks to be 30 pcf, however they are modeled with the same density (14 pcf, 15 pcf, or 16 pcf) as the base. Modeling the foam blocks with lighter density foam than specified in the design is conservative with respect to the possible incurred drop damage, and the accelerations near the base are not expected to be significantly affected because the foam properties are equivalent with the external base impact limiter. The crushable material for the foam is described in Section 2.12.4.2.3.4, *Polyurethane Foam (*mat_crushable_foam)*.

The base skin (external impact limiter shell), bell skin (enclosing the bolt tubes and foam blocks), bolt tubes, tube sheet, thermal shields, and internal impact limiter assemblies use type 16 fully integrated shell elements with Lobatto integration and type 8 hourglass control. Activating the Lobatto integration style calculates the stresses of the outer integration points at the outer surface of the shell. The Type 8 hourglass control is applicable for type 16 fully integrated shell elements, which activates full projection warping stiffness for accurate solutions. All shell elements have a shear correction factor of 5/6, as recommended by [6]. All the shell elements less than 1/2 inch thick have 3 integration points through their thickness. The shell elements that are 1/2 inch thick, which includes the internal impact limiter aluminum base plates and the main lodgment plates, have 5 integration points through their thickness.

The closure bolts are modeled with beam elements that are the type 9 (spot weld) with the cross section type set to circular and the default integration rule of 2. The cross section diameter is 1.1108 inch, which is the mean thread diameter of the 1 1/4 - 7UNC bolts, using Table 8-2 from [10]. The model is half symmetrical with the symmetry plane cutting thru two of the closure bolts. The bolts on the symmetry plane have a reduced beam cross section of 0.7854 inch that produces an area equivalent to half of the full symmetry bolt stress area. Therefore, the model has two half symmetry bolts and eleven full symmetry bolts. The beam elements are defined as beam type 9 (spot weld) and used in conjunction with the material type *mat_spotweld from Section 2.12.4.2.3.5 for the purpose of enabling the command *initial_axial_force_beam. The command *initial_axial_force_beam is used to initialize the axial force resultant in beam elements that are used to model bolts. The preload force used for all the simulations is 19,200 lb for the full symmetry bolts, and 9,600 lb for the half symmetry bolts. The preload is determined by using T = KFd, where the nominal bolt torque T is 300 ft-lb, K is an assumed torque (nut) factor of 0.15 from Section 2.6.1.5, *Closure Bolts*, and d is the bolt diameter of 1.25 inch.

The end drop (D1) and simultaneous side drop (D2) orientations are benchmarked without any thermal shields. CTU #1 does have a single thermal shield around the bell outer shell, however the thermal shield is not anticipated to significantly influence the drop results for the particular orientations benchmarked. The weight of the thermal shield is included in the model as an increased density factor across the other packaging components. The cg-over-top knuckle (D3) orientation benchmark does include the CTU side thermal shield and upper torispherical head thermal shield to be consistent with CTU #2, as this drop orientation may be affected by the strength of the thermal shields.

The lodgment is modeled entirely with shell elements, which have all the same attributes and features as described above for the bell, base, and internal impact limiter shells. The lodgment is an all aluminum structure that is modeled with plastic-kinematic properties as described in Section 2.12.4.2.3.3, *6061-T6 Aluminum (*mat_plastic_kinematic)*. The lodgment has upper and

lower halves that are connected with constrained nodal rigid bodies. The constrained nodal rigid bodies connect the nodes around the perimeter of the u-bracket holes in the upper lodgment with the nodes around the perimeter of the mid-plates in the lower lodgment. The constrained nodal rigid body part numbers are 120, 121, 122, and 123. The lodgment design calls for 1/2 inch stainless steel bolts to join the upper and lower halves. The bolts performed well with no breakages in certification testing and are not specifically considered in the model. The lodgment is also modeled without consideration for fillet weld effective throat areas being less than joint minimum plate thicknesses or as-welded aluminum material properties. The lodgment is considered in the simulations to conservatively contribute to the impact accelerations of the LTSS for the different orientations and to conservatively interface with packaging containment boundary. The lodgment design is proven by certification testing that demonstrates under worst-case impacts, the lodgment joints do not fail. Therefore failure in the simulations does not need to be considered.

The impact surface of the benchmark model includes a 2 inch thick by 300 inch wide by 150 inch deep rigid drop pad. The drop pad is modeled with the default type 1 constant stress solid elements, however the material is completely rigid as described in Section 2.12.4.2.3.6, *Rigid LTSS and Drop Pad (*mat_rigid)*. All nodes on the bottom surface of the drop pad are fully constrained. The LTSS is modeled in general size, shape, and weight. However, like the drop pad it is modeled with rigid material. The LTSS performance is demonstrated by the certification testing and does not require stress-strain simulation data, therefore modeling with rigid material conservatively loads the 435-B packaging in the FEA simulations while reducing computation time.

The FEA model includes a wide array of structural interfaces and contacts. Structural interfaces are modeled with merged nodes, where permitted by the mesh generation, or by tied contact definitions. For instance, the interface between the upper flange and bell shell is a merged node interface, i.e., the mesh is continuous between the parts. In other areas, like the lodgment, all the parts are connected with tied contact definitions. Tied contact definitions are used where the mesh between parts is not similar or continuous. The FEA model also has numerous contacts between parts. The most common contact definition used is automatic surface to surface with the optional card A set with soft equal to 2 for segment-based contact and the depth equal to 5 for checking surface and edge to edge penetrations. Friction between the various parts is defined through the contact cards. The majority of contact interfaces have a coefficient of friction of 0. However, a significant number of contact interfaces have a coefficient of friction 0.40, such as all the contacts involving foam and internal impact limiters. The coefficient of friction of 0.40 is used for both static and sliding conditions. The value is used in part by matching results between the benchmark simulations and certification testing. The value of 0.40 is also considered reasonable in comparison with a survey of dry sliding friction values in Table 3.2.4 of [9], where hard steel on hard steel is 0.42, mild steel on mild steel is 0.57, nickel on mild steel is 0.64, aluminum on mild steel is 0.47, and nickel on nickel is 0.53. The coefficient of friction used between the package and drop pad is 0.10, with two simulations using a value of 0 for demonstration purposes.

The benchmark model includes gravity as a body acceleration load of 386.4 in/sec^2. The benchmark model also includes an initial velocity of 561.5 in/sec that is equivalent to a combined 4 ft NCT and 30 ft HAC drop. This initial velocity of 561.5 in/sec applies all the drop energy of the 4 ft NCT and 30 ft HAC drops into one continuous impact simulation rather than

two distinct drop events. The purpose of applying this simulation method is to limit the number of necessary simulations, thereby decreasing the total calculation computer run time, required data storage space, and post-processing labor while producing reasonable simulation results. The benchmark simulation results in Section 2.12.4.5.1, *Benchmark Results* justify the applicability of this method by comparison with the certification test results. Additionally, one benchmark orientation is simulated with sequential and cumulative, NCT and HAC drops for comparative information.

See Figure 2.12.4-2 through Figure 2.12.4-12 for the FEA model components and mesh. See Table 2.12.4-5 and Table 2.12.4-6 for a summary of the benchmark cases and their respective parameters.

2.12.4.3.1.2 Slapdown (Prototypic) Model

The second phase of the work in this calculation is to take the benchmarked FEA model and perform a series of slapdown free drops to demonstrate the certification test orientations are appropriate for the license application. The benchmark model is slightly adjusted for the slapdown simulations. The primary differences include 1) Weight. The benchmark model uses the as-tested LTSS weight of 4,460 lb, from Table 2.12.3-1, and the slapdown model uses the estimated design gross weight of 4,650 lb, essentially equal to the maximum weight of 4,660 lb from Table 2.1-2, 2) The bell shell and upper torispherical head strength. The benchmark model uses 45 ksi yield strength from the CTU CMTR, while the slapdown model uses 40 ksi yield strength from the SAR drawings in Appendix 1.3.3, *Packaging General Arrangement Drawings*, and 3) The aluminum plate thickness. The benchmark model uses 0.53 inch thick main lodgment plates and internal impact limiter base plates from the CTU fabrication, while the slapdown model uses 0.50 inch thick from the SAR drawings. All the slapdown simulations have the CTU side thermal shield and upper torispherical head thermal shield like the D3 benchmark simulation, i.e., D3_benchmark_302_6JN0.

The different FEA models are grouped in Table 2.12.4-7 with their respective component weights. Note that the "Loaded Package" weight for the slapdown simulations of 9,935 lb is only 1.6% less than the maximum weight of 10,100 lb given in Table 2.1-2. A complete summary of the FEA model components and descriptions is in Table 2.12.4-8, and a complete summary of the FEA model component parameters (material and thickness) is in Table 2.12.4-9. The material references in Table 2.12.4-9 are from Section 2.12.4.2.3, *Material Properties* where the ID # refers to the curves in Section 2.12.4.2.3.2, *Type 304 Stainless Steel (*mat_piecewise_linear plasticity)* and 304 PK refers to the Plastic Kinematic material in Section 2.12.4.2.3.1, *Type 304 Stainless Steel (*mat_plastic_kinematic)*. The foam densities refer to the material curves in Section 2.12.4.2.3.4, *Polyurethane Foam (*mat_crushable_foam)*.

2.12.4.4 Acceptance Criteria

The objective of simulations performed in this calculation is to demonstrate that the certification test orientations performed are appropriate for the licensing basis. The primary method by which this will be demonstrated is comparison of the package free drop accelerations and package impact surface dimensions ("impact patch") between the simulations and the certification test results. The certification test orientations are the worst case and conservatively demonstrate the structural NCT and HAC free drop safety effectiveness of the package. If a governing

performance parameter was not obtained from the certification testing, then the simulation results are utilized to obtain the required parameter.

2.12.4.5 Results

There are two primary groups of simulations. The benchmark simulations are developed for comparison with the certification test results. The prototypic (slapdown) simulations are developed for trending the effects of drop orientation, to confirm the certification test orientations represent the worst case. The differences between the two groups of simulations are not great. The benchmark simulations use as-tested material properties for the bell shell and upper torispherical head, and the as-tested LTSS weight as discussed in Section 2.12.4.3.1.2, *Slapdown (Prototypic) Model*. The prototypic (slapdown) simulations use design specified material properties for the bell shell and upper torispherical head, and the gross LTSS weight.

In all cases, the time history data obtained from the numerical simulation contains high frequency structural vibration and numerically-induced noises that are filtered out to provide an accurate assessment of the loadings on the package. In post-processing these analyses, the time history data is processed with a low-pass Butterworth filter. The cutoff frequency is 500Hz as referenced from Section 2.12.3.2.2, *Instrumentation* of the certification test results. The cutoff frequency was determined in Section 2.12.3.2.2 based on guidance given in Section 701.9 of TS-G-1.1 [8].

The CTUs were instrumented with accelerometers for the NCT and HAC certification free drops. The accelerometers were attached to the bell (lid) at four locations, two upper and two lower. The accelerometers were located at the azimuth of the seal test port and opposite the seal test port, as shown in Figure 2.12.3-1. To benchmark the FEA model and compare the CTU accelerations, the accelerations of the bell are processed at the approximate corresponding locations for the FEA model. The nodal accelerations are post-processed for 12 nodes at each upper and lower location. The 12 nodes at each location represent an area representative of the accelerometer blocks welded to the CTUs. The accelerations of the nodes are averaged and then filtered at 500Hz. See Figure 2.12.4-13 through Figure 2.12.4-15 for the FEA model nodes that are equivalent to the CTU accelerometer blocks.

The upper, lower, and average bell accelerations are the primary metric used to compare the FEA model results with certification testing, where the average is simply, (upper + lower) / 2. The impact patch dimensions including the circumferential width and axial height of the side drop and cg-over-top knuckle certification test damage are also used as a metric for comparison with the FEA model results. The impact patches are defined as the approximate region that contacts the drop pad surface. The CTU impact patches were measured by scuff marks (abrasions) indicating contact with the drop pad. The simulation impact patches are measured by observation of the time history animation to determine the extent of contact between the package and drop pad.

The upper, lower, and average bell accelerations are also the primary metric used to trend the simulation results for the severity of the various free drop orientations. Supplemental data used to trend the various free drop orientation severity includes the LTSS rigid body acceleration, maximum axial bolt force, containment boundary effective cumulative plastic strain, and minimum foam thickness near the seal region. In general, the benchmark simulations correlate well with the certification test results having accelerations and impact patch dimensions within

10%, and the slapdown free drop simulations demonstrate the worst case orientations were chosen for certification testing. Detailed comparison and evaluation of the benchmark simulations is discussed on Section 2.12.4.5.1, *Benchmark Results*. Detailed comparison and evaluation of the prototypic (slapdown) free drop simulations is discussed in Section 2.12.4.5.2, *Slapdown Free Drop Results* and warm simulation results are presented in Section 2.12.4.5.3, *Warm Free Drop Results*.

2.12.4.5.1 Benchmark Results

The FEA model is benchmarked with results from the full-scale certification testing. Three simulations are performed, including the D1 end drop, the D2 side drop (where the impact limiter and upper torispherical head contact the drop pad at the same time), and the D3 cg-over-knuckle drop. All the certification test results are referenced from Appendix 2.12.3, *Certification Test Results*. The certification testing included a 4 ft NCT drop followed by a 30 ft HAC drop to assess cumulative damage in the D1, D2, and D3 test orientations.

The FEA simulations are performed with a combined drop where the drop energy equivalent to 34 ft is applied in one continuous event. This combined drop height method is applicable based on comparison with a cumulative (rather than combined) test simulation and the certification test results. The D1 free drop orientation is simulated with a cumulative 4ft NCT and 30 ft HAC drop via a restart process and the results are compared to the certification testing and the combined drop simulations. The 30 ft HAC drop simulation with cumulative NCT drop damage produced an average bell acceleration of 804 g while the combined 34 ft drop simulation produced an average bell acceleration of 819 g. The 30 ft HAC certification drop, D1H, recorded an average bell acceleration of 768 g. The combined drop height simulation produced results that are conservative compared to the sequential drop simulation and to the drop test results. Therefore, a combined drop height of 34 ft was used for all benchmark and slapdown simulations. See all the results in Table 2.12.4-10 and Table 2.12.4-11 for the cumulative cases labeled D1_benchmark_NCT and D1_benchmark_HAC, and the equivalent combined case D1_benchmark302_6JN0.

All the benchmark results are presented in Table 2.12.4-12, where the acceleration results are compared with HAC certification test results from Appendix 2.12.3, and the impact patch dimensions (where deformation exists from contact with the drop pad), and internal impact limiter tube crush dimensions are compared with certification test measurements collected after each HAC event.

The effect of friction between the package and the drop pad is considered in the benchmark simulations. The benchmark simulations use a low coefficient of friction with the pad of 0.10, except for one test case that uses 0.0. See simulation results for D2_benchmark_309_6JN0 in Table 2.12.4-10 and Table 2.12.4-11 for 0.0 friction with the pad. The friction coefficient of 0.10 is used because of good correlation with the certification test results and because the 0.0 friction coefficient has tendency to produce an unrealistic slipping of the impact limiter in the shallow slapdown and side drop orientations, where the foam appears to squirt out the base of the package from between the impact limiter shell and base flange. This behavior was not observed in certification testing.

The benchmark simulation results are shown in Figure 2.12.4-16 through Figure 2.12.4-41, and are compared with the certification test results in Table 2.12.4-12. The impact g's of the benchmark simulations have a difference with the certification test data that ranges between

0.6% to 10.0%. The impact patches of the benchmark simulations range between 0.25 inches to 1.6 inches difference with the certification test data. The benchmark simulations show the FEA model produces results very similar to those seen in full-scale testing. These results demonstrate that the FEA model of the 435-B is capable of reliably predicting the behavior of the real package.

2.12.4.5.2 Slapdown Free Drop Results

The slapdown free drops are all the simulations in Table 2.12.4-13 and Table 2.12.4-14. These simulations include some orientations that do not physically slapdown. The slapdown connotation is used to separate this complete set of simulations from the benchmark simulations. The slapdown set of simulations includes 19 simulations that vary only by orientation, which ranges from end drop to bell drop. See Figure 2.12.4-42 for the drop orientation terminology. Four additional runs are included in this set to consider specific variables such as friction with the pad and elevation of the payload cg relative to the maximum bolt load.

Terminology of the drop simulation names is relative to these abbreviations: sar = safety analysis report, ilp = impact limiter primary, kp = knuckle (of upper torispherical head) primary, fr = coefficient with the drop pad, simu = simultaneous side drop, number = package angle in degrees. For example, sar_kp63 = safety analysis report, knuckle primary slapdown at 63 degrees. See Figure 2.12.4-69 for this orientation.

All the slapdown free drop simulation results are included in Table 2.12.4-13 and Table 2.12.4-14. The slapdown free drop simulation results are plotted versus drop orientation in Figure 2.12.4-43 through Figure 2.12.4-47. The maximum average bell (lid) acceleration of 797 g occurred in the end drop orientation, with the second highest average bell acceleration of 311 g occurring in the simultaneous side drop orientation, see Figure 2.12.4-43. The upper bell accelerations are predominantly higher than the lower bell accelerations, which is reasonable given the lower location is nearer the package CG and much closer to the foam impact limiter. The maximum impact at the upper bell, excluding the end drop, is 429 g for the impact limiter primary 0 degree slapdown (ILP0). Of note, an additional run is performed at ILP0, but using 0 friction with the drop pad. In this case, upper, lower, and LTSS accelerations are slightly less than the simulation with 0.10 friction although the containment boundary maximum cumulative effective plastic strain is slightly more. Since the change in results is less than 10% and no clear bounding condition exists that includes each evaluated characteristic the friction coefficient factor of 0.10 is used for all other cases.

The dip in the acceleration plot for the ILP-7 orientation appears to be a function of geometry. The package just slightly impacts the top edge of the base impact limiter, which does not induce the slapdown rotation like the ILP0 orientation or the blunt initial impact of the simultaneous side drop.

The simultaneous side orientation clearly produces the maximum LTSS impact, 228 g, as shown in Figure 2.12.4-44. This orientation produces a higher payload impact than the end drop, which is 206 g. The payload impact is mitigated in the end drop by the internal impact limiter. The simultaneous side drop orientation also causes the most impact limiter foam crush near the seal region. This is demonstrated in Figure 2.12.4-45 that shows the minimum remaining foam thickness versus drop orientation. The foam crush relative to the remaining foam thickness is important near the containment seal for thermal protection of the o-ring. Orientations, such as ILP45, that may have more foam crush than the simultaneous side drop are not checked for

minimum remaining foam because the crush region is not adjacent to the containment o-ring and the available foam thickness is large.

The maximum containment boundary cumulative effective plastic strain is demonstrated in Figure 2.12.4-46 to be caused by the cg-over-top knuckle orientation. The maximum containment boundary cumulative effective plastic strain occurs for a knuckle primary drop (onto the upper torispherical head) with an angle between 70° and 63°. The cumulative effective plastic strain for the knuckle primary 70° case is 32.3% and for the knuckle primary 63° case is 31.0%, as shown in Table 2.12.4-14. The difference in plastic strain between the 70° and 63° simulations is approximately 1.3%, which is negligible for austenitic stainless steel. Therefore, the D3 certification test at 63° is sufficiently bounding for containment boundary maximum strain.

The maximum bolt load is demonstrated in Figure 2.12.4-47 to be caused by the impact limiter primary 75° orientation. The maximum bolt load appears to be caused by the payload contacting the bell shell in near vertical end drop orientations. Three additional simulations are performed to evaluate the effect of the payload cg height on the maximum bolt load in this orientation. One simulation is performed at 75° with the payload elevated, (i.e., suspended and touching the top of the payload cavity prior to impact) and two simulations are performed with the payload upside down and elevated in the payload cavity at 68° and 75° orientations. The lodgment that controls the LTSS in the payload cavity is biased to keep the LTSS cg low in the payload cavity. Therefore, flipping the loaded lodgment upside down in the payload cavity and elevating it in the payload cavity prior to impact is a conservative simulation condition for determining the maximum bolt load. This is further discussed in Section 2.7.1.5.1, *Maximum Closure Bolt Stress*. Doing so generates a maximum bolt load of 35,774 lb in simulation sar_ilp68_udep, where udep = upside down elevated payload. This bolt load occurs for the maximum (cold) impact, with a payload gap at the bottom, and the maximum payload c.g. height. See the results summary in Table 2.12.4-13 and Table 2.12.4-14.

Figures for a sample of the simulation results used to create the data plots versus drop orientation are included in the following pages. For simulation sar_simu see Figure 2.12.4-48 through Figure 2.12.4-54. For simulation sar_ilp0 see Figure 2.12.4-55 through Figure 2.12.4-61. For simulation sar_ilp68_udep see Figure 2.12.4-62 through Figure 2.12.4-68. For simulation sar_kp63 see Figure 2.12.4-69 through Figure 2.12.4-75.

The deformation of the upper torispherical head for the top down drop simulation, sar_lid, is shown in Figure 2.12.4-76. The flat region created in the upper torispherical head by the top down drop has an approximate outer diameter of 38 inches, which is further considered for the HAC fire event in Section 2.7.4.3, *Stress Calculations*.

2.12.4.5.3 Warm Free Drop Results

The certification testing included a test series, D4, for determining the minimum remaining foam thickness near the seal region. The D4 test series was performed on CTU #2 with 14 pcf foam. The foam was heated and recorded to be approximately 117 °F before the HAC drop. The drop orientation was the simultaneous side drop, which has been shown to be the worst orientation for minimum foam thickness near the seal region.

The crush strength of the polyurethane foam is shown in Figure 2.12.4-1. The as-tested 14 pcf foam has a slightly higher crush strength at 117 °F than the prototypic 15 pcf foam has at the

NCT temperature of 150 °F. Therefore, two simulations are performed to determine the crush factor between the as-tested foam and prototypic foam. The actual remaining foam values from the simulations are not intended for use in the thermal evaluation, but only to adjust the measurements made on CTU #2. This is further discussed in Section 2.7.1.5.2, *Maximum Impact Limiter Crush Deformation.* The accelerations for the as-tested simulation compare well with the D4 drop results in Section 2.12.3.4.6, *Test Series D4*, lower bell accelerations of 186 g simulation and 183 g test, upper bell accelerations of 406 g simulation and 374 g test. However, the minimum remaining foam does not compare well being 2.5 inches simulation and 5.13 inches test. The certification test minimum remaining foam is shown to be 5.13 inches per Figure 2.12.3-48. The warm simulation results are shown in Table 2.12.4-15 and Table 2.12.4-16.

The objective of the two warm simulations is to determine the minimum remaining foam for each foam crush strength (14 pcf at 117 °F and 15 pcf at 150 °F), such that a comparative factor can be created to compensate the certification test result minimum remaining foam for the decreased prototypic foam crush strength. The compensated minimum remaining foam will then be considered in the thermal evaluation. For creating the comparative factor, the as-tested foam simulation has a minimum remaining foam thickness of 2.5 inches near the seal region, see Figure 2.12.4-77. Likewise, the prototypic foam simulation has a minimum remaining foam thickness of 2.0 inches near the seal region, see Figure 2.12.4-78. The comparative factor is calculated in Section 2.7.1.5.2, *Maximum Impact Limiter Crush Deformation,* and used in the thermal analysis in Chapter 3, *Thermal Analysis.*

2.12.4.6 FEA Summary

This document provides supporting drop simulation data for the certification testing performed on the 435-B package. The licensing basis for the package is primarily by full-scale test of Hypothetical Accident Condition (HAC) free drop and puncture. Analysis is used for all Normal Conditions of Transport (NCT), except the NCT free drop, to determine the worst-case orientations for test, to determine the performance in orientations not tested, and for the HAC fire event. The analysis performed in this calculation is for supporting the worst-case orientations tested, and to determine the performance in orientations not tested.

The primary method by which this will be demonstrated is comparison of the package free drop accelerations between the simulations and certification testing. The certification test orientations must be the worst case and conservatively demonstrate the structural NCT and HAC free drop safety effectiveness of the package. If a governing performance parameter was not obtained from the certification testing, then the simulation results are utilized to obtain the required parameter.

The FEA simulations performed in this calculation include benchmark orientations that are compared directly to the certification test results. Free drop impact deformation and acceleration results are used to benchmark the finite element analysis model for use in non-tested orientations and conditions. The non-tested orientations are slapdown free drops with both the base impact limiter primary and the bell (lid) torispherical head primary in a wide range of angles.

As discussed in Section 2.12.4.5, the simulation results compare well with the certification test results. The benchmark simulations show impact accelerations and impact patch sizes have a difference less than or equal to 10%. This is reasonable and useful, given the nature of variation

in physical testing, and that a simulations outcome is dependent on numerous inputs, modeling techniques, and code capabilities.

The slapdown series of simulations demonstrates that the appropriate certification test orientations were performed. The end drop has the highest average packaging impact with an acceleration of 797 g. The simultaneous side drop has the second highest average packaging impact with an acceleration of 311 g. This orientation is the highest impact perpendicular to the package axis. The simultaneous side drop also rivals the 0° slapdown for the highest upper bell acceleration (excluding the end drop), having a difference less than 3%. The simultaneous side orientation also produces the maximum LTSS acceleration, 228 g, and has the least amount of remaining foam near the seal region. Lastly, the cg-over-top knuckle drop generates the maximum cumulative effective plastic strain in the containment boundary. Therefore, all the certification tests are demonstrated by this calculation and the test plan, Appendix 2.12.2, *Certification Test Plan*, to be worst case, and appropriate for the license application. The only supplemental information necessary for the license application is the maximum bolt load (35,774 lb) from the simulations and the warm minimum remaining polyurethane foam comparative factor data.

Table 2.12.4-1 – True Plastic Stress-Strain Curves for Type 304 Stainless Steel at 70 °F

Strain (in/in)	Stress (psi)	Stress (psi)	Stress (psi)
	Material ID 15	Material ID 16	Material ID 17
0.000	40,137	51,697	45,192
0.002	42,779	55,100	48,167
0.004	44,575	57,414	50,189
0.006	46,148	59,440	51,961
0.008	47,592	61,300	53,586
0.010	48,947	63,044	55,112
0.020	54,935	70,757	61,854
0.030	60,180	77,513	67,759
0.040	64,993	83,713	73,179
0.050	69,510	89,530	78,264
0.060	73,803	95,059	83,098
0.070	77,918	100,360	87,732
0.080	81,888	105,473	92,202
0.090	85,734	110,427	96,532
0.100	89,474	115,244	100,743
0.150	106,960	137,766	120,431
0.200	123,008	158,437	138,501
0.250	138,066	177,832	155,455
0.300	152,378	196,267	171,570
0.350	166,100	213,940	187,020
0.400	179,334	230,987	201,921
0.500	204,627	263,563	230,399
0.600	228,667	294,528	257,468
0.700	251,715	324,214	283,418
0.800	273,945	352,847	308,448
0.900	295,484	380,590	332,700
1.000	316,428	407,566	356,282

Table 2.12.4-2 – Static Stress-Strain Curves for Polyurethane Foam

Strain (in/in)	Stress (psi)	Stress (psi)	Stress (psi)	Stress (psi)	Stress (psi)	Stress (psi)
	16 pcf at 75 °F	16 pcf at 75 °F	15 pcf at 75 °F	15 pcf at 75 °F	14 pcf at 75 °F	14 pcf at 75 °F
	CTU-1 Parallel	CTU-1 Perpendicular	Prototypic Parallel	Prototypic Perpendicular	CTU-2 Parallel	CTU-2 Perpendicular
0.00	0	0	0	0	0	0
0.10	755	741	629	603	606	607
0.20	769	770	630	625	615	627
0.30	822	824	668	670	656	668
0.40	930	934	754	769	737	749
0.50	1,176	1,175	964	977	917	927
0.60	1,727	1,727	1,436	1,445	1,326	1,338
0.65	2,263	2,272	1,886	1,903	1,728	1,750
0.70	3,185	3,212	2,645	2,691	2,421	2,456
0.75	4,273	4,328	3,551	3,629	3,231	3,287
0.80	5,803	5,902	4,819	4,952	4,365	4,453
0.85	7,880	8,048	6,540	6,758	5,898	6,033
	Actual Test Data		Nominal		Actual Test Data	

Table 2.12.4-3 – Averaged and Temperature Adjusted Static Stress-Strain Curves for Polyurethane Foam

Strain (in/in)	Stress (psi)	Stress (psi)	Stress (psi)	Stress (psi)
	16 pcf at -10 °F, no bias	15 pcf at -40 °F, +10% bias	14 pcf at 117 °F, no bias	15 pcf at 150 °F, -10% bias
	CTU-1	Prototypic Cold	CTU-2	Prototypic Warm
0.00	0	0	0	0
0.10	981	969	489	381
0.20	998	974	507	397
0.30	1,060	1,028	546	430
0.40	1,200	1,169	619	496
0.50	1,498	1,471	766	627
0.60	2,178	2,152	1,118	943
0.65	2,798	2,759	1,459	1,240
0.70	3,814	3,703	2,132	1,840
0.75	5,000	4,820	2,889	2,519
0.80	6,619	6,324	3,988	3,518
0.85	8,762	8,299	5,507	4,913

Table 2.12.4-4 – Dynamic Adjusted Stress-Strain Curves for Polyurethane Foam

Strain (in/in)	Stress (psi)	Stress (psi)	Stress (psi)	Stress (psi)
	16 pcf at -10 °F	15 pcf at -40 °F	14 pcf at 117 °F	15 pcf at 150 °F
	CTU-1	Prototypic Cold	CTU-2	Prototypic Warm
0.00	0	0	0	0
0.10	1,597	1,578	777	601
0.20	1,507	1,470	762	596
0.30	1,545	1,499	799	629
0.40	1,700	1,656	875	701
0.50	2,026	1,989	1,042	854
0.60	2,730	2,699	1,418	1,199
0.65	3,312	3,266	1,750	1,492
0.70	3,974	3,863	2,275	1,976
0.75	5,151	4,974	3,045	2,670
0.80	6,741	6,453	4,148	3,678
0.85	8,821	8,374	5,651	5,066

Table 2.12.4-5 – Benchmark Summary

CTU#	Certification Test Series	Simulation Test Description	Foam Type	Side Thermal Shield	Head Thermal Shield
1	D1	4-ft NCT, bottom down	cold 16 pcf	Single Wall (no mesh in model, mass added by density factor)	No
		30-ft HAC, bottom down			
		34-ft (NCT + HAC), bottom down			
	D2	34-ft (NCT + HAC) side orient			
		34-ft (NCT + HAC) side orient, zero friction			
2	D3	34-ft (NCT + HAC), c.g.-over-top knuckle	warm 14 pcf	Single Wall	Prototypic
	D4	Not benchmarked, side orientation			
3	D5	Not benchmarked, bottom down	cold 16 pcf	Prototypic	No
	D6	Not benchmarked, side orientation			

Table 2.12.4-6 – Benchmark Parameters

Computer Run	Initial Velocity	Orientation
D1_benchmark_302_6JN0	-561.5 (34 ft)	End 90°
D1_benchmark_HAC	-527.5 (30 ft)	End 90°
D1_benchmark_NCT	-192.6 (4ft)	End 90°
D2_benchmark_302_6JN0	-561.5 (34 ft)	Side - 13°
D2_benchmark_309_6JN0	-561.5 (34 ft)	Side - 13°
D3_benchmark_302_6JN0	-561.5 (34 ft)	Top - 63°

Table 2.12.4-7 – FEA Model Weights

Component	D1 & D2 Benchmarks	D3 Benchmark	Slapdown Simulations
	lb	lb	lb
Base Assembly	2,285	2,218	2,259
Lid Assembly	2,352	2,433	2,482
Empty Package	4,669	4,682	4,772
Lodgment	510	510	512
LTSS	4,460	4,460	4,651
Loaded Package	9,639	9,652	9,935

Table 2.12.4-8 – FEA Model Part Descriptions

Component Model Part #	Model Part Description
1	lid flange (lid is equivalent to bell)
2	lid shell (includes upper torispherical head)
3	lid skin 0.25 thk (angle tube sheet)
4	lid skin 0.12 thk (lid foam and bolt tube enclosure sheet)
5	lid aluminum plate 0.5 thk (of upper internal impact limiter)
7	lid foam (foam blocks between bolt access tubes)
9	bolt tubes (closure bolt access tubes)
10	impact limiter base blocks (internal impact limiter clips)
11	base flange (includes lower torispherical head)
12	base skin 0.25 thk (bottom and outer skin of impact limiter)
13	base skin 0.12 thk (inner skin of impact limiter by lid)
14	base aluminum plate 0.5 thk (of lower internal impact limiter)
16	base foam (base external impact limiter foam)
21	bolts (closure bolts)
22	symmetry bolts
25	bolt shell tops (rigid shells connecting bolt tops)
26	bolt shell bottoms (rigid shell connecting bolt bottoms)
48	ltss (Long Term Storage Shield)
71	upper tubes (upper internal impact limiter tubes)
72	upper support plate (upper internal impact limiter dome sheet)
73	lower tubes (lower internal impact limiter tubes)
74	lower support plate (lower internal impact limiter dome sheet)
75	lower center tube (centers the lower internal impact limiter)
80	knuckle thermal shield
81	head thermal shield
82	thermal shield spacer (on upper head near hoist ring boss)
83	side thermal shield (single layer side thermal shield)
100	Upper Lodgment Main Plates
101	Upper Lodgment Center Tube
102	Upper Lodgment Top Plate
103	Upper Lodgment Perim Plate (circular plate)
104	Upper Lodgment Top Angles
105	Upper Lodgment Mid Angles
106	Upper Lodgment Dbl Angles
107	Upper Lodgment Dbl Plates
108	Lower Lodgment Mid Plates
109	Lower Lodgment Main Plates
110	Lower Lodgment Center Tube
111	Lower Lodgment Bot Plate
112	Lower Lodgment Perim Plate (circular plate)
113	Lower Lodgment Bot Angles
114	Lower Lodgment Dbl Angles
115	Lower Lodgment Dbl Plates
116	Upper Lodgment U-Brackets

Table 2.12.4-9 – FEA Model Parameters

Component	D1 & D2 Benchmarks		D3 Benchmark		Slapdown Simulations		Warm		Warm Test	
Model Part #	Mat	Thk	Mat	Thk	Mat	Thk	Mat	Thk	Mat	Thk
1	304 PK	0.50	304 PK	0.50	304 PK	0.50	304 PK	0.50	304 PK	0.50
2	304 ID 17	0.50	304 ID 17	0.50	304 ID 15	0.50	304 ID 15	0.50	304 ID 15	0.50
3	304 ID 15	0.25	304 ID 15	0.25	304 ID 15	0.25	304 PK	0.25	304 PK	0.25
4	304 ID 15	0.12	304 ID 15	0.12	304 ID 15	0.12	304 PK	0.12	304 PK	0.12
5	6061-T6	0.53	6061-T6	0.53	6061-T6	0.50	6061-T6	0.50	6061-T6	0.50
7	16 pcf at -10°F		14 pcf at 117°F		16 pcf at -10°F		15 pcf at 150°F		14 pcf at 117°F	
9	304 ID 15	0.12	304 ID 15	0.12	304 ID 15	0.12	304 PK	0.12	304 PK	0.12
10	304 ID 15	1.25	304 ID 15	1.25	304 ID 15	1.25	304 ID 15	1.25	304 ID 15	1.25
11	304 PK	0.50	304 PK	0.50	304 PK	0.50	304 PK	0.50	304 PK	0.50
12	304 ID 15	0.25	304 ID 15	0.25	304 ID 15	0.25	304 PK	0.25	304 PK	0.25
13	304 ID 15	0.12	304 ID 15	0.12	304 ID 15	0.12	304 PK	0.12	304 PK	0.12
14	6061-T6	0.53	6061-T6	0.53	6061-T6	0.50	6061-T6	0.50	6061-T6	0.50
16	16 pcf at -10°F		14 pcf at 117°F		16 pcf at -10°F		15 pcf at 150°F		14 pcf at 117°F	
21	A320 L43	1.11	A320 L43	1.11	A320 L43	1.11	A320 L43	1.11	A320 L43	1.11
22	A320 L43	0.78	A320 L43	0.78	A320 L43	0.78	A320 L43	0.78	A320 L43	0.78
25	rigid	0.10	rigid	0.10	rigid	0.10	rigid	0.10	rigid	0.10
26	rigid	0.10	rigid	0.10	rigid	0.10	rigid	0.10	rigid	0.10
48	rigid 4,460 lb	na	rigid 4,460 lb	na	rigid 4,651 lb	na	rigid 4,651 lb	na	rigid 4,651 lb	na
71	304 ID 16	.035	304 ID 16	.035	304 ID 16	.035	304 ID 16	.035	304 ID 16	.035
72	304 PK	.105	304 PK	.105	304 PK	.105	304 PK	.105	304 PK	.105
73	304 ID 16	.035	304 ID 16	.035	304 ID 16	.035	304 ID 16	.035	304 ID 16	.035
74	304 PK	.105	304 PK	.105	304 PK	.105	304 PK	.105	304 PK	.105
75	304 PK	.049	304 PK	.049	304 PK	.049	304 PK	.049	304 PK	.049
80	-	-	304 ID 16	.105	304 ID 16	.105	304 PK	.105	304 PK	.105
81	-	-	304 ID 16	.105	304 ID 16	.105	304 PK	.105	304 PK	.105
82	-	-	304 ID 16	.105	304 ID 16	.105	304 PK	.105	304 PK	.105
83	-	-	304 ID 15	.105	304 ID 15	.105	304 PK	.105	304 PK	.105
100	6061-T6	0.53	6061-T6	0.53	6061-T6	0.50	6061-T6	0.50	6061-T6	0.50
101	6061-T6	0.24	6061-T6	0.24	6061-T6	0.24	6061-T6	0.24	6061-T6	0.24
102	6061-T6	0.53	6061-T6	0.53	6061-T6	0.50	6061-T6	0.50	6061-T6	0.50
103	6061-T6	0.53	6061-T6	0.53	6061-T6	0.50	6061-T6	0.50	6061-T6	0.50
104	6061-T6	0.25	6061-T6	0.25	6061-T6	0.25	6061-T6	0.25	6061-T6	0.25
105	6061-T6	0.25	6061-T6	0.25	6061-T6	0.25	6061-T6	0.25	6061-T6	0.25
106	6061-T6	0.25	6061-T6	0.25	6061-T6	0.25	6061-T6	0.25	6061-T6	0.25
107	6061-T6	0.25	6061-T6	0.25	6061-T6	0.25	6061-T6	0.25	6061-T6	0.25
108	6061-T6	0.53	6061-T6	0.53	6061-T6	0.50	6061-T6	0.50	6061-T6	0.50
109	6061-T6	0.53	6061-T6	0.53	6061-T6	0.50	6061-T6	0.50	6061-T6	0.50
110	6061-T6	0.24	6061-T6	0.24	6061-T6	0.24	6061-T6	0.24	6061-T6	0.24
111	6061-T6	0.53	6061-T6	0.53	6061-T6	0.50	6061-T6	0.50	6061-T6	0.50
112	6061-T6	0.53	6061-T6	0.53	6061-T6	0.50	6061-T6	0.50	6061-T6	0.50
113	6061-T6	0.25	6061-T6	0.25	6061-T6	0.25	6061-T6	0.25	6061-T6	0.25
114	6061-T6	0.25	6061-T6	0.25	6061-T6	0.25	6061-T6	0.25	6061-T6	0.25
115	6061-T6	0.25	6061-T6	0.25	6061-T6	0.25	6061-T6	0.25	6061-T6	0.25
116	6061-T6	0.35	6061-T6	0.35	6061-T6	0.35	6061-T6	0.35	6061-T6	0.35

Table 2.12.4-10 – Benchmark Simulation Acceleration Results Summary

Drop Simulation	Lower Bell Acceleration	Upper Bell Acceleration	Average Bell Acceleration	LTSS Acceleration
	Y-acceleration (g)	Y-acceleration (g)	Y-acceleration (g)	Resultant-acceleration (g)
D1_benchmark_302_6JN0	800	838	819	206
D2_benchmark_302_6JN0	224	445	335	256
D2_benchmark_309_6JN0 (0 Friction with Pad)	214	462	338	261
D3_benchmark_302_6JN0	172	195	184	216
D1_benchmark_NCT (4 ft)	313	338	326	167
D1_benchmark_HAC (30 ft) Cumulative	786	822	804	226

Table 2.12.4-11 – Benchmark Simulation Results Summary

Drop Simulation	Axial Bolt Force	Containment Boundary Plastic Strain	Minimum Foam Thickness
	Maximum for all Bolts (lb)	Cumulative Effective (%, inch/inch)	Near Seal (inch)
D1_benchmark_302_6JN0	21,648	5.6	
D2_benchmark_302_6JN0	25,012	23.4	4.3
D2_benchmark_309_6JN0 (0 Friction with Pad)	27,682	22.0	4.1
D3_benchmark_302_6JN0	21,798	28.9	
D1_benchmark_NCT (4 ft)	20,386	0.9	
D1_benchmark_HAC (30 ft) Cumulative	21,495	6.1	

Table 2.12.4-12 – Benchmark Simulation and CTU Results Comparison

Case[1]	Test Weight	Model Weight	Test Upper Impact	Model Upper Impact	Difference	Test Lower Impact	Model Lower Impact	Difference		
	lb	lb	g	g	Δ g, %	g	g	Δ g, %		
D1	9,642	9,639	776	838	+62, +8.0	760	800	+40, +5.3		
D2	9,642	9,639	466	445	-21, -4.5	249	224	-25, -10.0		
D3	9,653	9,652	183[3]	195	+12, +6.6	171[3]	172	+1, +0.6		
Case	**Test Upper Patch Width**	**Model Upper Patch Width**	**Test Upper Patch Height**	**Model Upper Patch Height**	**Test Lower Patch Width**	**Model Lower Patch Width**	**Test Lower Patch Height**	**Model Lower Patch Height**	**Test[2] Tube Crush**	**Model Tube Crush**
	inch	inch	inch	inch	inch	inch	inch	inch	inch	inch
D1	NA	NA	NA	NA	NA	NA	NA	NA	1.43	2.0
D2	18.0	18.5	12.0	12.8	33.25	33.6	25.25	25.0	NA	NA
D3	33.5	33.1	21.0	22.6	NA	NA	NA	NA	NA	NA

Notes:

1. D1 is the End Drop orientation, D2 is the Side Drop orientation (where the base impact limiter and upper torispherical head knuckle contact the drop pad simultaneously), and D3 is the CG-Over-Top Knuckle orientation.
2. Axial crush of the lower internal impact limiter tubes. The CTU and model are measured for the change in length between the top of the lodgment and underside of the internal impact limiter clips (base blocks) to determine the tube crush.
3. The accelerations for D3 test data are from Appendix 2.12.3, *Certification Test Results*. The T/U and OT/U average and OT/L accelerations are resolved for comparison with the upper and lower model impact g's with the method discussed in Appendix 2.12.3, of dividing by the cosine of 27 degrees to resolve the average 159g to 178g for compensating the angle of the drop with the mounting orientation of the accelerometers.
4. The patch width and height are the respective packaging deformations in the circumferential and axial directions caused by impact with the drop pad surface.
5. Figure 2.12.4-16 through Figure 2.12.4-41 demonstrate the results summarized in Table 2.12.4-12 for the three benchmark simulations. All the results plots have been filtered at 500 Hz as discussed in Section 2.12.4.5, *Results*.

Table 2.12.4-13 – Slapdown Simulation Acceleration Results Summary

Drop Simulation	Lower Bell Acceleration	Upper Bell Acceleration	Average Bell Acceleration	LTSS Acceleration
	Y-acceleration (g)	Y-acceleration (g)	Y-acceleration (g)	Resultant-acceleration (g)
sar_end	787	806	797	206
sar_ilp83	198	203	201	188
sar_ilp75	197	194	196	139
sar_ilp75_ep (elevated payload)	148	158	153	142
sar_ilp75_udep (upside down elevated payload)	151	148	150	193
sar_ilp68	112	162	137	128
sar_ilp68_udep (upside down elevated payload)	129	166	148	182
sar_ilp60	116	156	136	133
sar_ilp45	138	157	148	148
sar_ilp30	134	96 (-117)	115	140
sar_ilp15	188	382	285	204
sar_ilp0	178	429	304	199
sar_ilp0_0fr (0 Friction with Pad)	160	419	290	189
sar_ilp-7	220	333	277	194
sar_simu	204	418	311	228
sar_kp20	203	326	265	192
sar_kp30	130	272	201	193
sar_kp45	139	227	183	185
sar_kp55	140	175	158	194
sar_kp63	158	167	163	188
sar_kp70	169	174	172	193
sar_kp75	179	185	182	180
sar_lid	154	165	160	139

Note:

Terminology of the drop simulation names is relative to these abbreviations: sar = safety analysis report, ilp = impact limiter primary, kp = knuckle (of upper torispherical head) primary, fr = coefficient with the drop pad, simu = simultaneous side drop, number = package angle in degrees. For example, sar_kp63 = safety analysis report, knuckle primary slapdown at 63 degrees.

Table 2.12.4-14 – Slapdown Simulation Results Summary

Drop Simulation	Axial Bolt Force	Containment Boundary Plastic Strain	Minimum Foam Thickness
	Maximum for all Bolts (lb)	Cumulative Effective (%, inch/inch)	Near Seal (inch)
sar_end	21,628	6.0	
sar_ilp83	29,703	4.6	
sar_ilp75	33,373	8.7 (minor area at hoist ring boss)	
sar_ilp75_ep (elevated payload)	34,871	4.8	
sar_ilp75_udep (upside down elevated payload)	35,693	5.3	
sar_ilp68	30,550	2.4	
sar_ilp68_udep (upside down elevated payload)	35,774	5.0	
sar_ilp60	26,692	2.3	
sar_ilp45	22,871	1.7	
sar_ilp30	19,735	2.3	
sar_ilp15	23,584	21.5	
sar_ilp0	22,228	24.6	5.5
sar_ilp0_0fr (0 Friction with Pad)	22,311	26.6	5.5
sar_ilp-7	22,510	25.8	5.2
sar_simu	25,451	23.8	4.2
sar_kp20	26,684	23.8	4.4
sar_kp30	23,557	24.1	5.1
sar_kp45	21,450	26.8	
sar_kp55	20,987	23.1	
sar_kp63	21,869	31.0	
sar_kp70	21,820	32.3	
sar_kp75	21,148	29.1	
sar_lid	19,928	6.0	

Note:

Terminology of the drop simulation names is relative to these abbreviations: sar = safety analysis report, ilp = impact limiter primary, kp = knuckle (of upper torispherical head) primary, fr = coefficient with the drop pad, simu = simultaneous side drop, number = package angle in degrees. For example, sar_kp63 = safety analysis report, knuckle primary slapdown at 63 degrees.

Table 2.12.4-15 – Warm Simulation Acceleration Results Summary

Drop Simulation	Lower Bell Acceleration	Upper Bell Acceleration	Average Bell Acceleration	LTSS Acceleration
	Y-acceleration (g)	Y-acceleration (g)	Y-acceleration (g)	Resultant-acceleration (g)
sar_warm_simu (15pcf @ 150F)	170	401	286	201
sar_warm_simu_test (14pcf @ 117F)	186	406	296	205

Table 2.12.4-16 – Warm Simulation Results Summary

Drop Simulation	Axial Bolt Force	Containment Boundary Plastic Strain	Minimum Foam Thickness
	Maximum for all Bolts (lb)	Cumulative Effective (%, inch/inch)	Near Seal (inch)
sar_warm_simu (15pcf @ 150F)	23,205	23.8	2.0
sar_warm_simu_test (14pcf @ 117F)	23,303	24.2	2.5

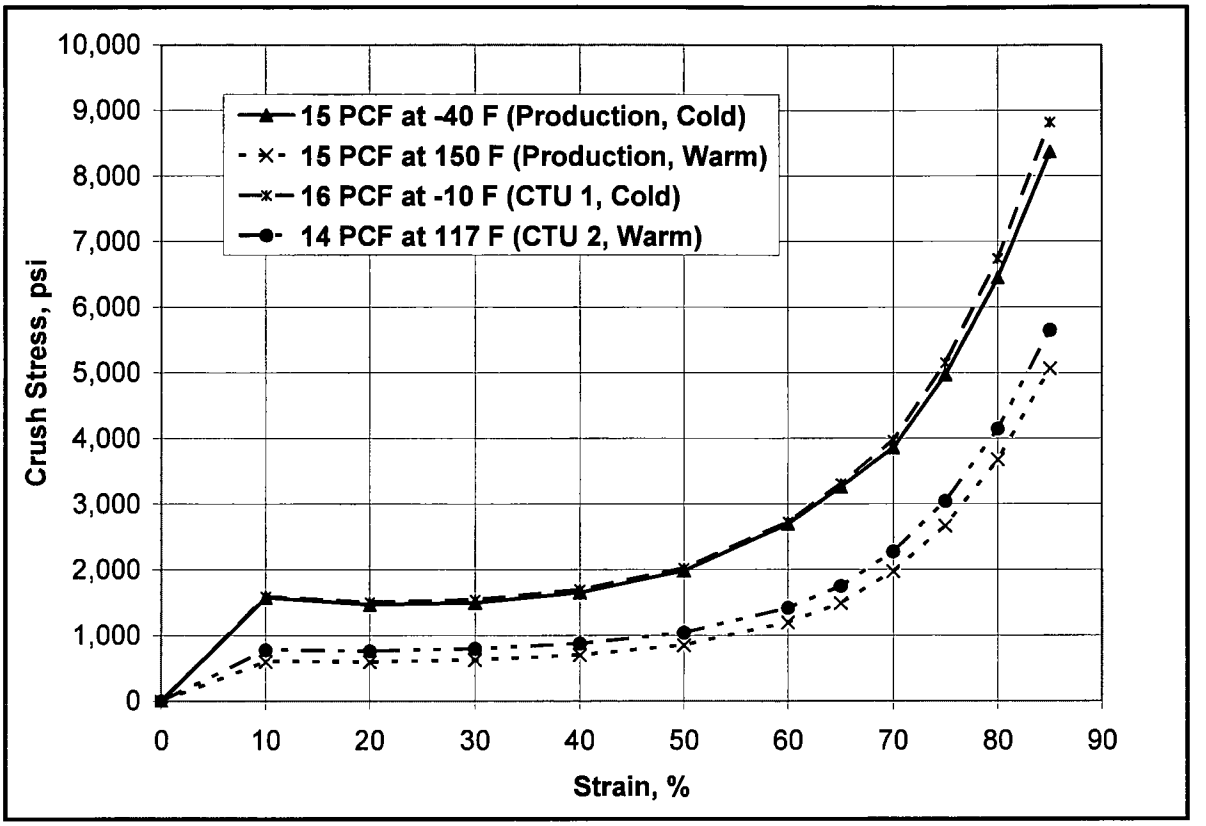

Figure 2.12.4-1 – Polyurethane Foam CTU and Prototypic (Production) Crush Strength Curves

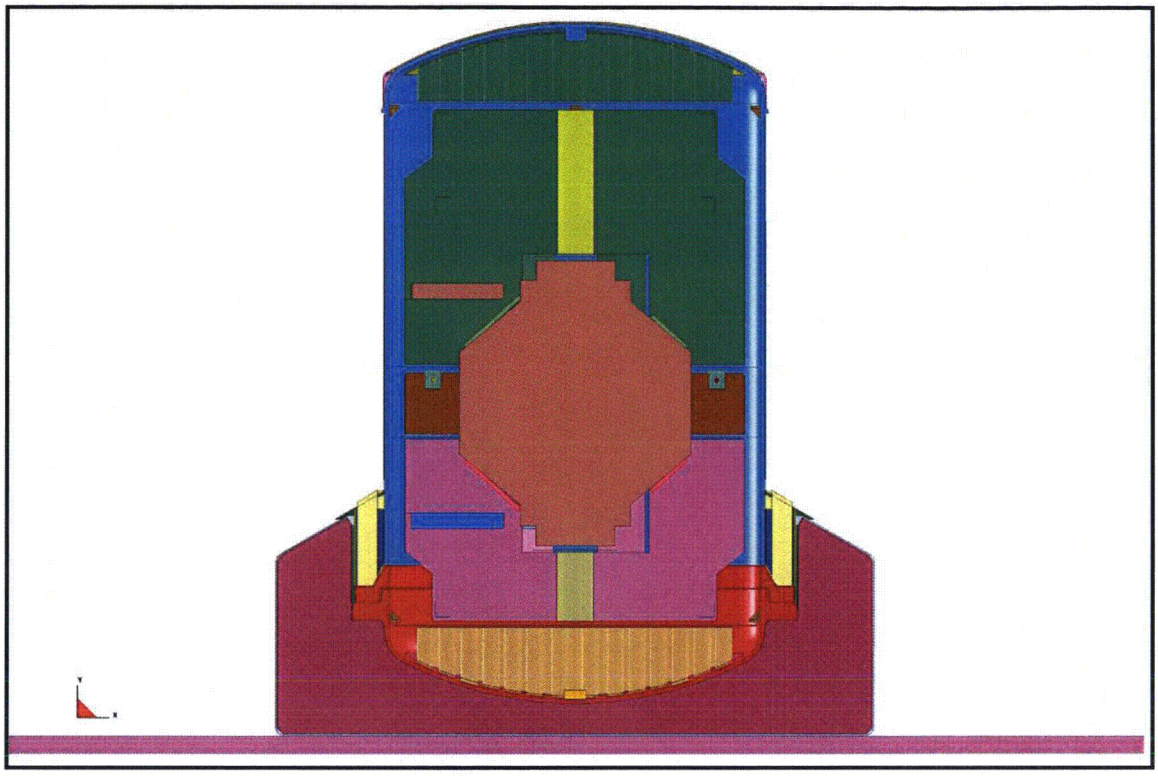

Figure 2.12.4-2 – 435-B FEA Model

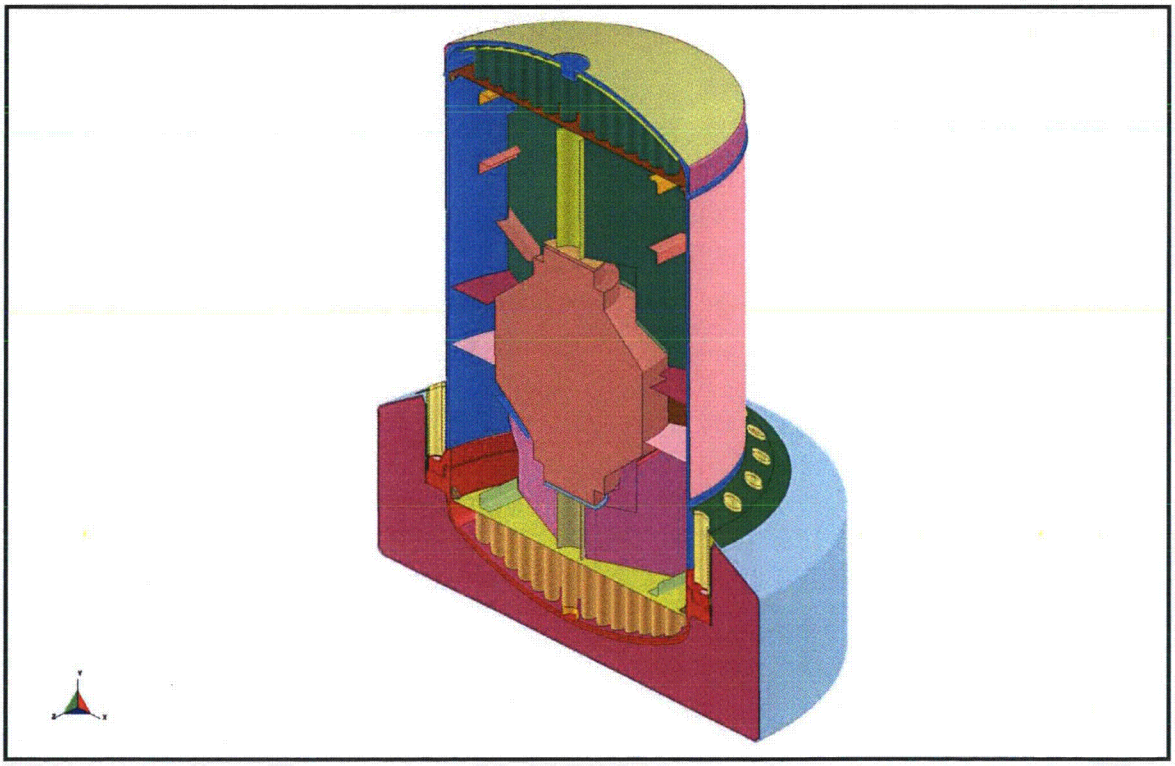

Figure 2.12.4-3 – 435-B FEA Model, Iso-View, Drop Pad Removed

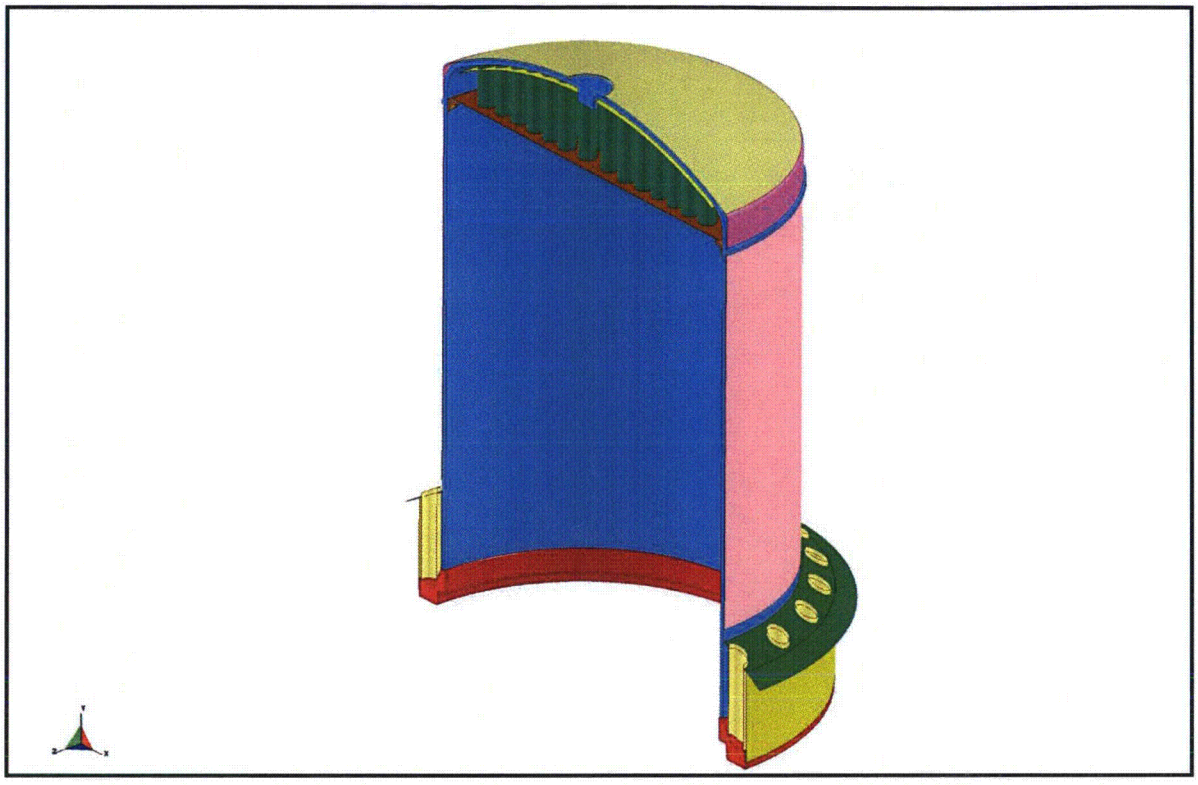

Figure 2.12.4-4 – 435-B FEA Model Bell (Lid)

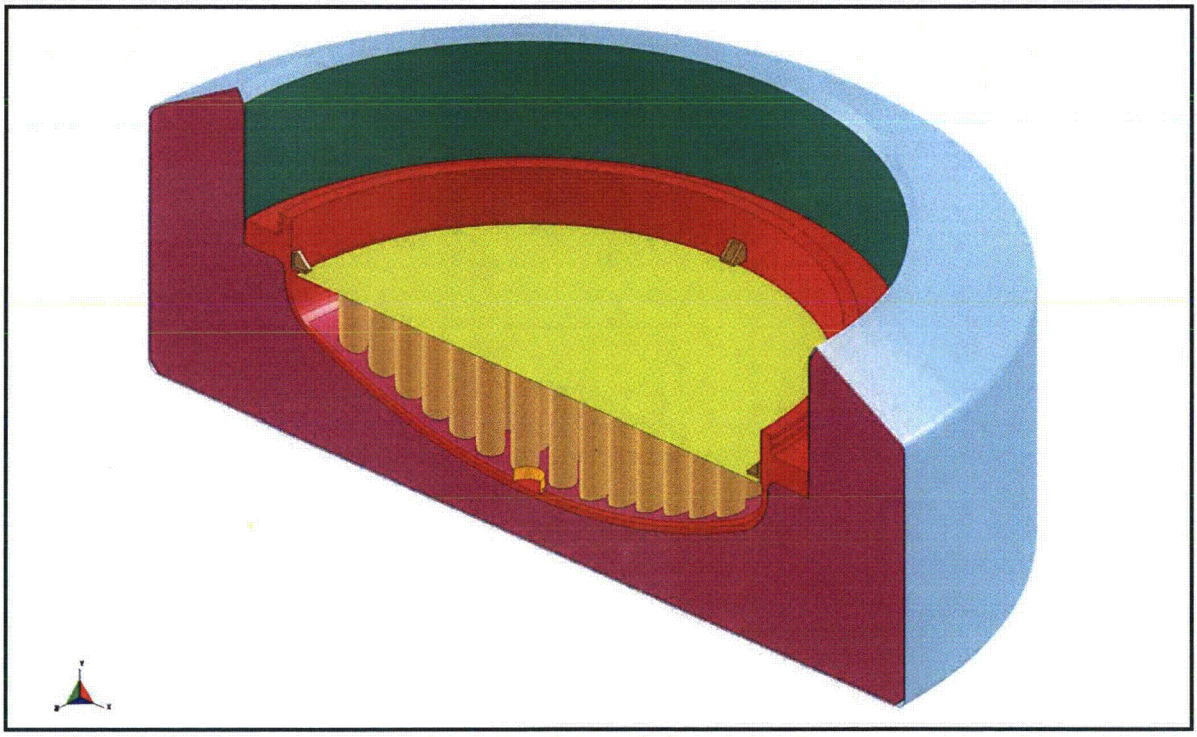

Figure 2.12.4-5 – 435-B FEA Model Base

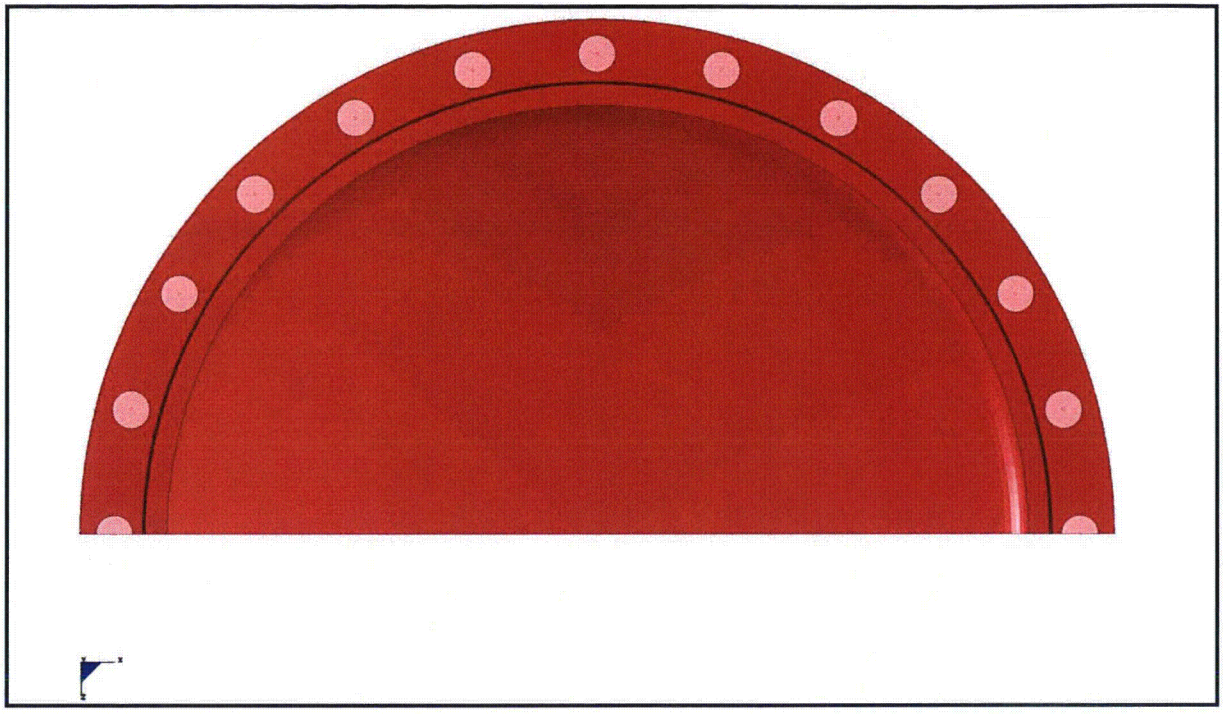

Figure 2.12.4-6 – 435-B FEA Model Closure Bolt Locations

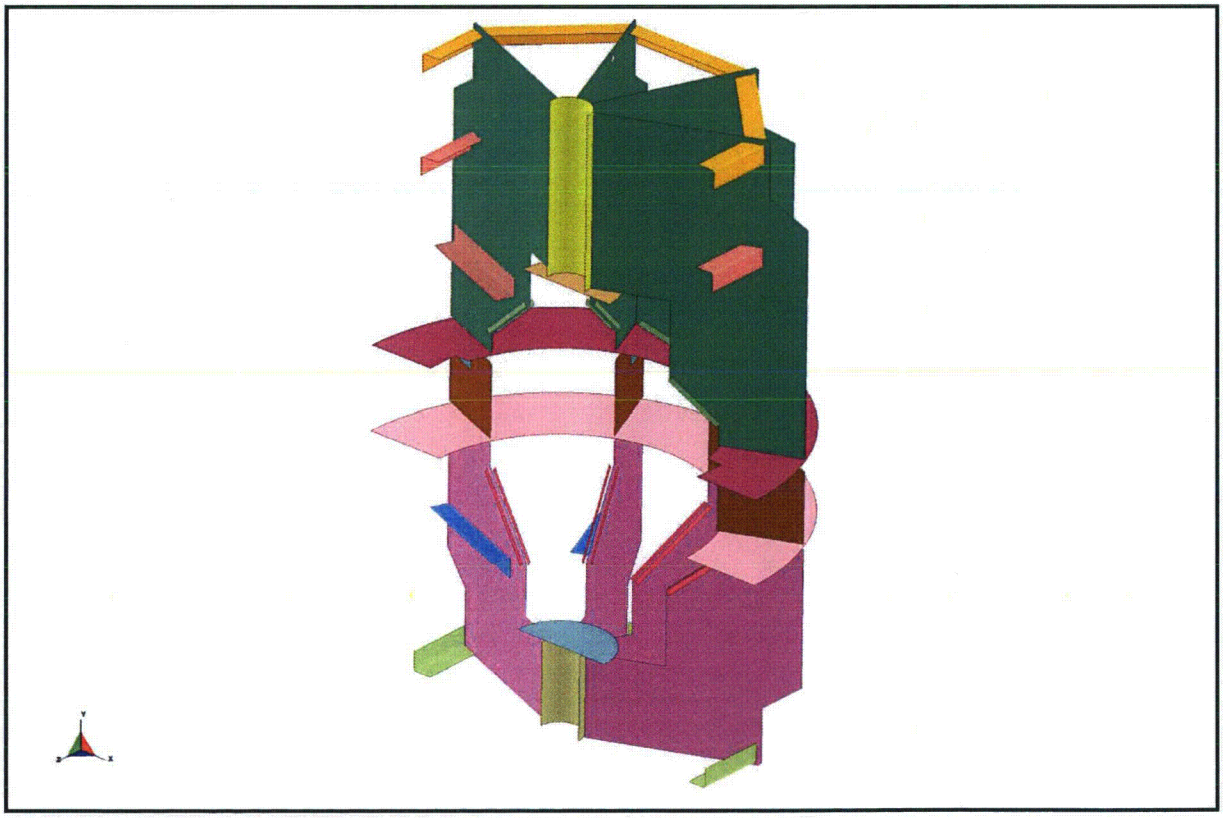

Figure 2.12.4-7 – 435-B FEA Model LTSS Lodgment

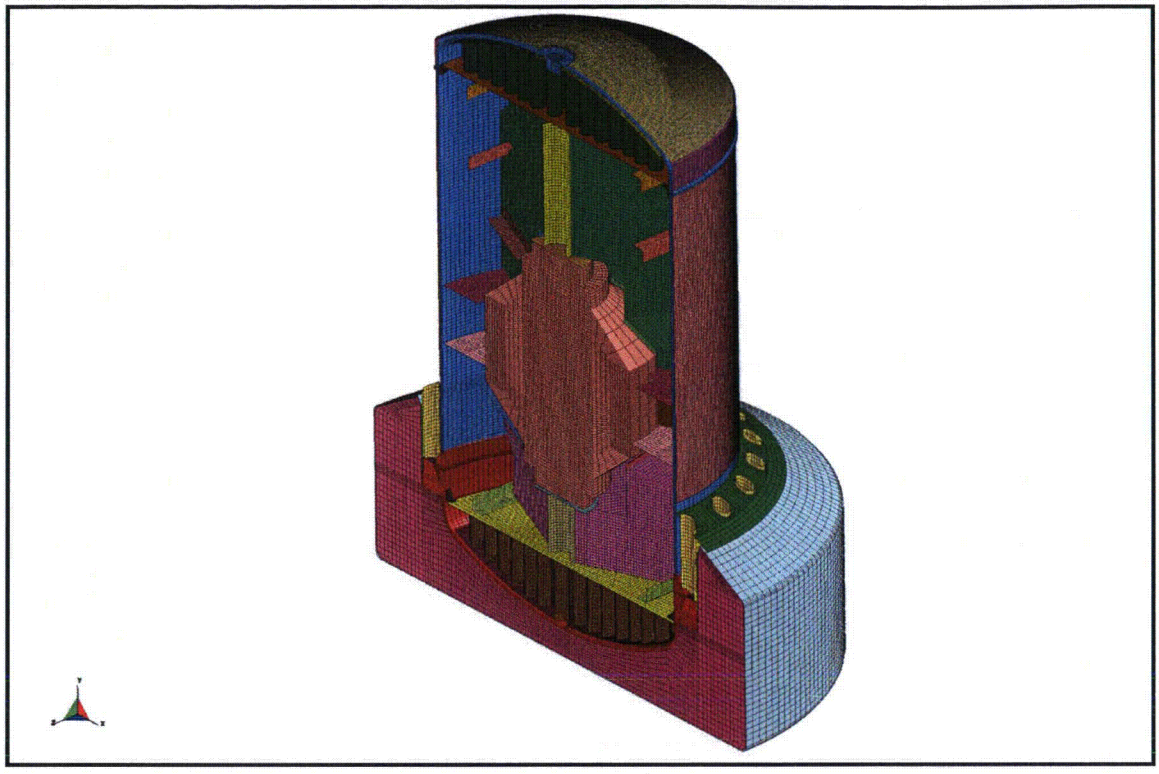

Figure 2.12.4-8 – 435-B FEA Model Mesh, Iso-View, Drop Pad Removed

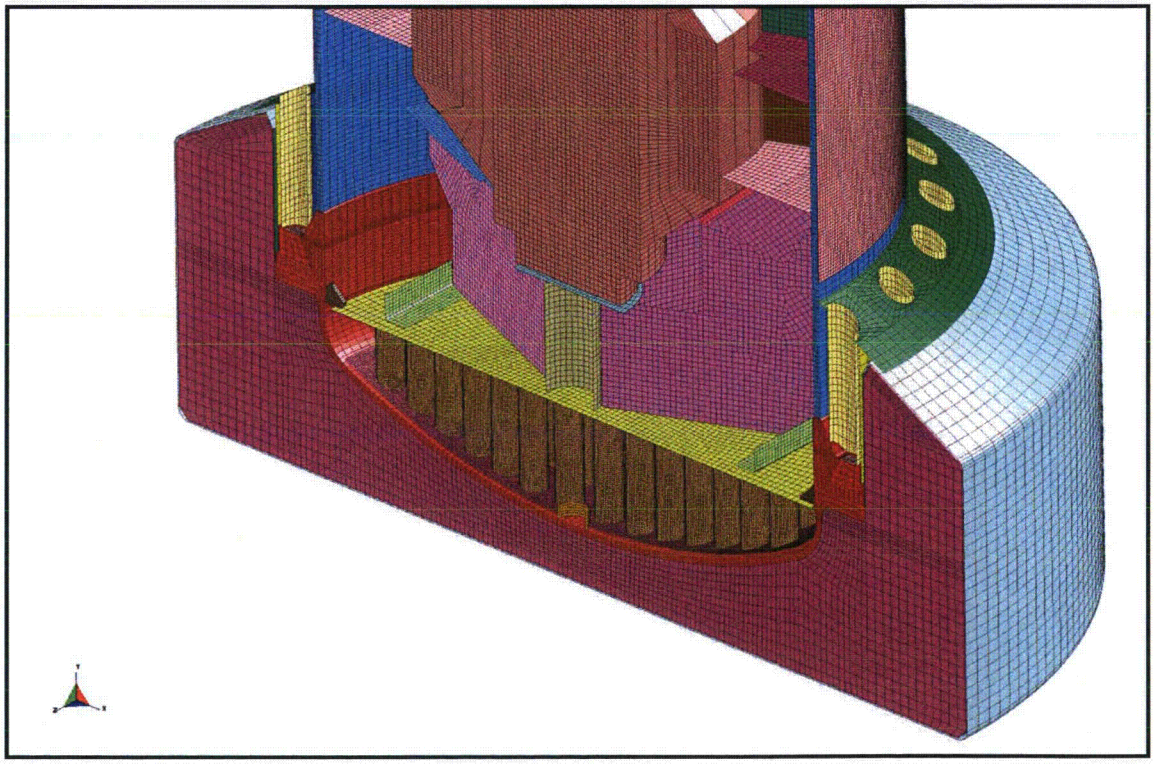

Figure 2.12.4-9 – 435-B FEA Model Mesh, Iso-View, Lower Half

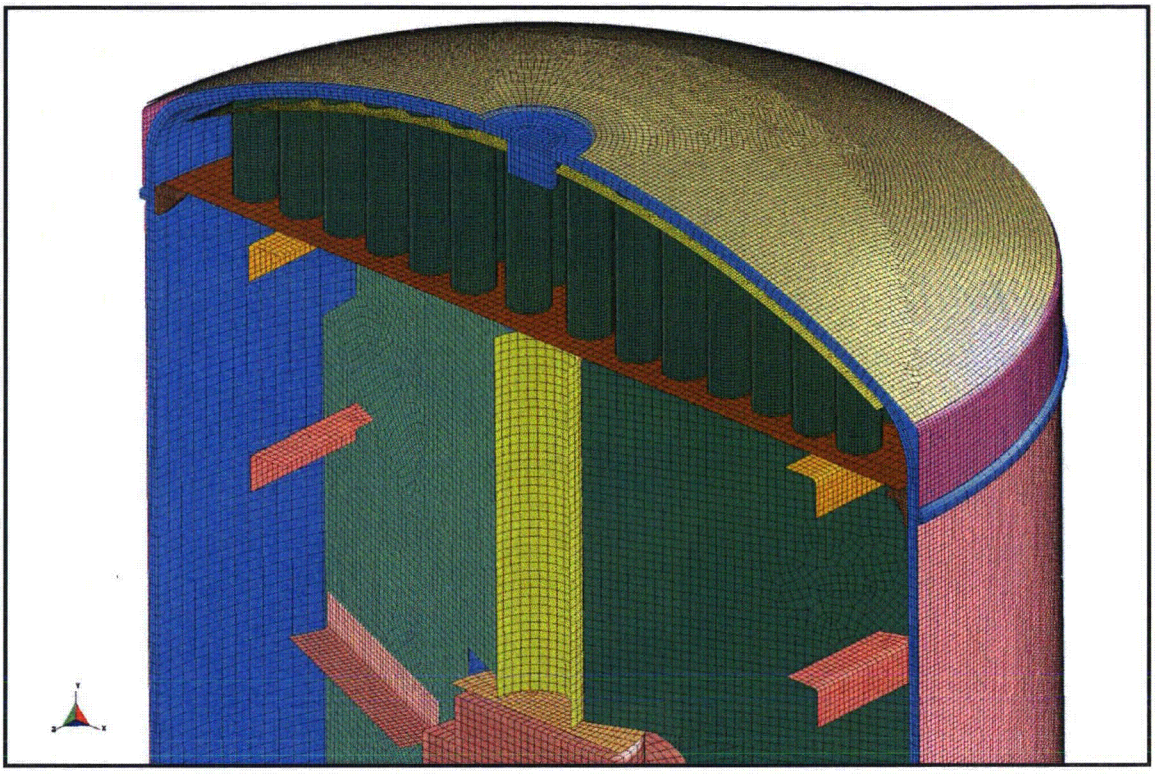

Figure 2.12.4-10 – 435-B FEA Model Mesh, Iso-View, Upper Half

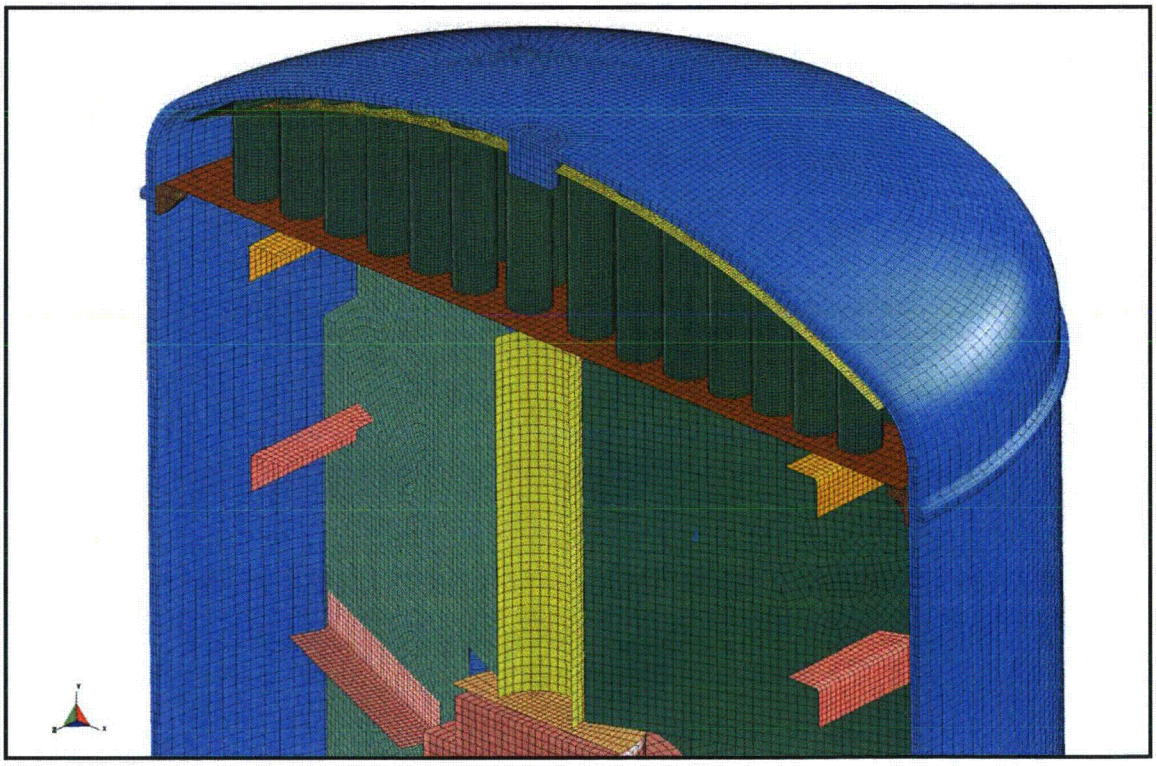

Figure 2.12.4-11 – 435-B FEA Model Mesh, Upper Half, Thermal Shields Removed

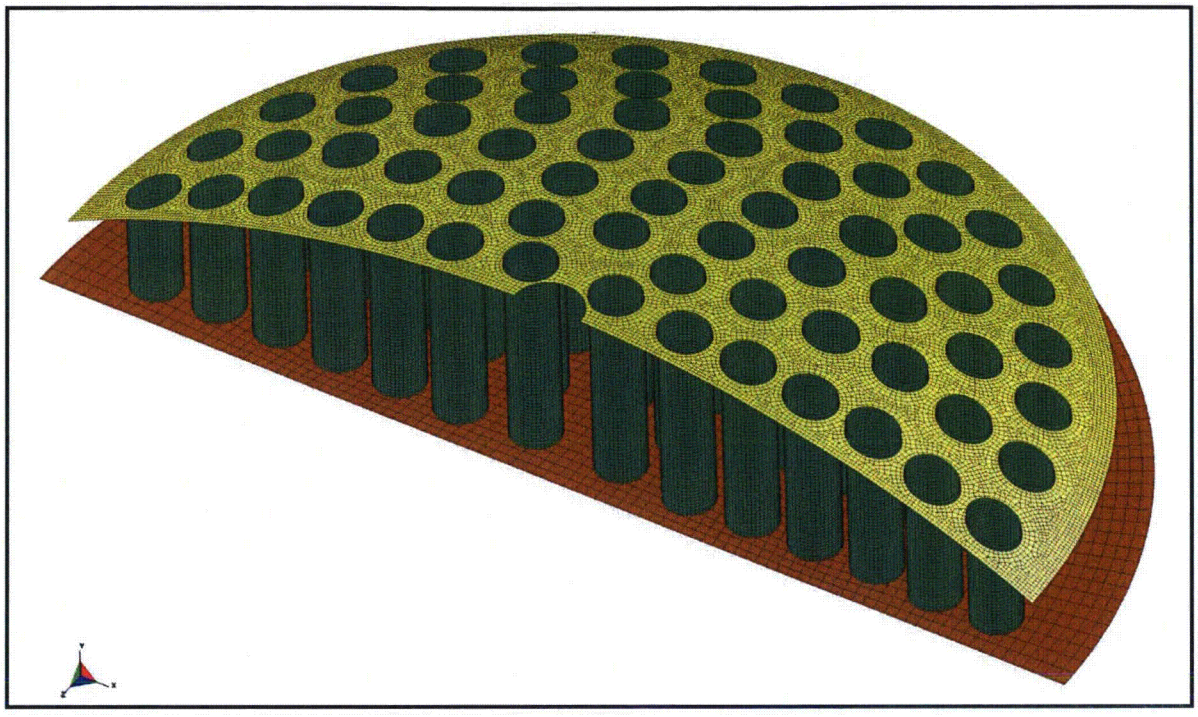

Figure 2.12.4-12 – 435-B FEA Model Mesh, Iso-View, Internal Impact Limiter

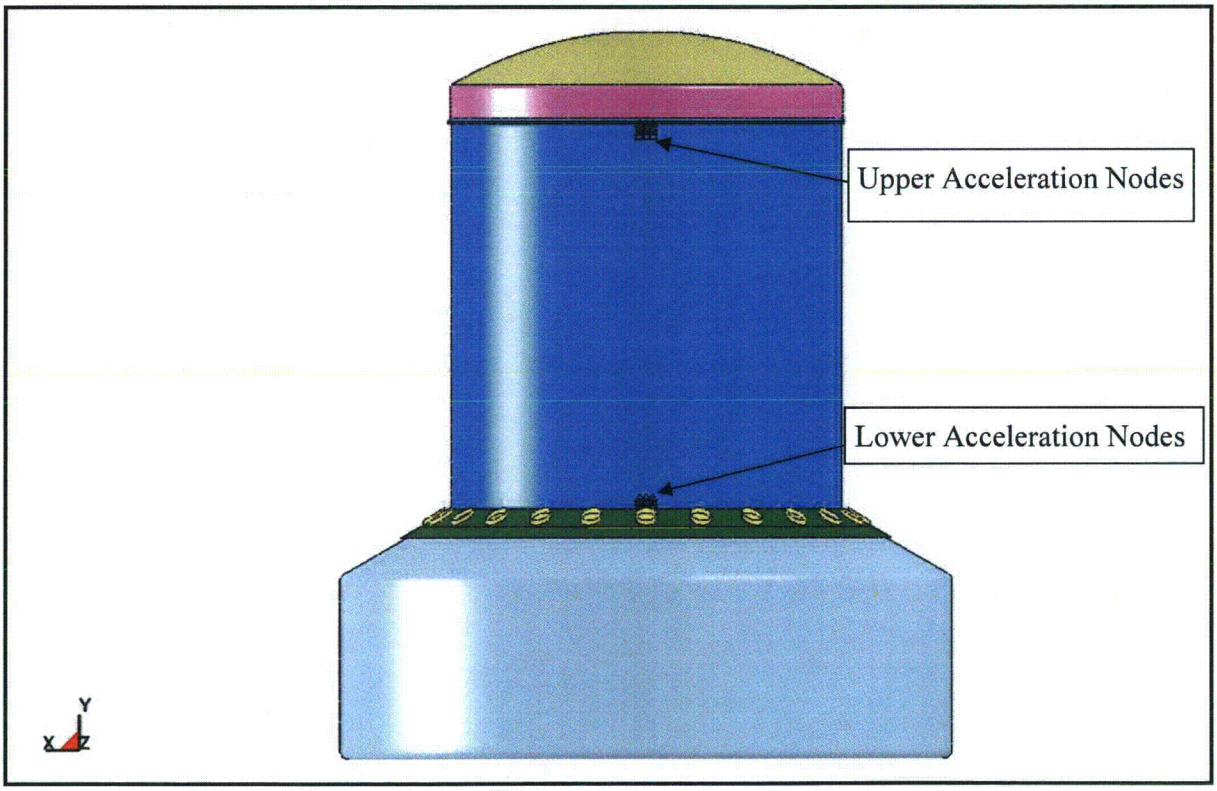

Figure 2.12.4-13 – FEA Model Nodes Equivalent to CTU Accelerometer Blocks

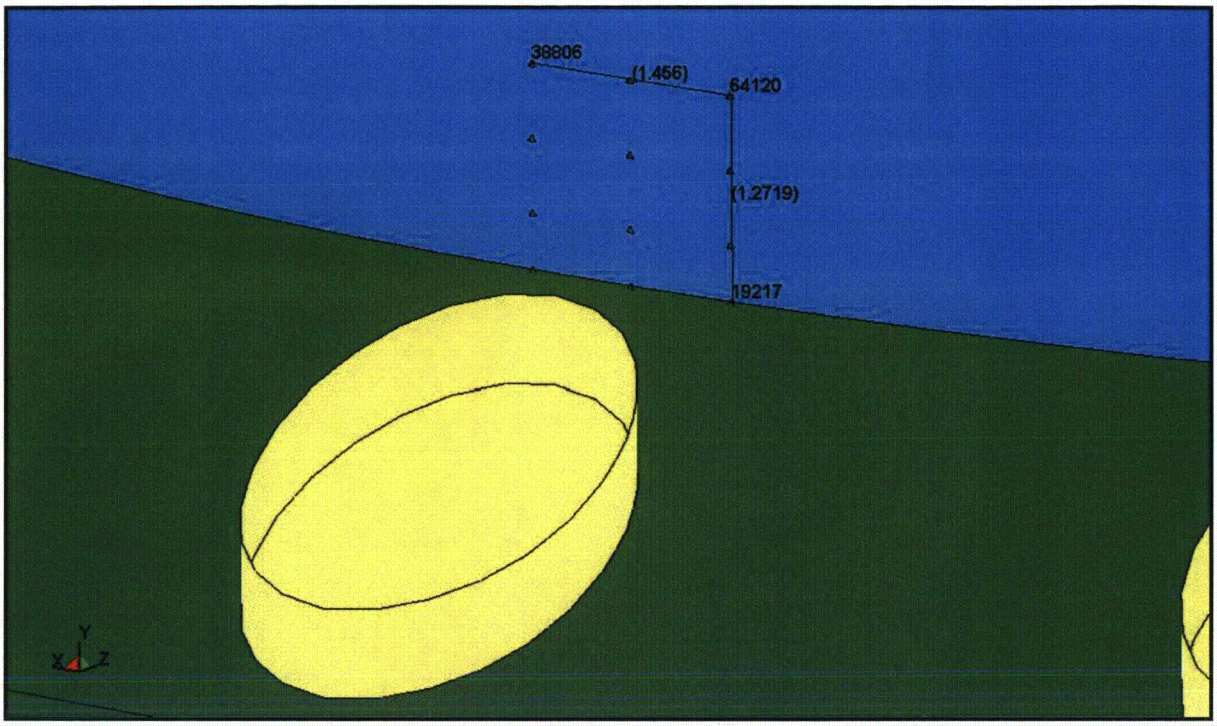

Figure 2.12.4-14 – FEA Model Nodes Equivalent to CTU Accelerometer Blocks (Lower)

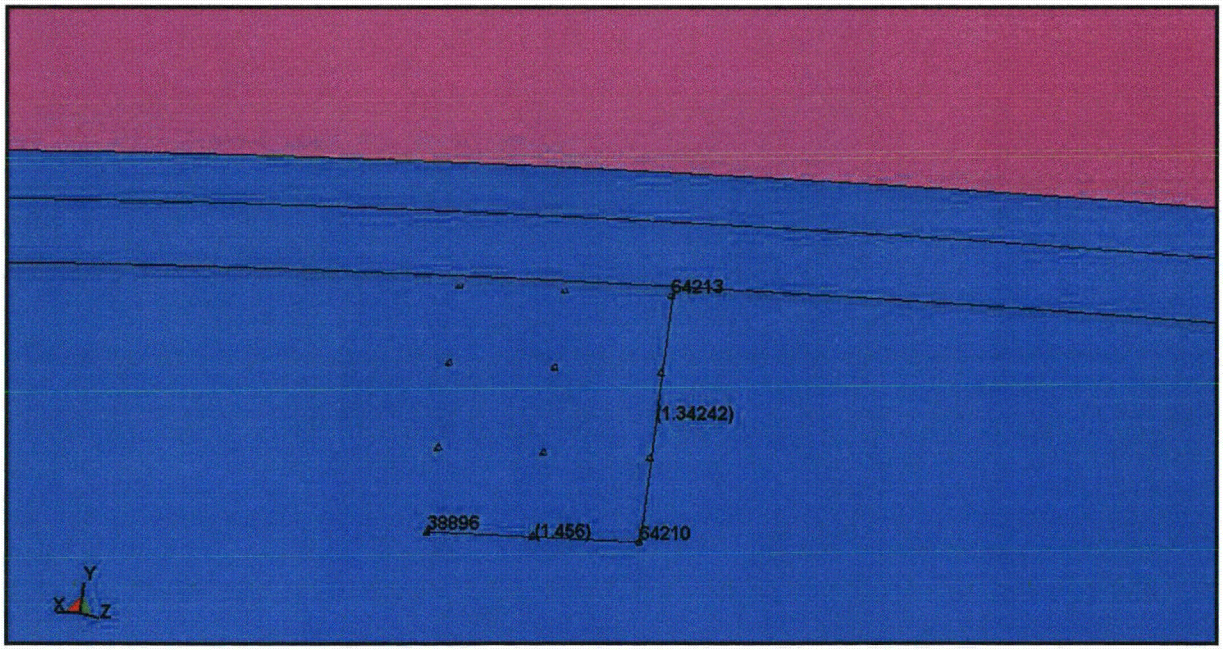

Figure 2.12.4-15 – FEA Model Nodes Equivalent to CTU Accelerometer Blocks (Upper)

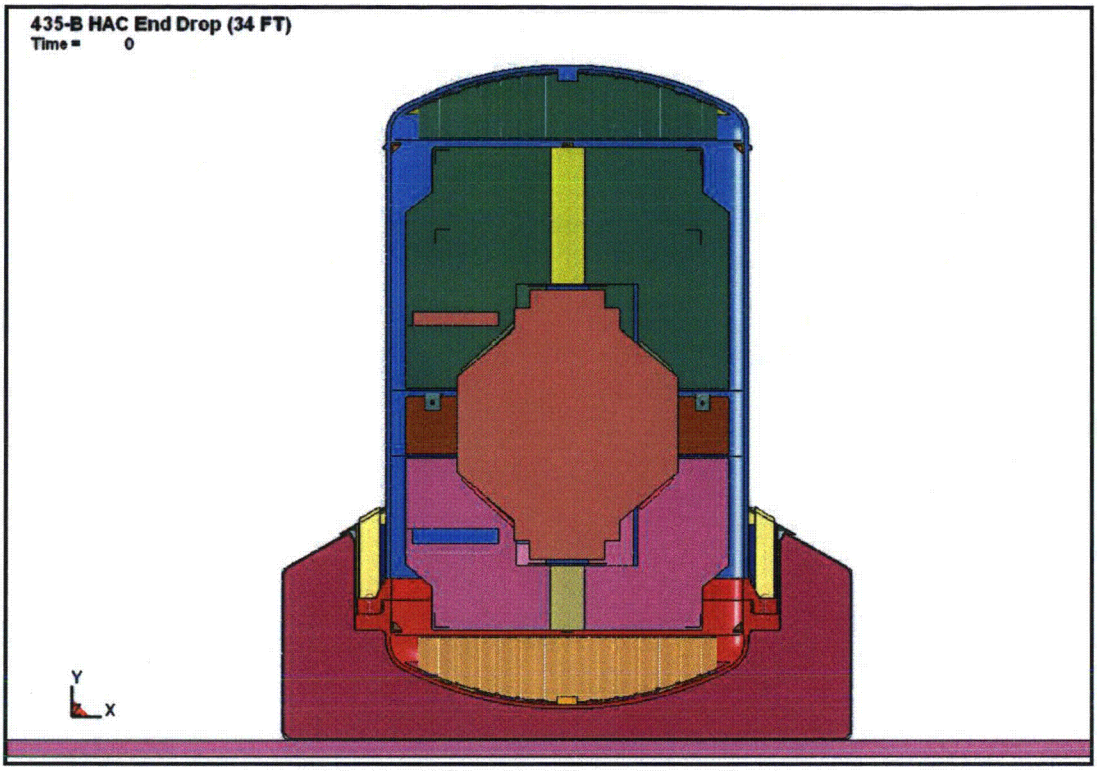

Figure 2.12.4-16 – D1 Benchmark Initial State

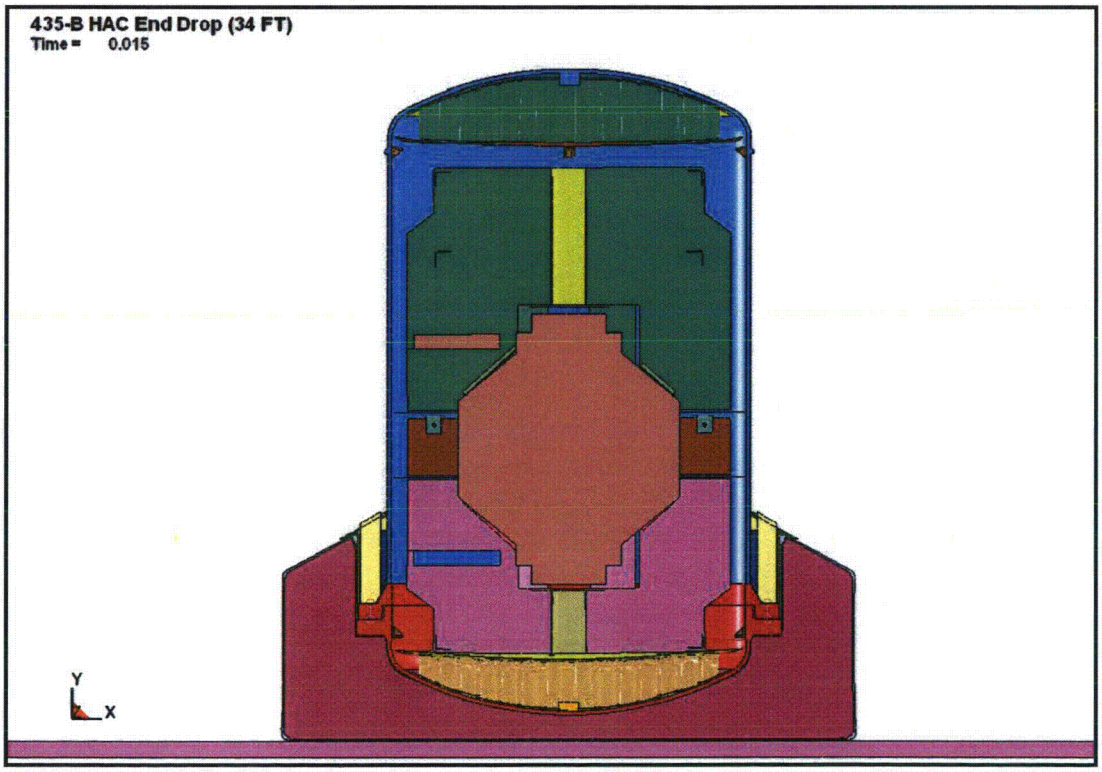

Figure 2.12.4-17 – D1 Benchmark Final State

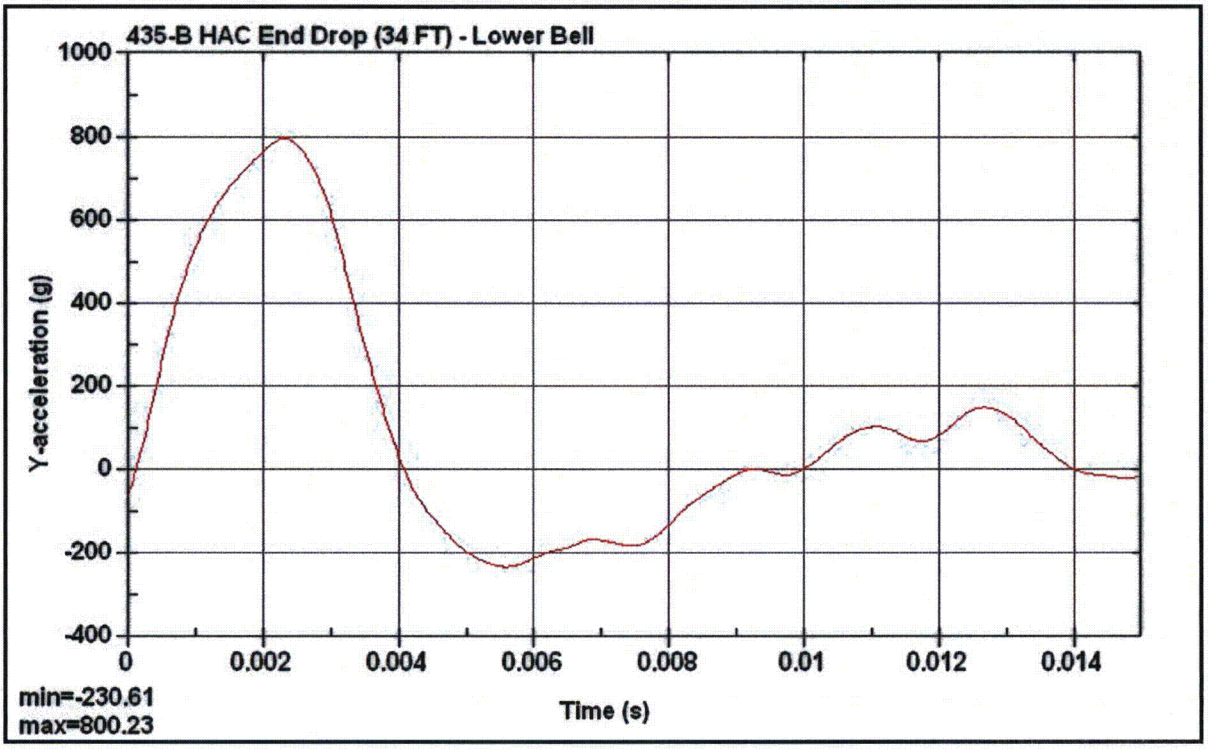

Figure 2.12.4-18 – D1 Benchmark Lower Bell Acceleration

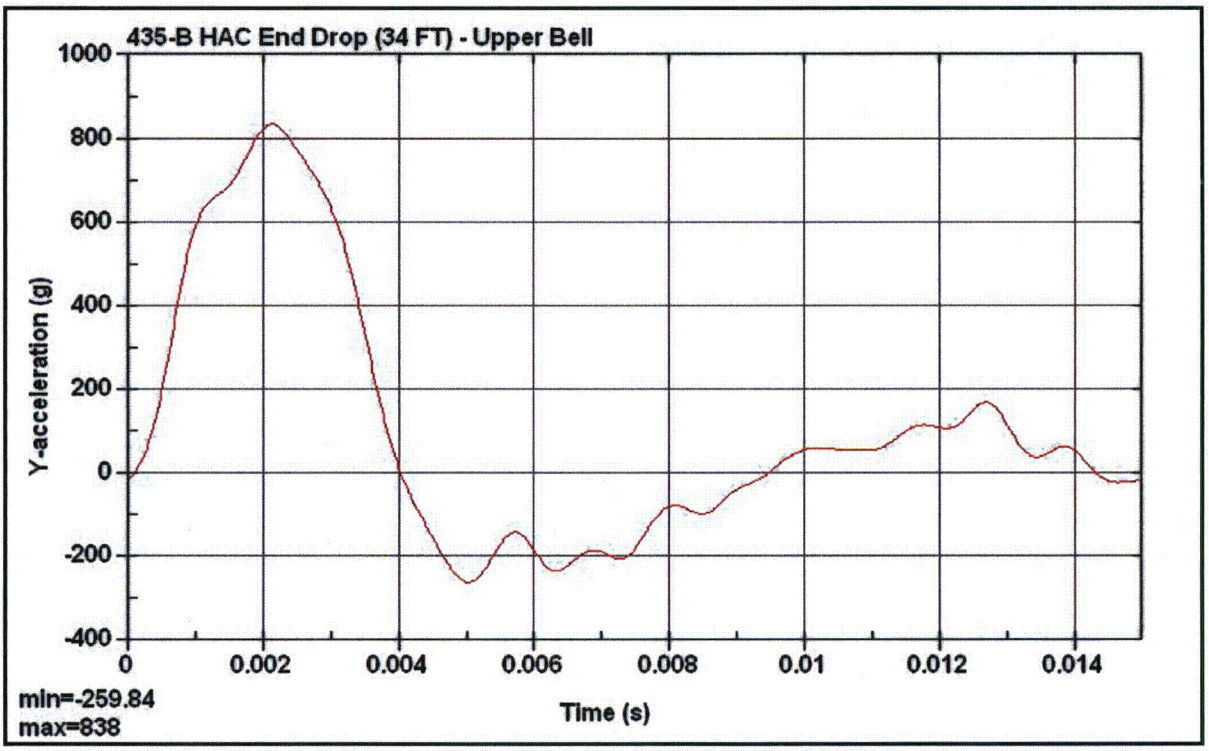

Figure 2.12.4-19 – D1 Benchmark Upper Bell Acceleration

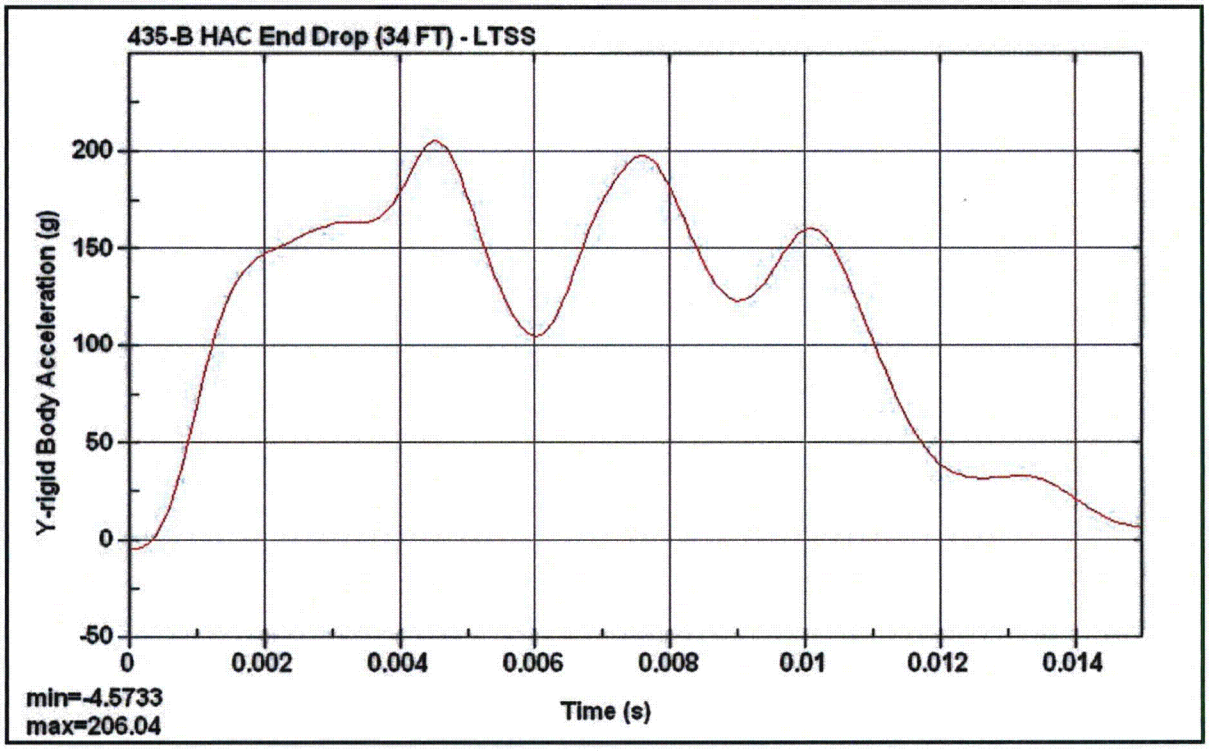

Figure 2.12.4-20 – D1 Benchmark LTSS Acceleration

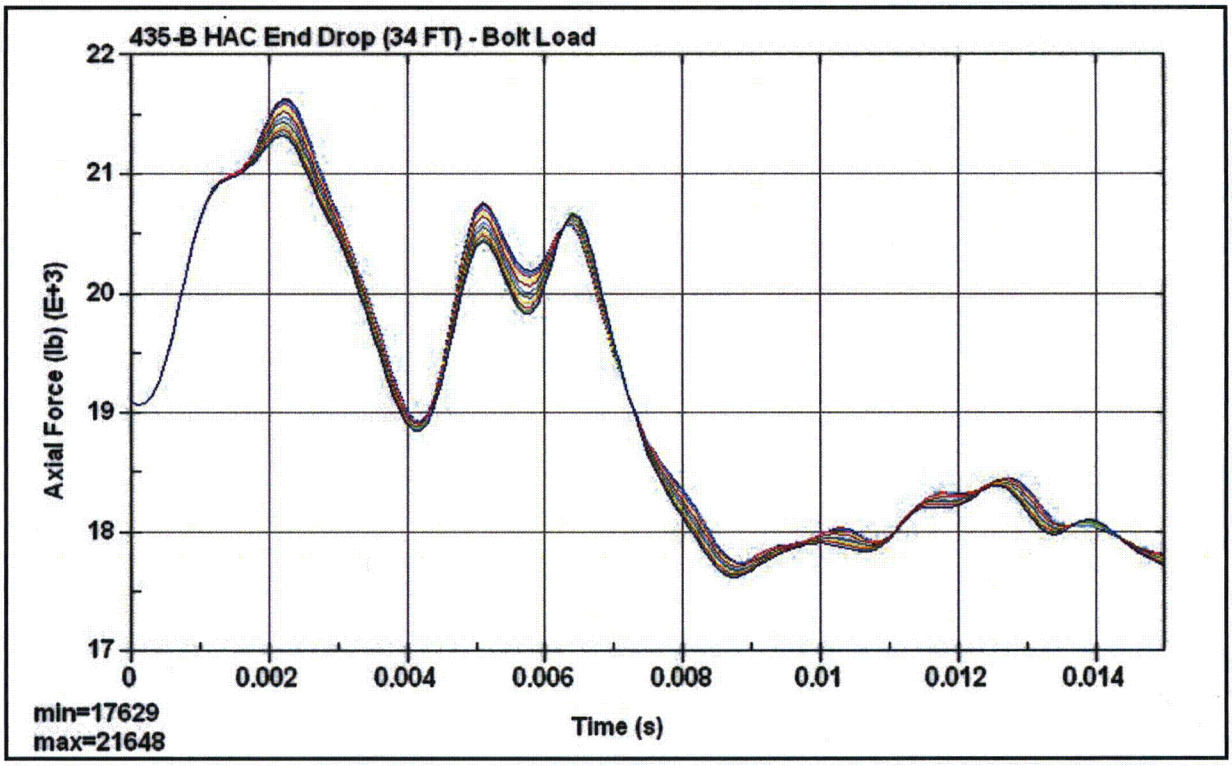

Figure 2.12.4-21 – D1 Benchmark Axial Bolt Force

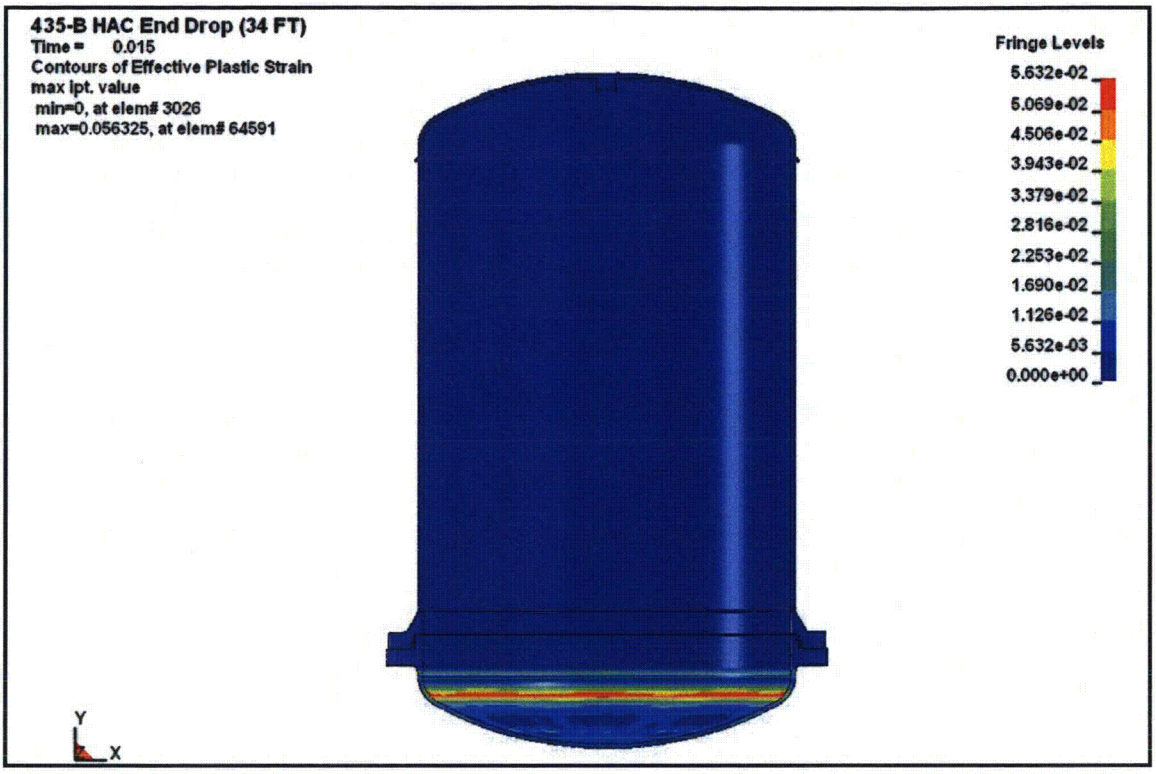

Figure 2.12.4-22 – D1 Benchmark Containment Boundary Cumulative Effective Plastic Strain

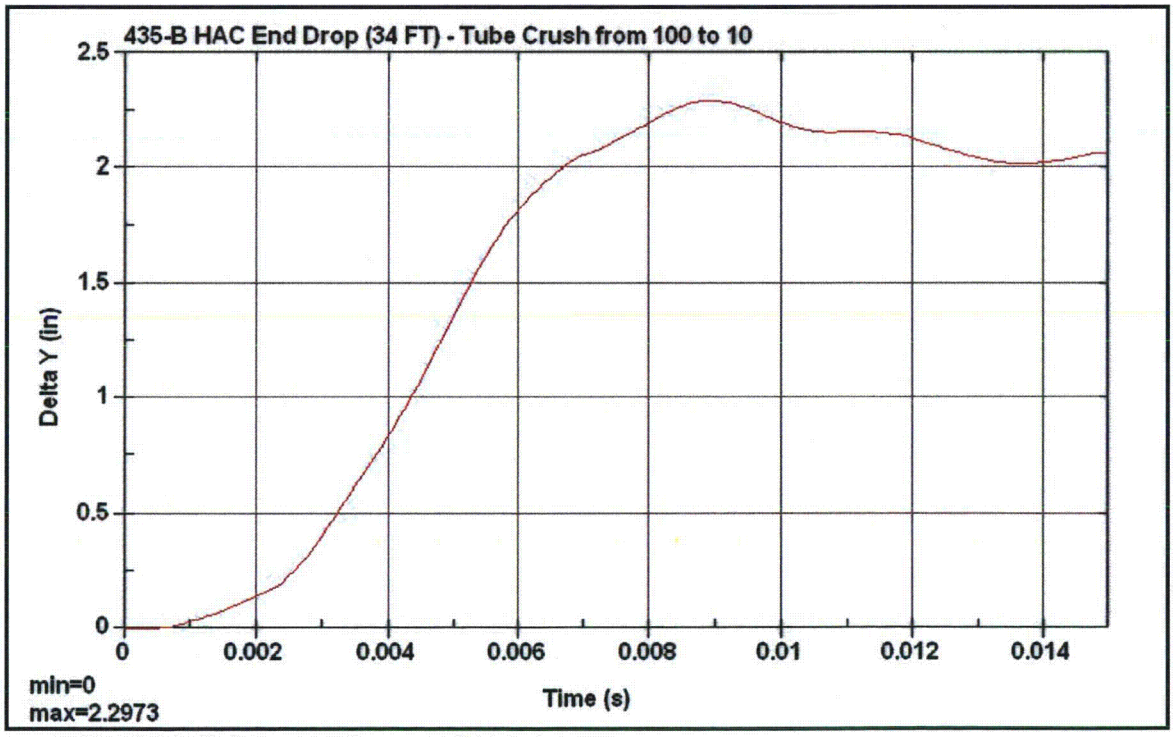

Figure 2.12.4-23 – D1 Benchmark Tube Crush from Lodgment (Part 100) to the Clips (Part 10)

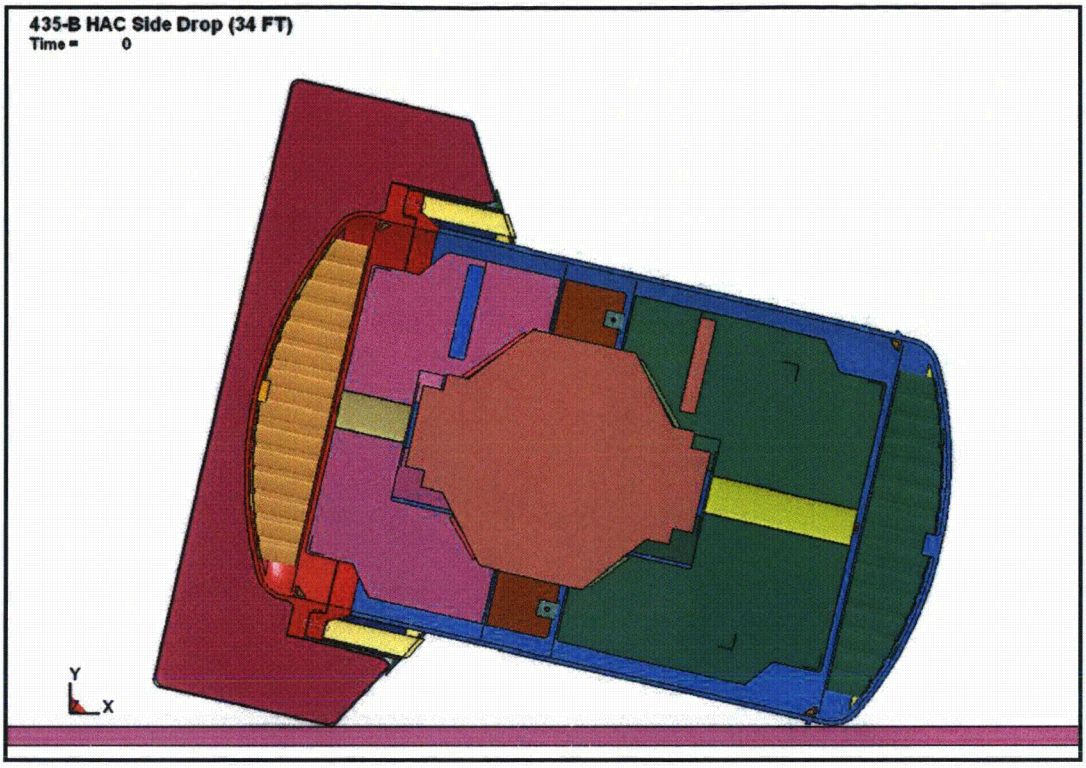

Figure 2.12.4-24 – D2 Benchmark Initial State

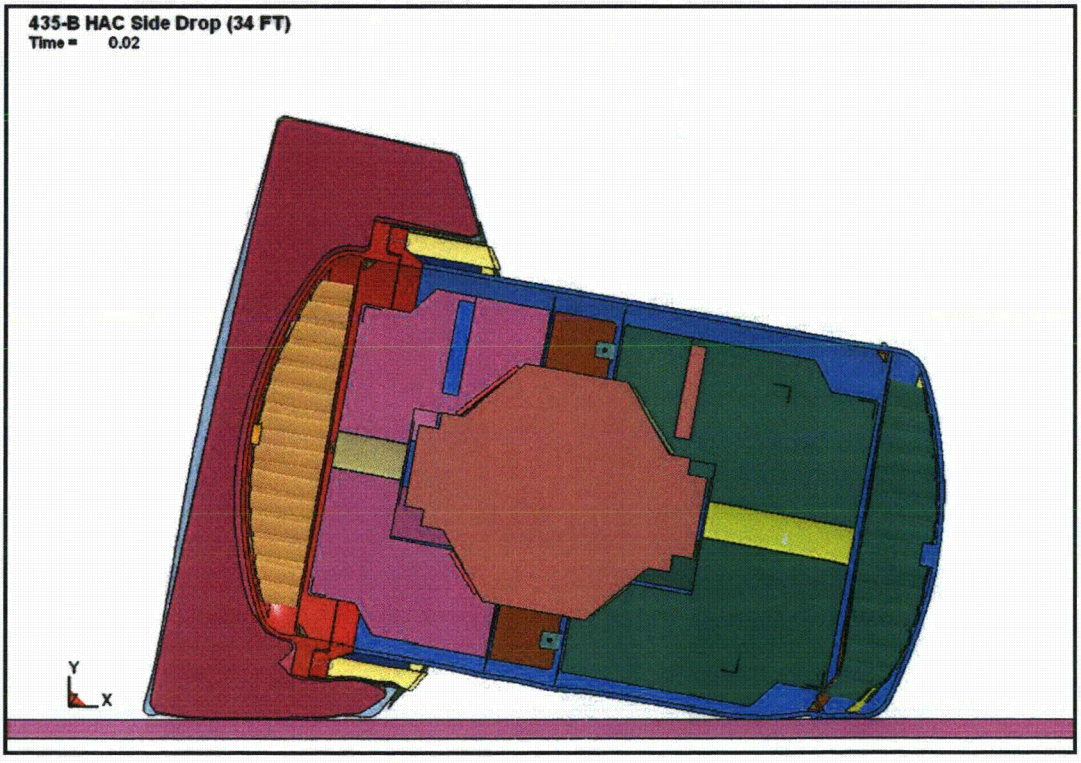

Figure 2.12.4-25 – D2 Benchmark Final State

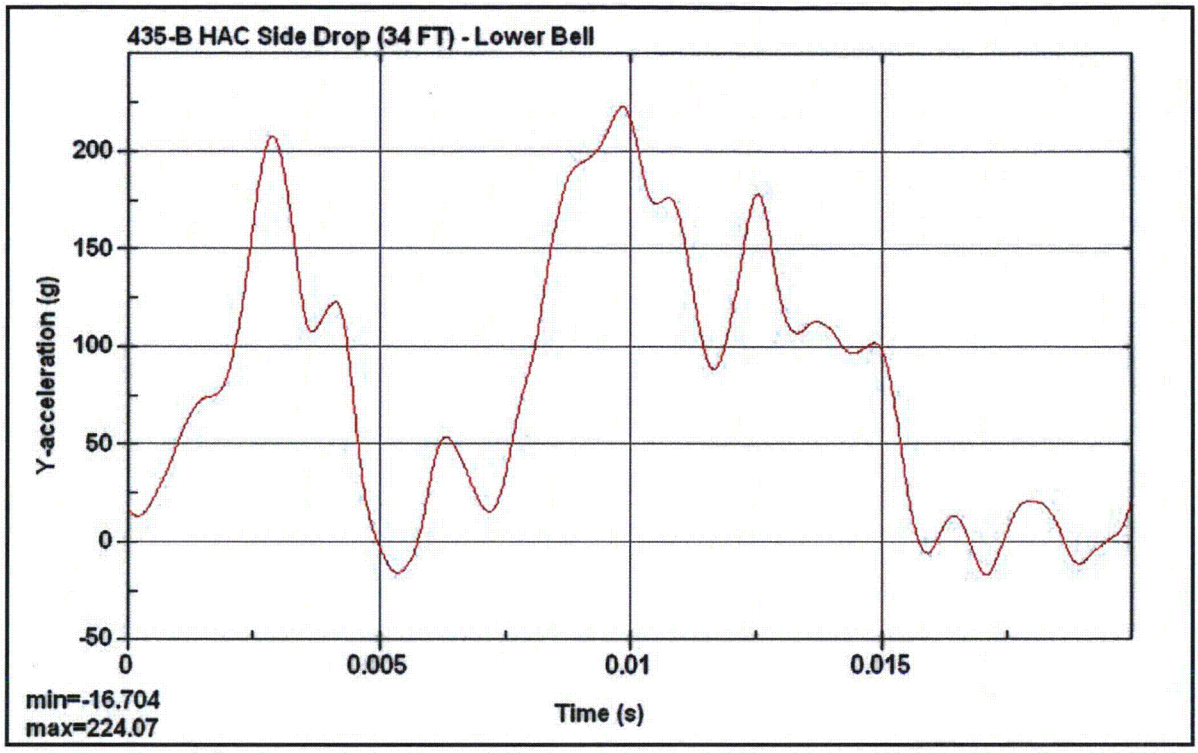

Figure 2.12.4-26 – D2 Benchmark Lower Bell Acceleration

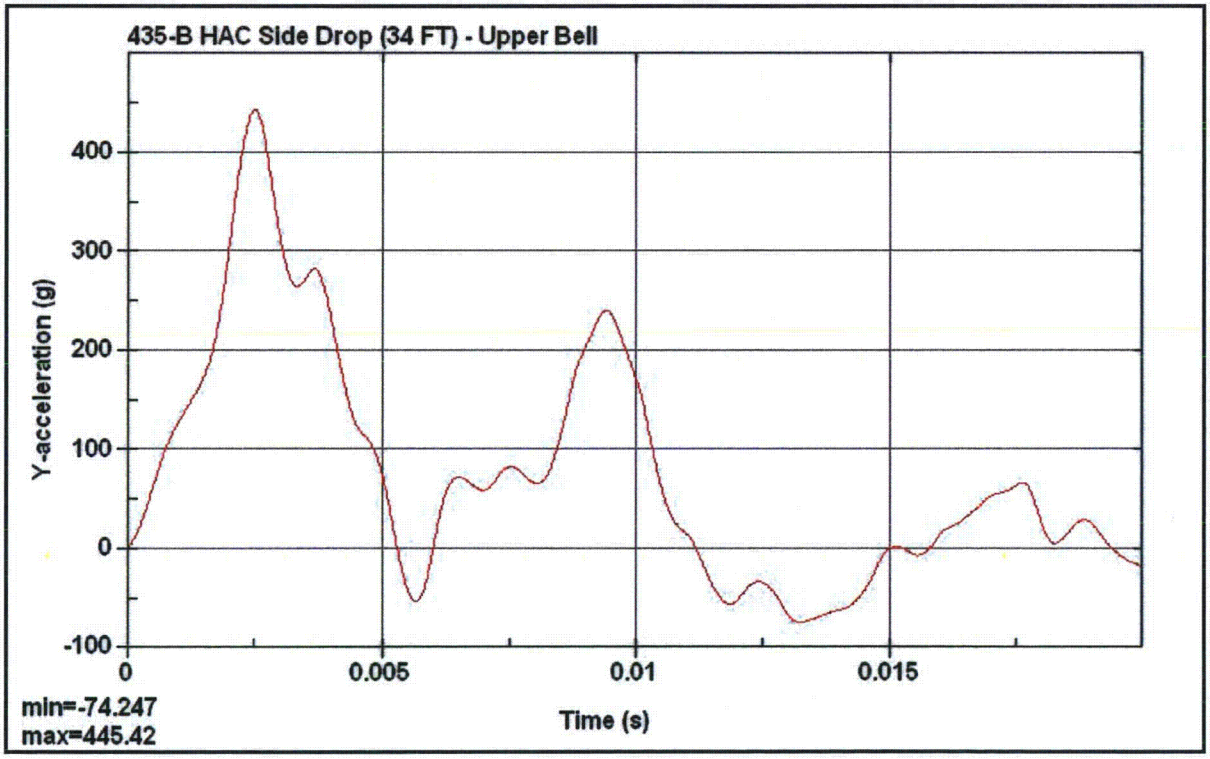

Figure 2.12.4-27 – D2 Benchmark Upper Bell Acceleration

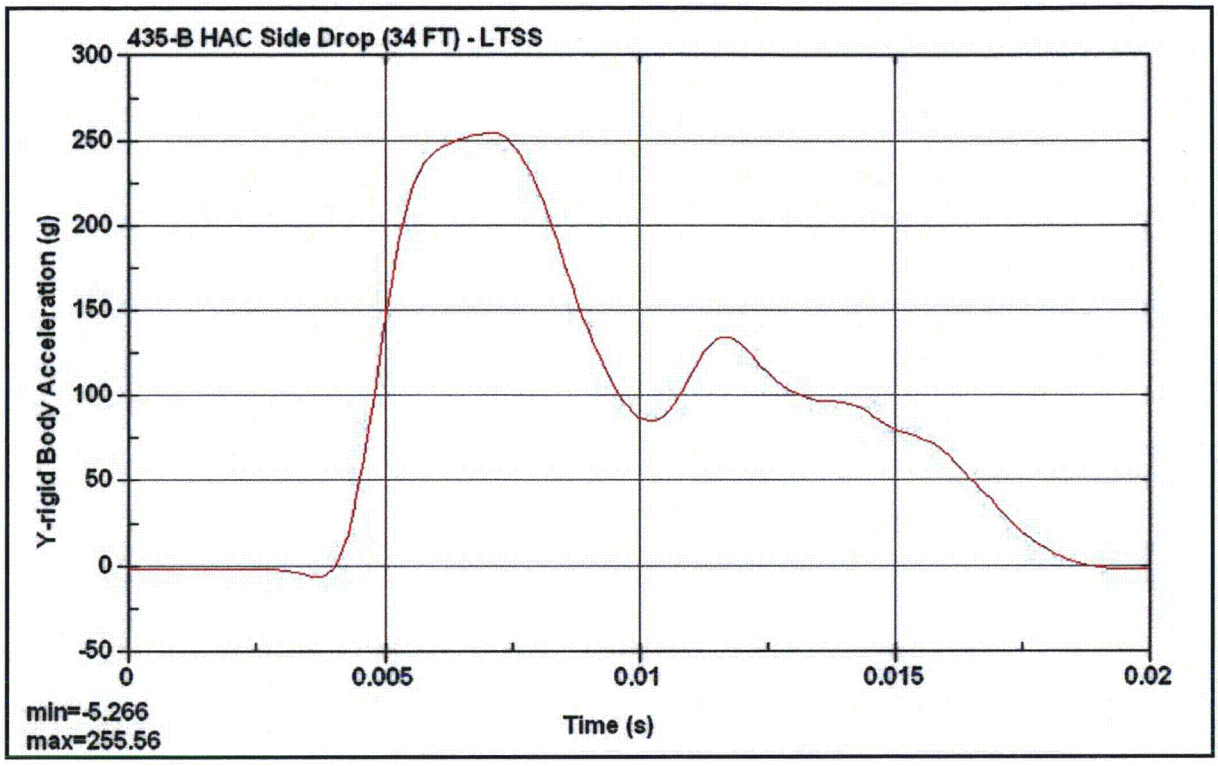

Figure 2.12.4-28 – D2 Benchmark LTSS Acceleration

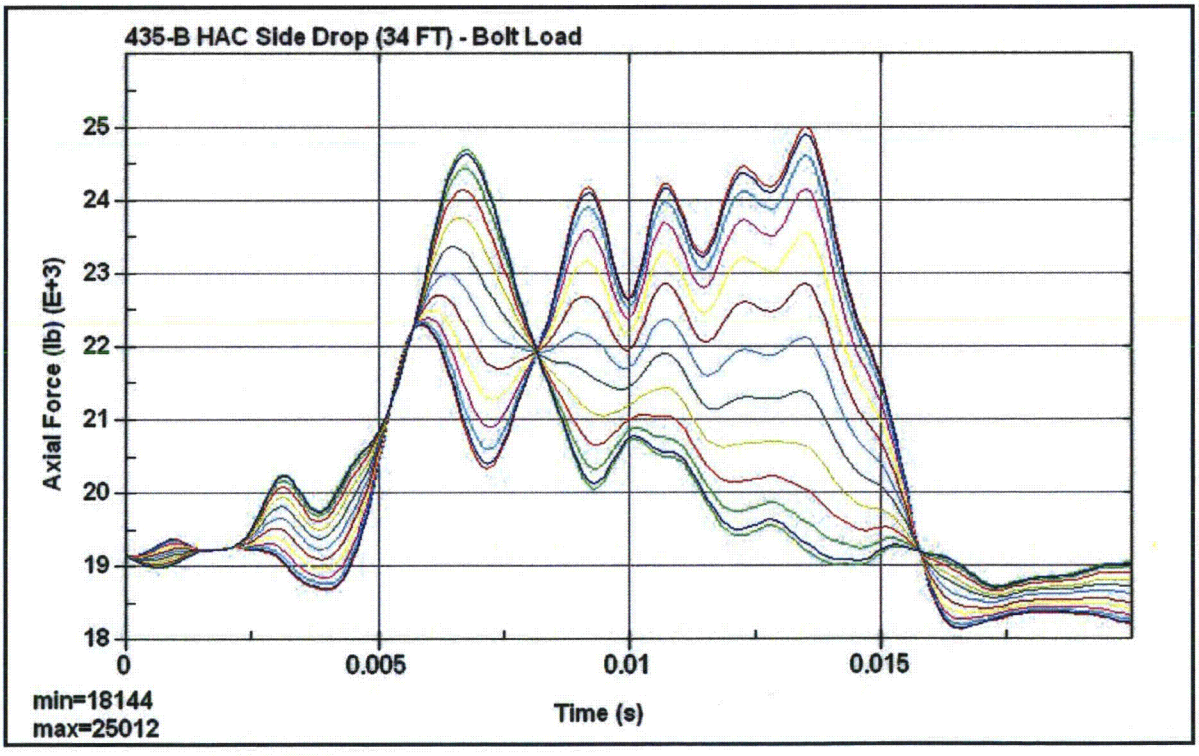

Figure 2.12.4-29 – D2 Benchmark Axial Bolt Force

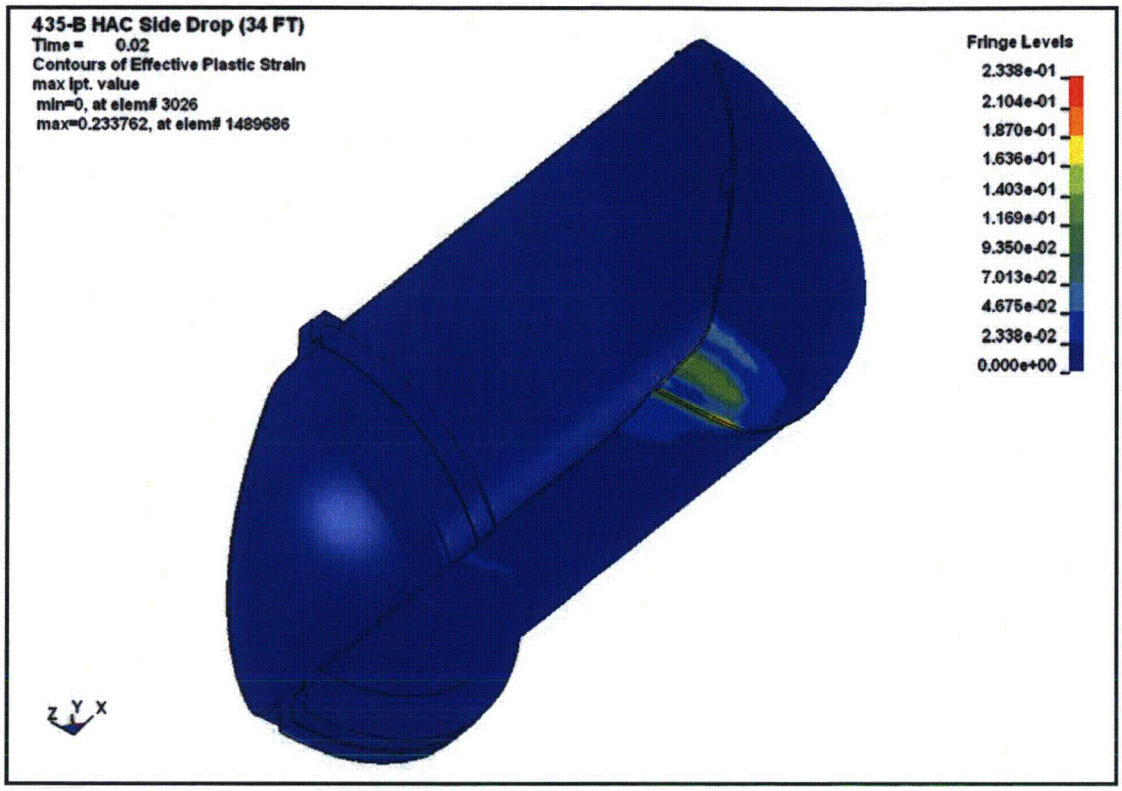

Figure 2.12.4-30 – D2 Benchmark Containment Boundary Cumulative Effective Plastic Strain

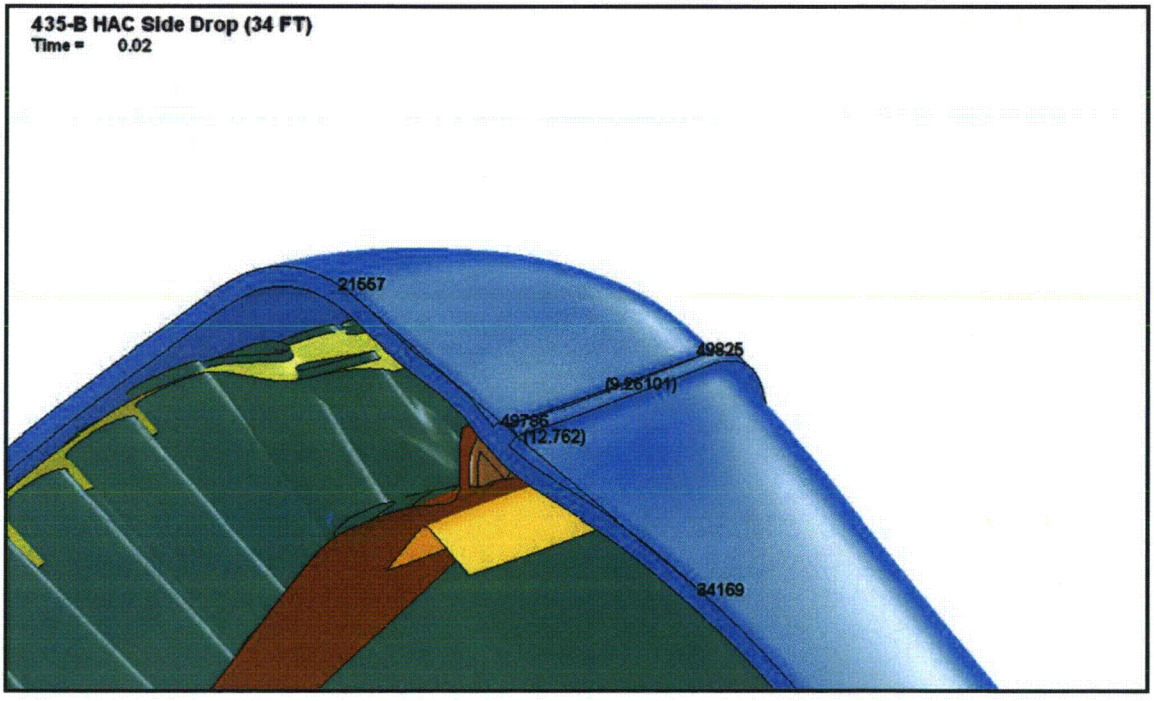

Figure 2.12.4-31 – D2 Benchmark Upper Impact Patch

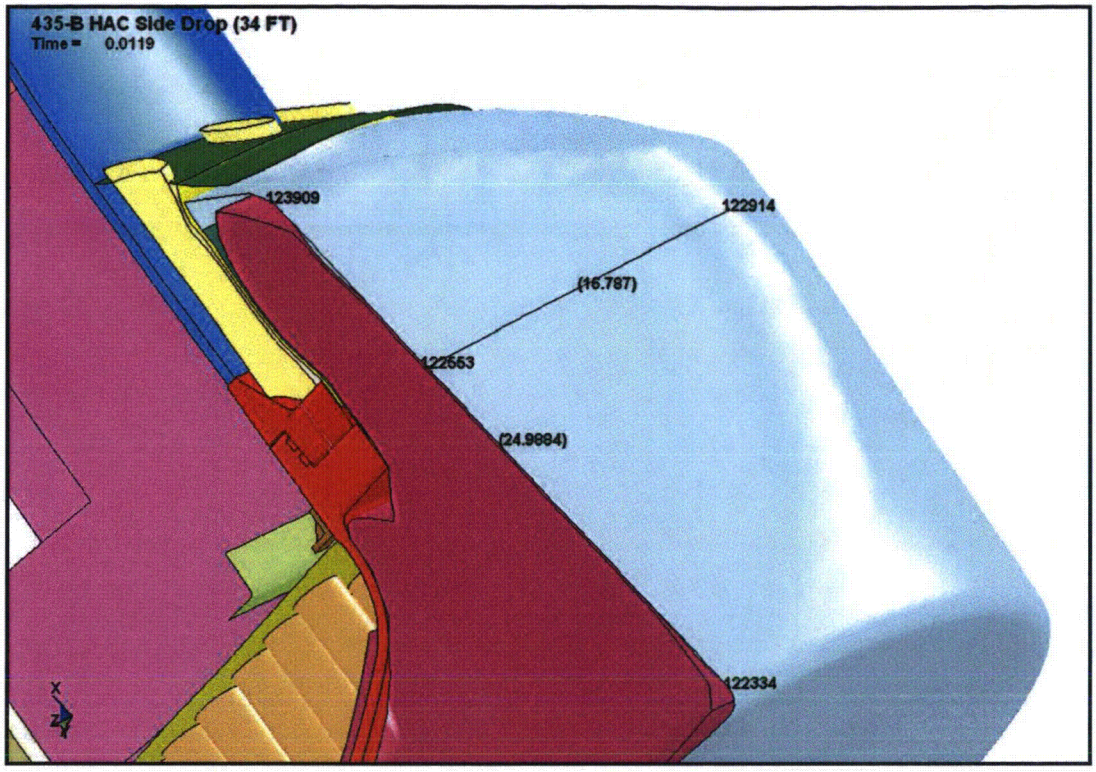

Figure 2.12.4-32 – D2 Benchmark Lower Impact Patch

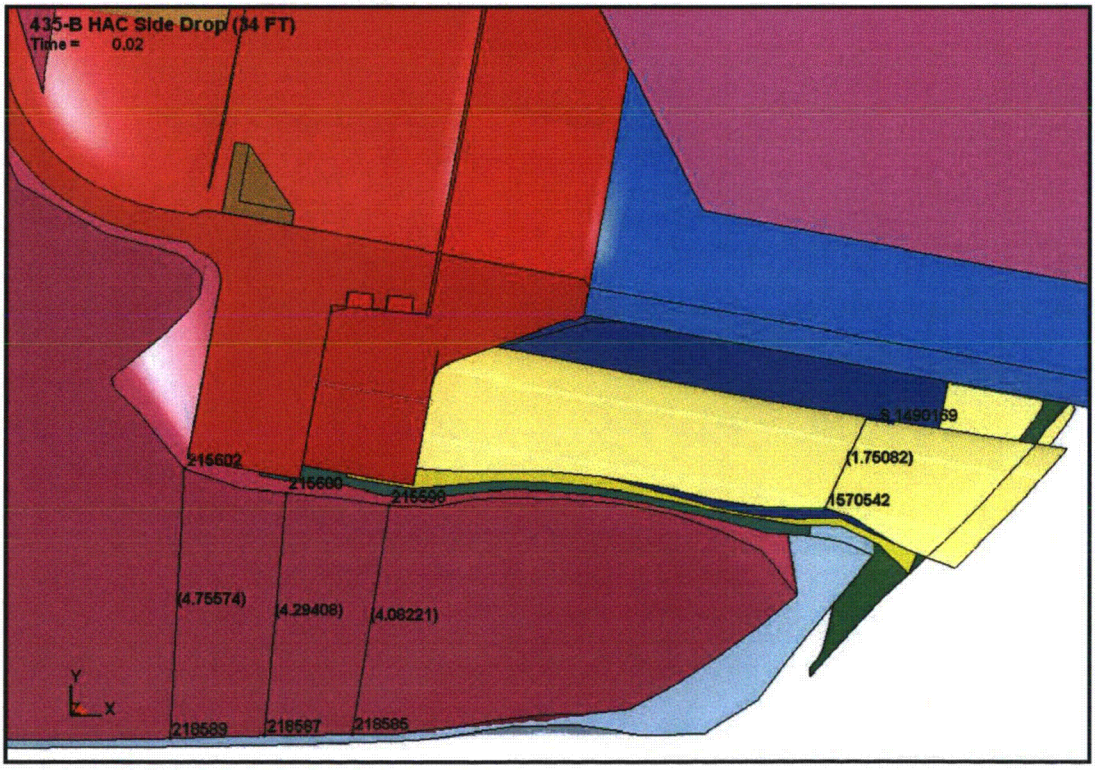

Figure 2.12.4-33 – D2 Benchmark Minimum Foam Near Seal

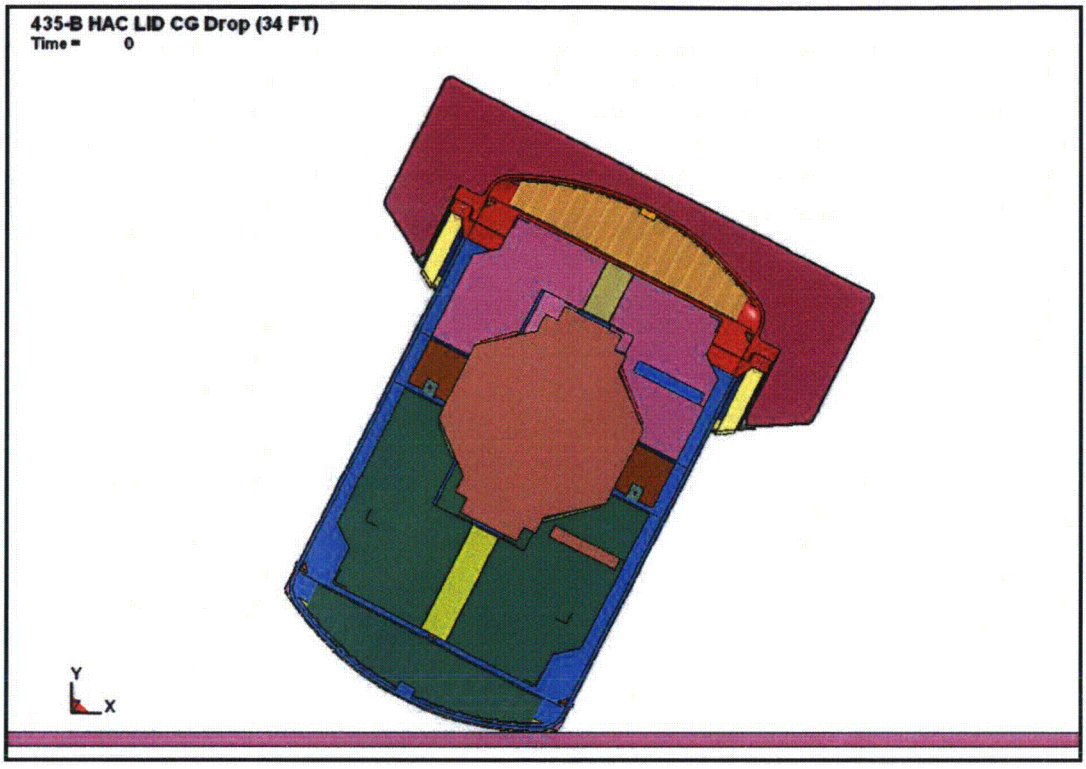

Figure 2.12.4-34 – D3 Benchmark Initial State

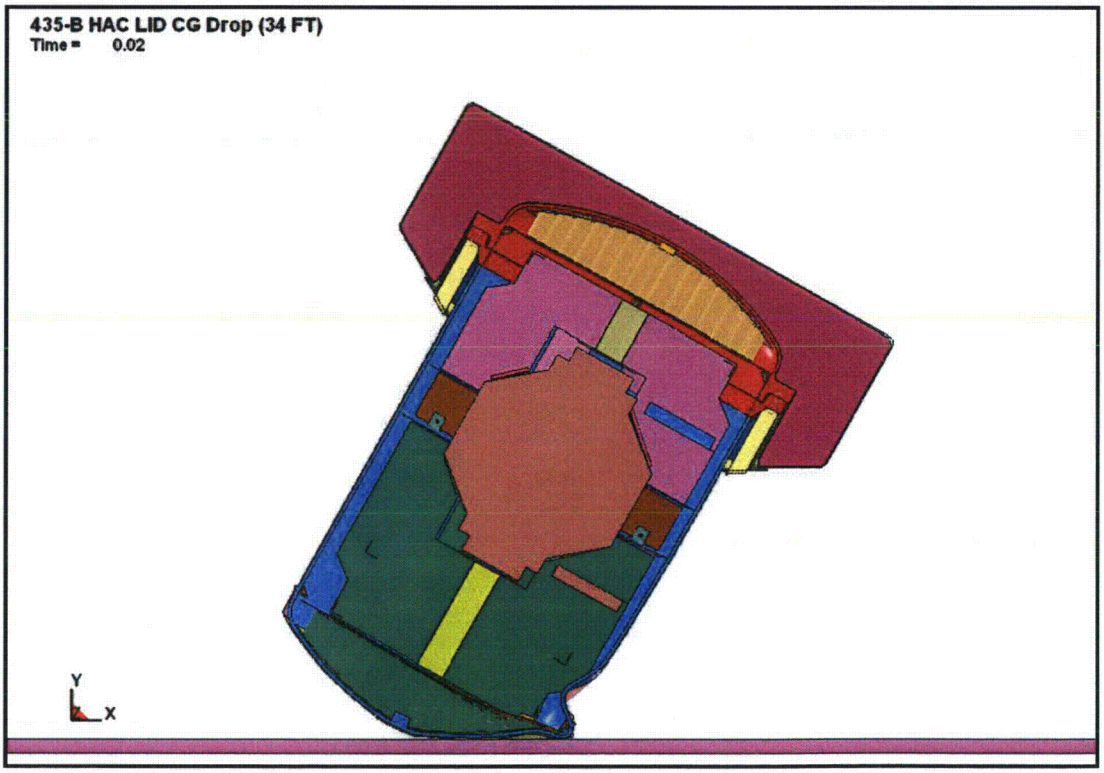

Figure 2.12.4-35 – D3 Benchmark Final State

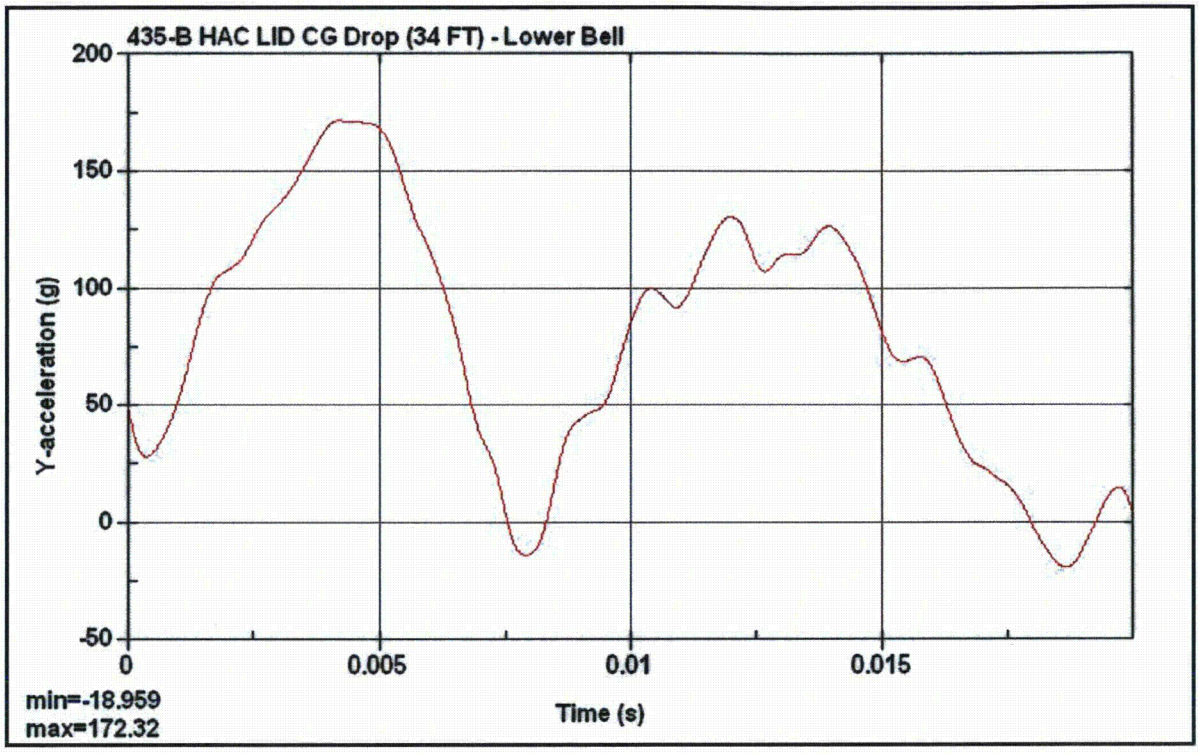

Figure 2.12.4-36 – D3 Benchmark Lower Bell Acceleration

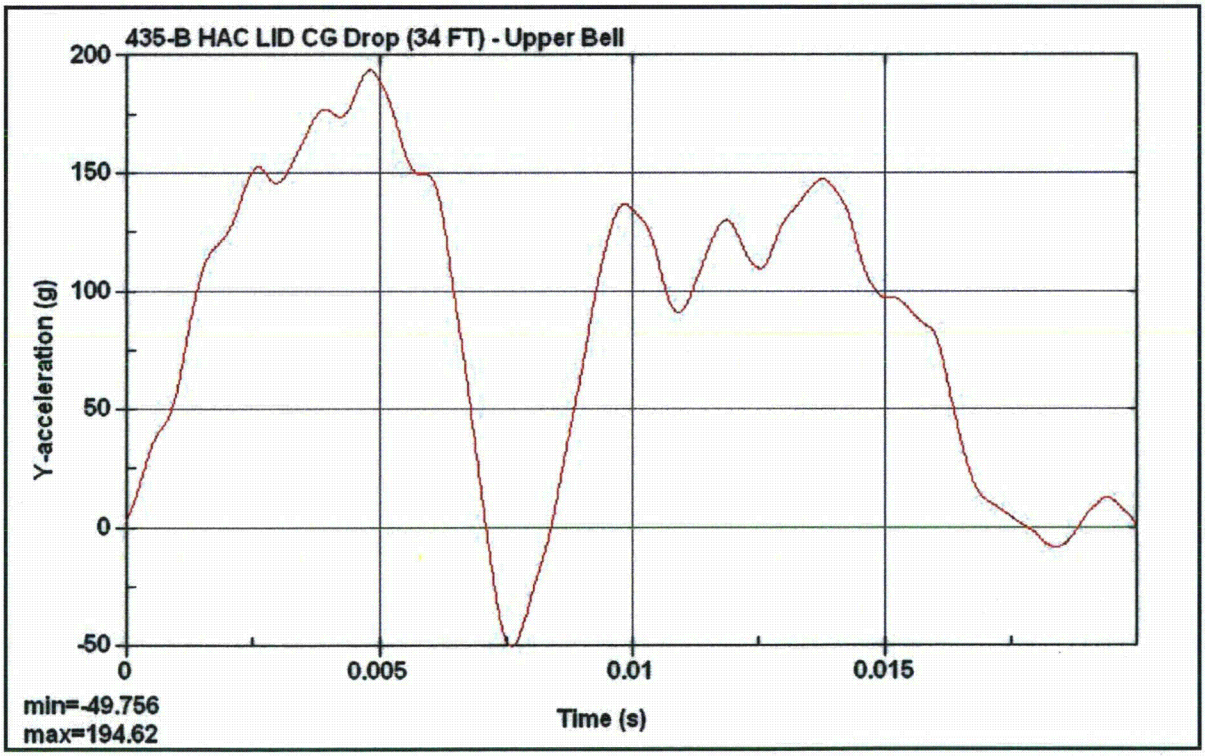

Figure 2.12.4-37 – D3 Benchmark Upper Bell Acceleration

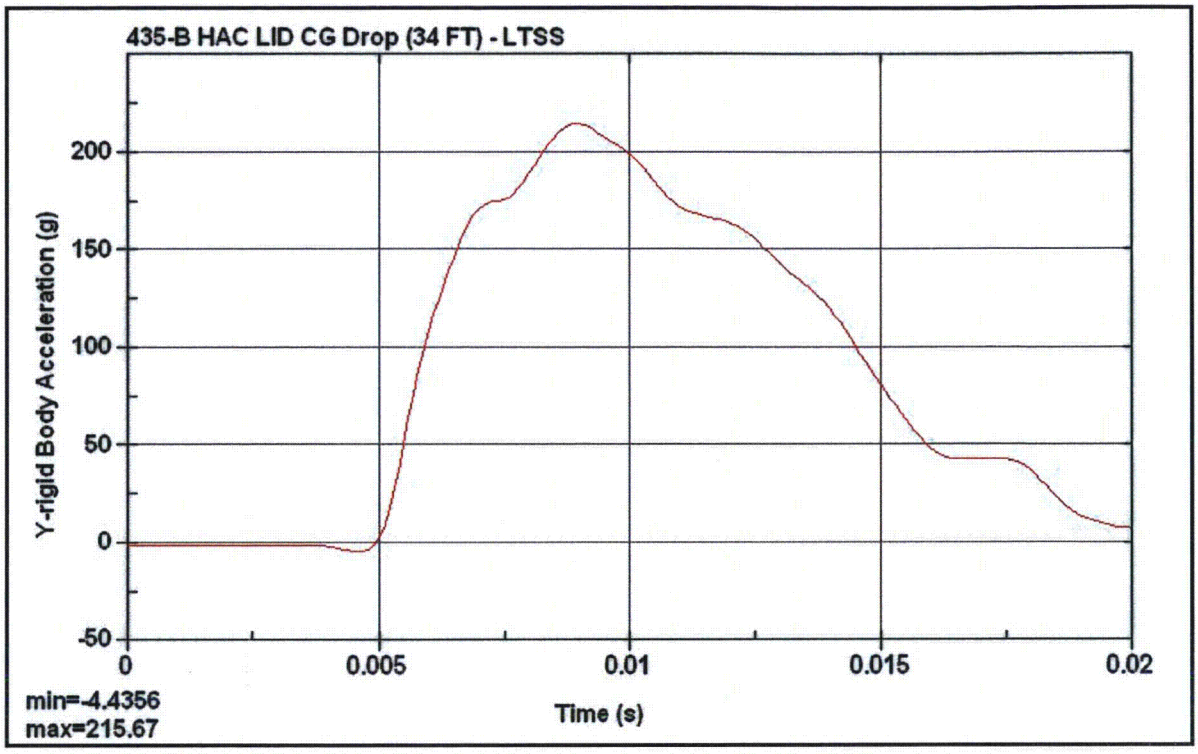

Figure 2.12.4-38 – D3 Benchmark LTSS Acceleration

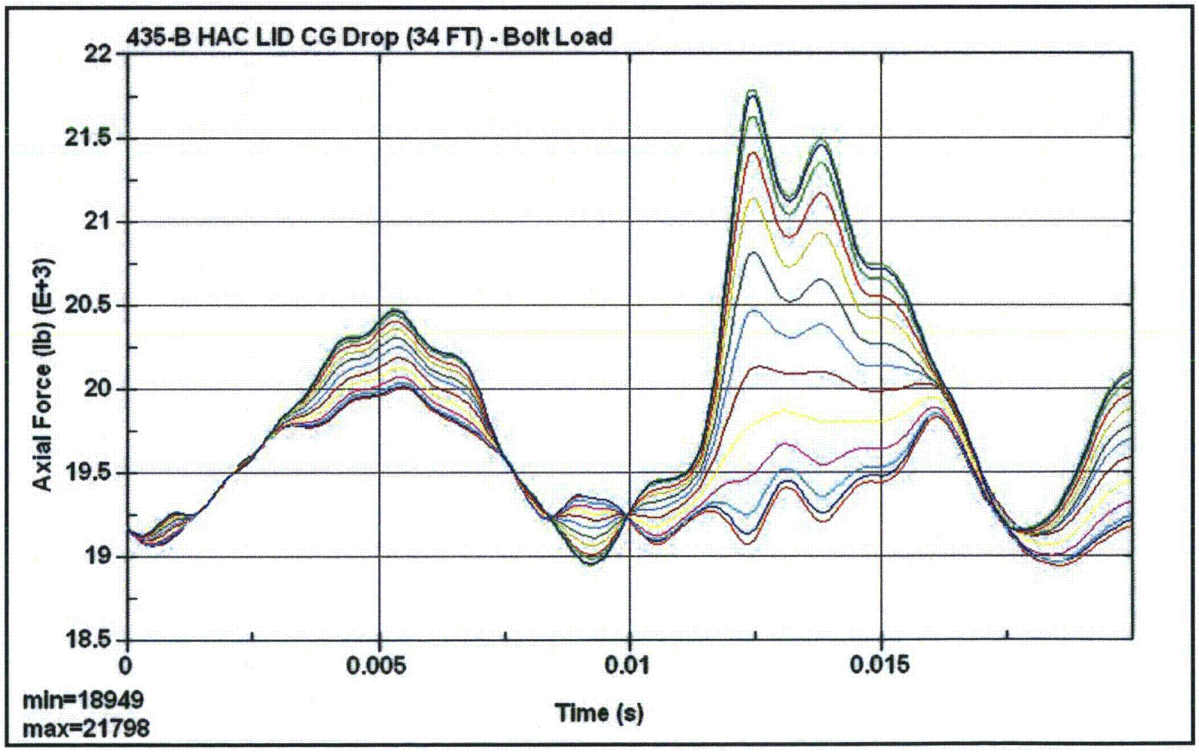

Figure 2.12.4-39 – D3 Benchmark Axial Bolt Force

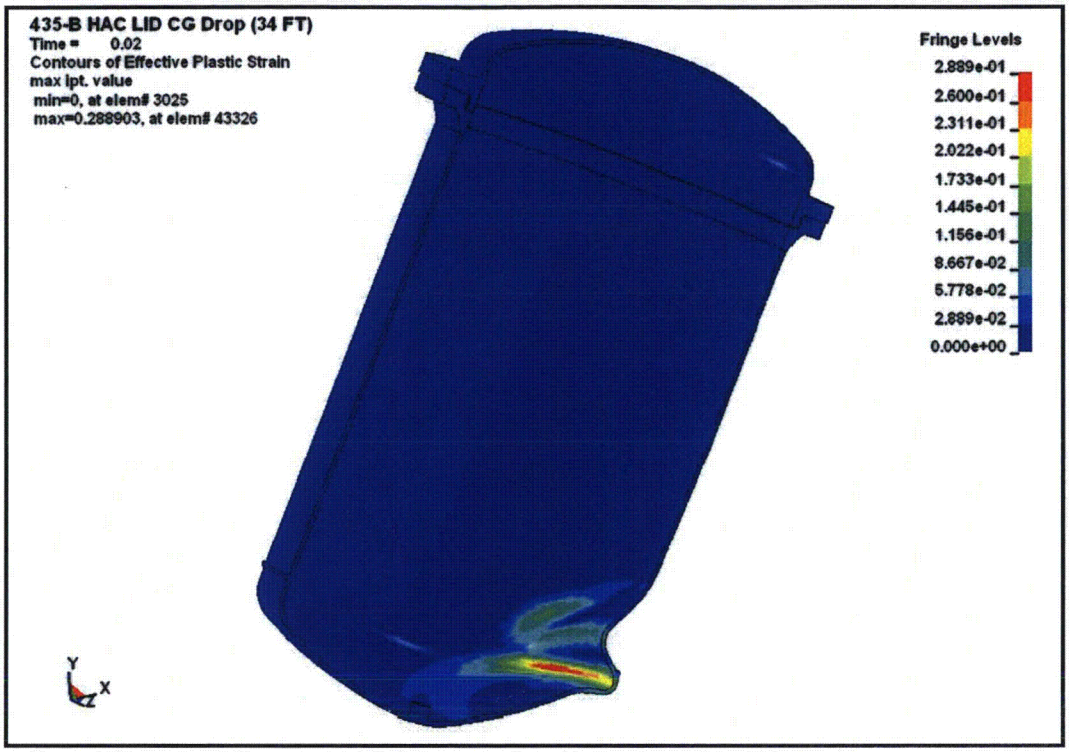

Figure 2.12.4-40 – D3 Benchmark Containment Boundary Cumulative Effective Plastic Strain

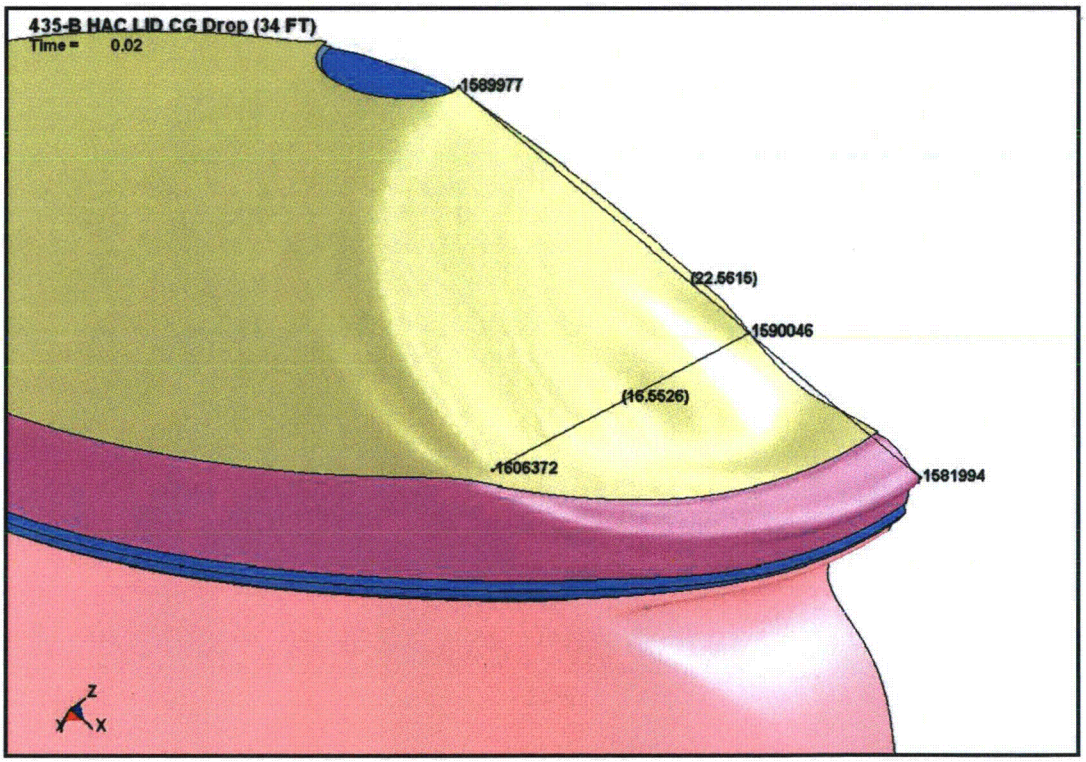

Figure 2.12.4-41 – D3 Benchmark Upper Impact Patch

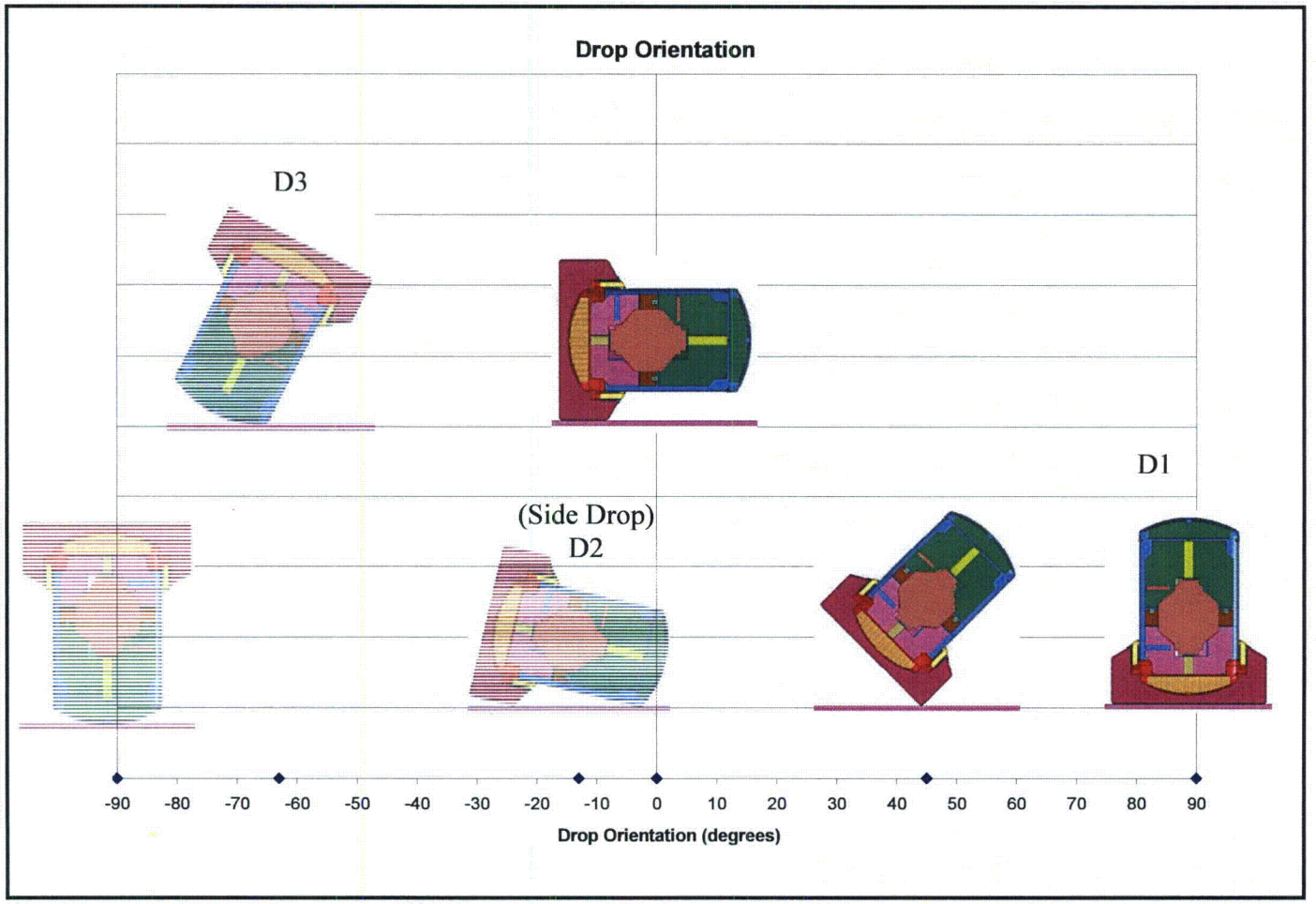

Figure 2.12.4-42 – Drop Orientation Terminology (Sampling of Orientations Only)

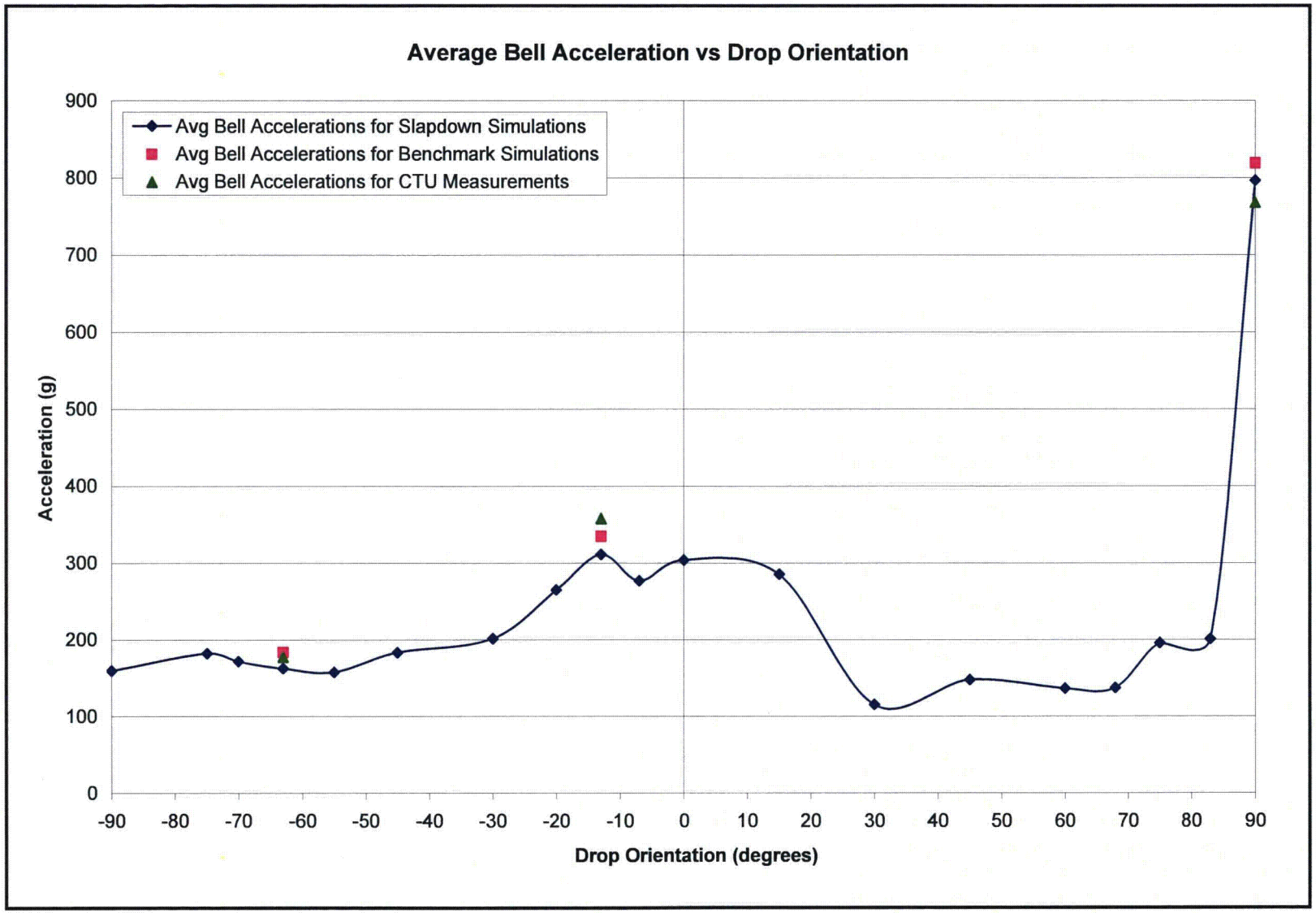

Figure 2.12.4-43 – Average Bell Acceleration vs Drop Orientation

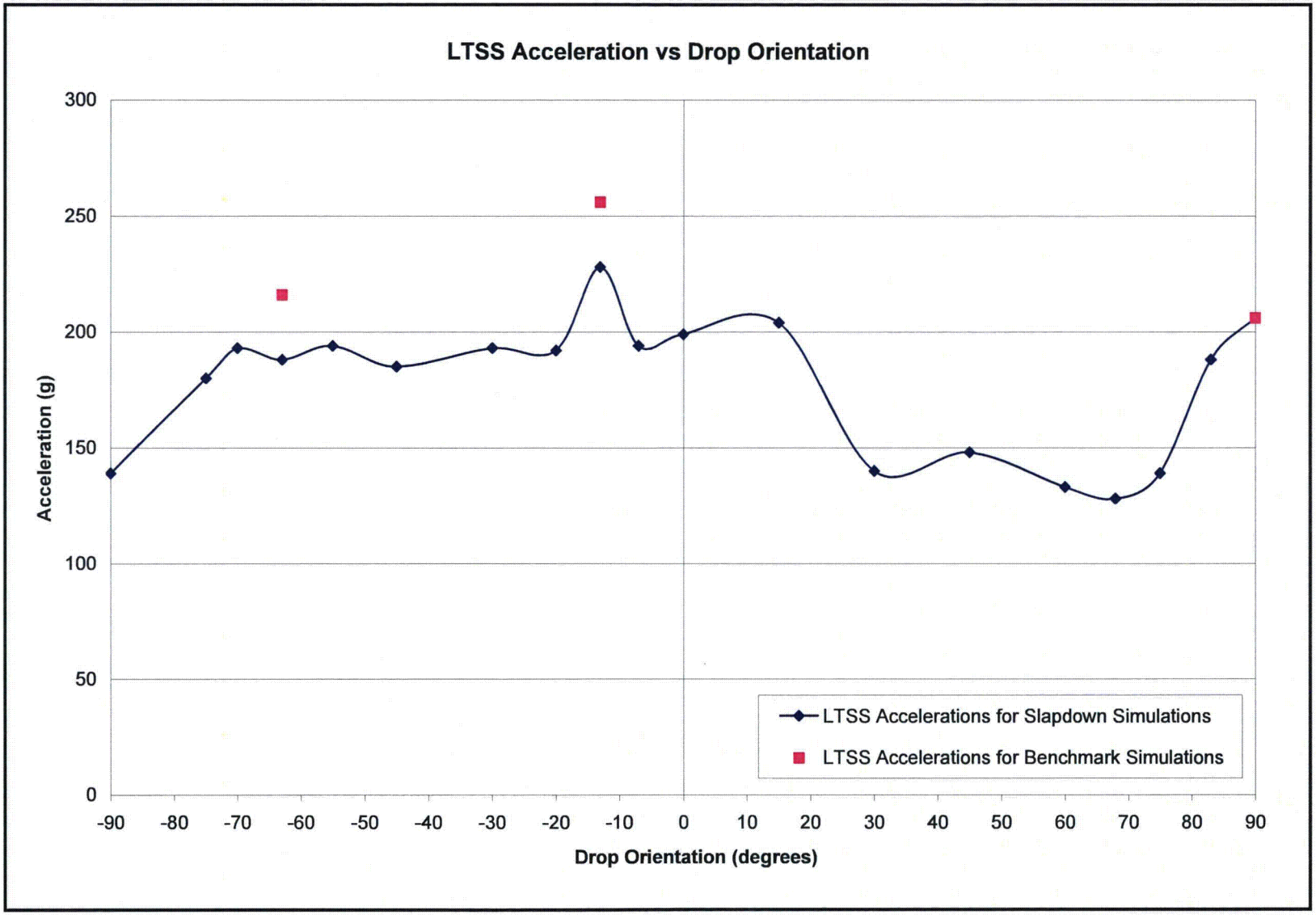

Figure 2.12.4-44 – LTSS Acceleration vs Drop Orientation

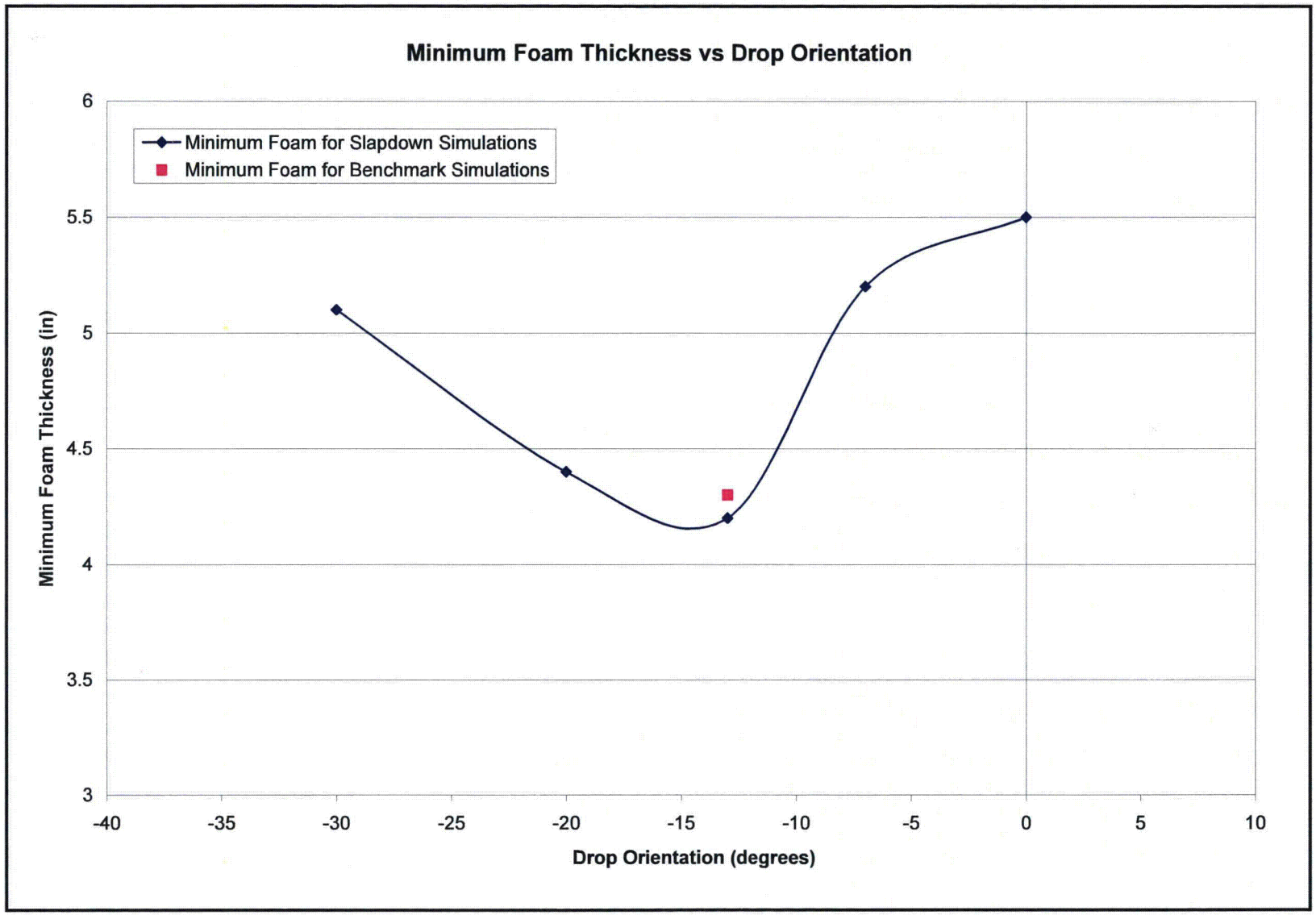

Figure 2.12.4-45 – Minimum Foam Thickness vs Drop Orientation

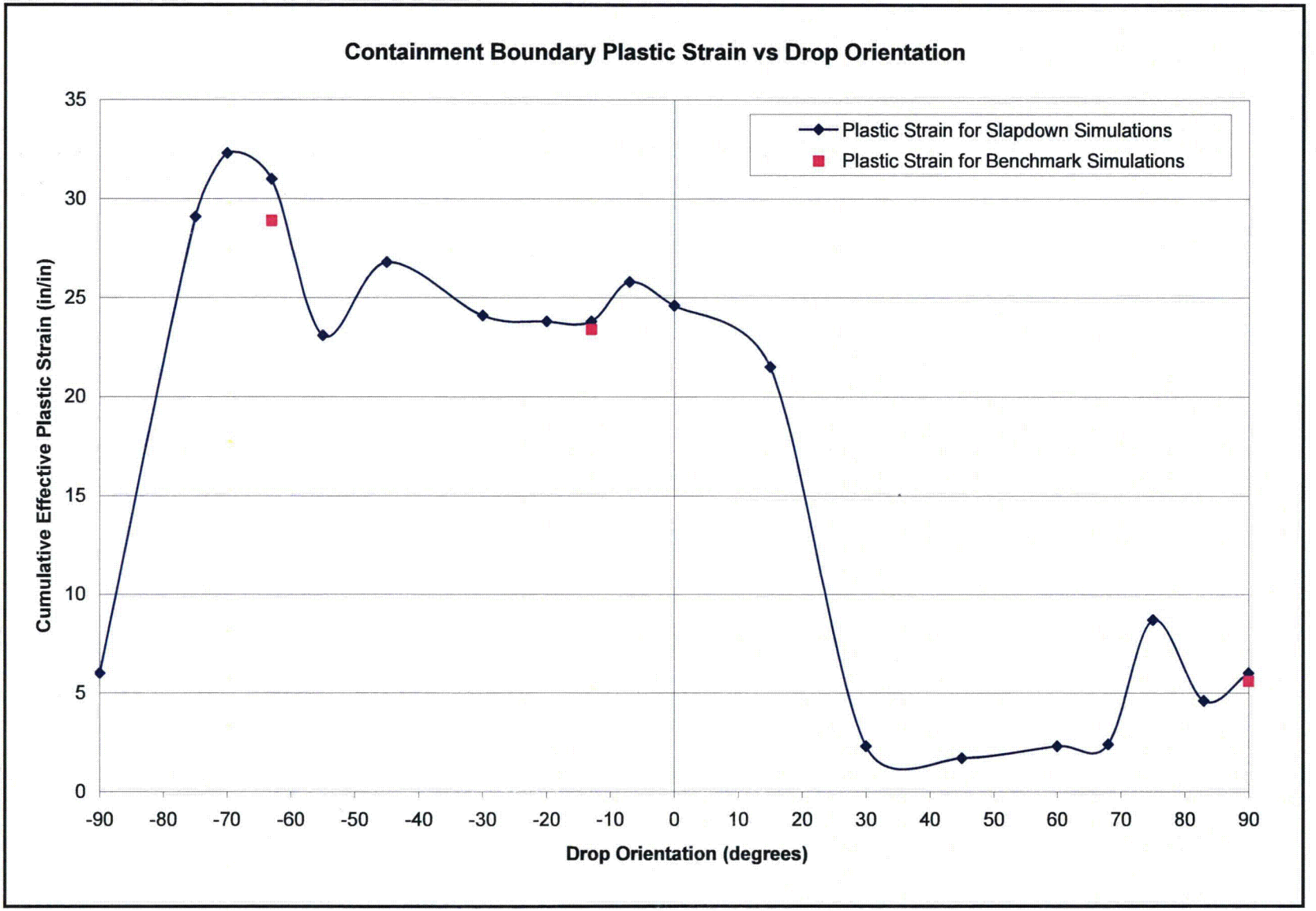

Figure 2.12.4-46 – Containment Boundary Plastic Strain vs Drop Orientation

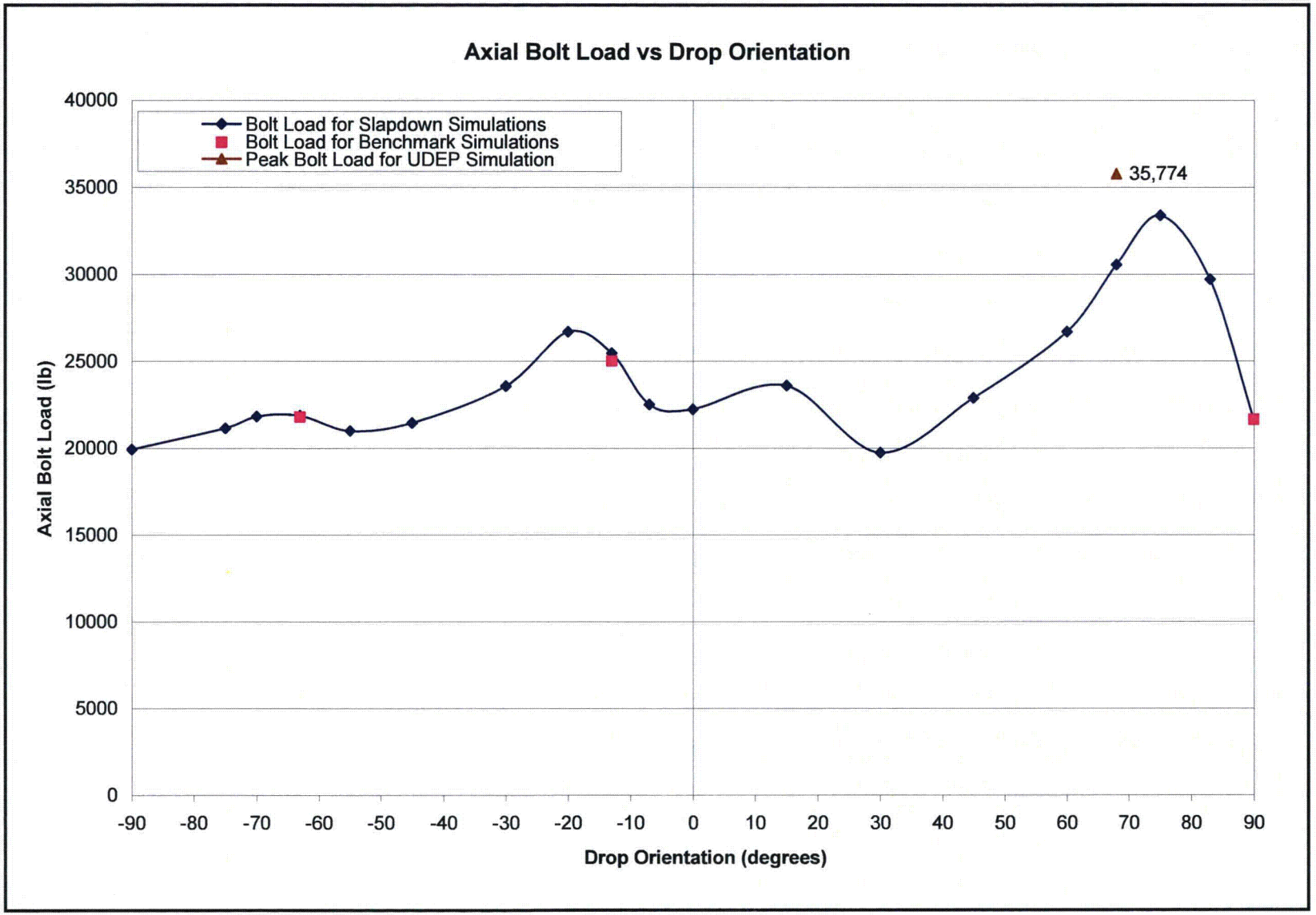

Figure 2.12.4-47 – Axial Bolt Load vs Drop Orientation

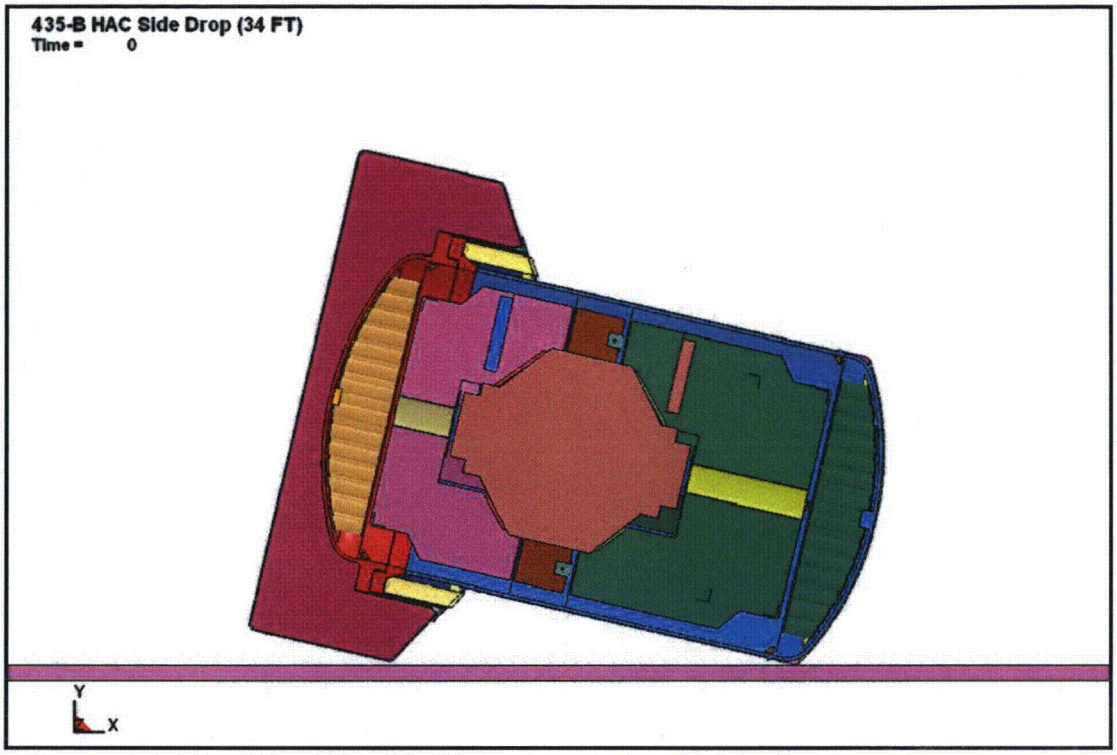

Figure 2.12.4-48 – Simultaneous Side Drop Initial State

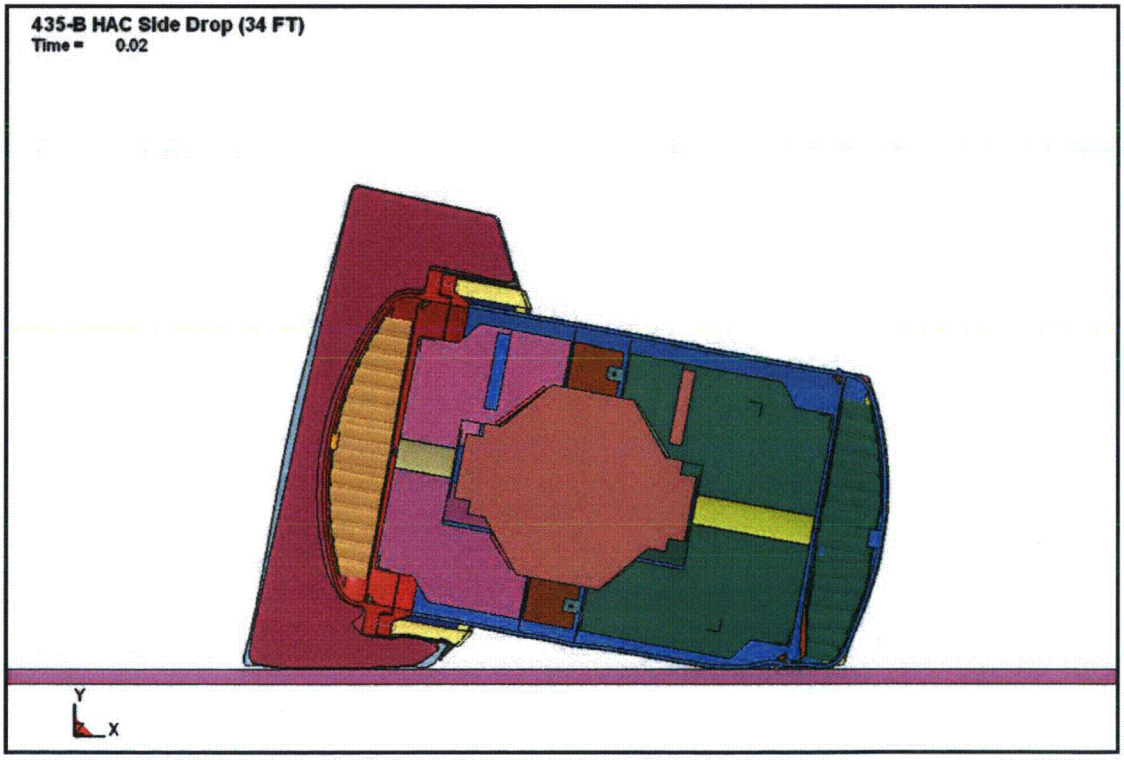

Figure 2.12.4-49 – Simultaneous Side Drop Final State

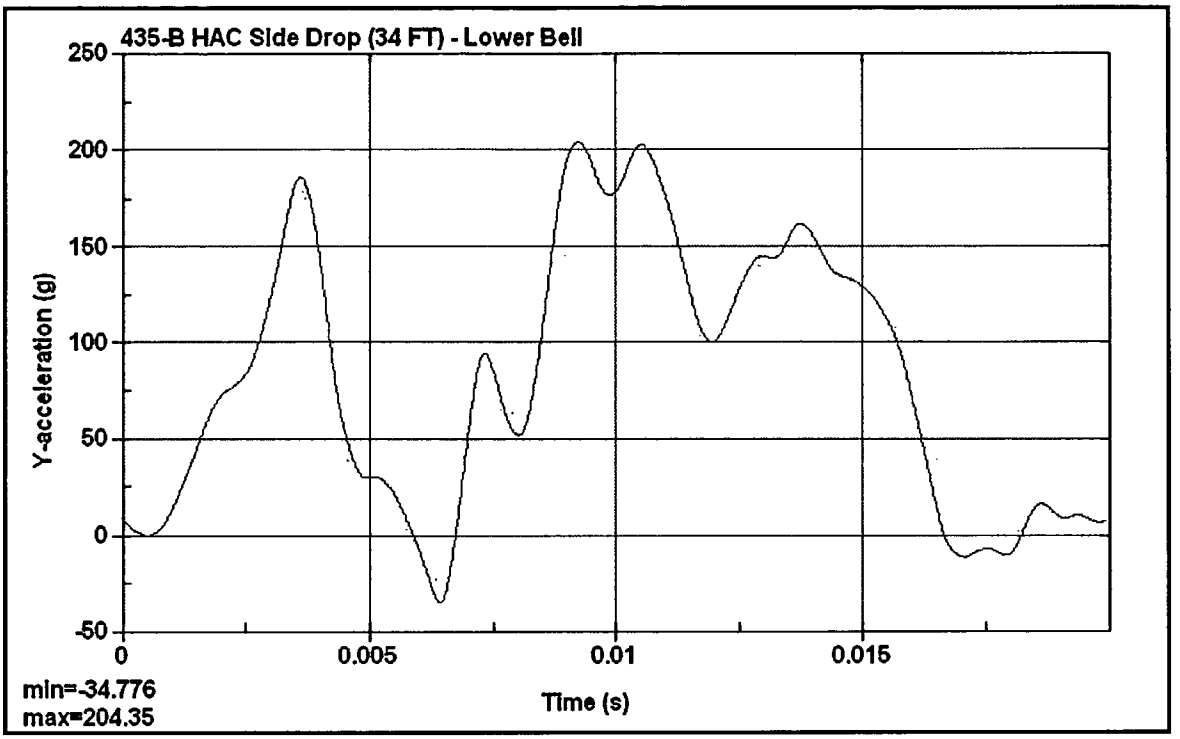

Figure 2.12.4-50 – Simultaneous Side Drop Lower Bell Acceleration

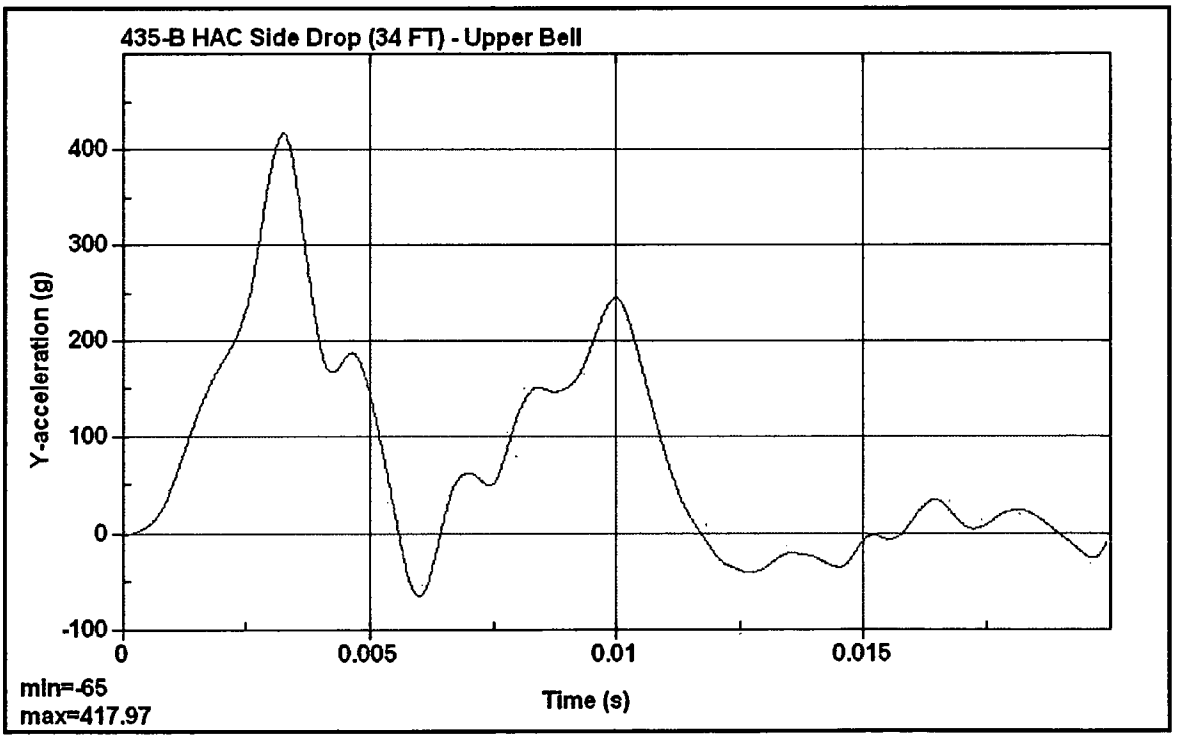

Figure 2.12.4-51 – Simultaneous Side Drop Upper Bell Acceleration

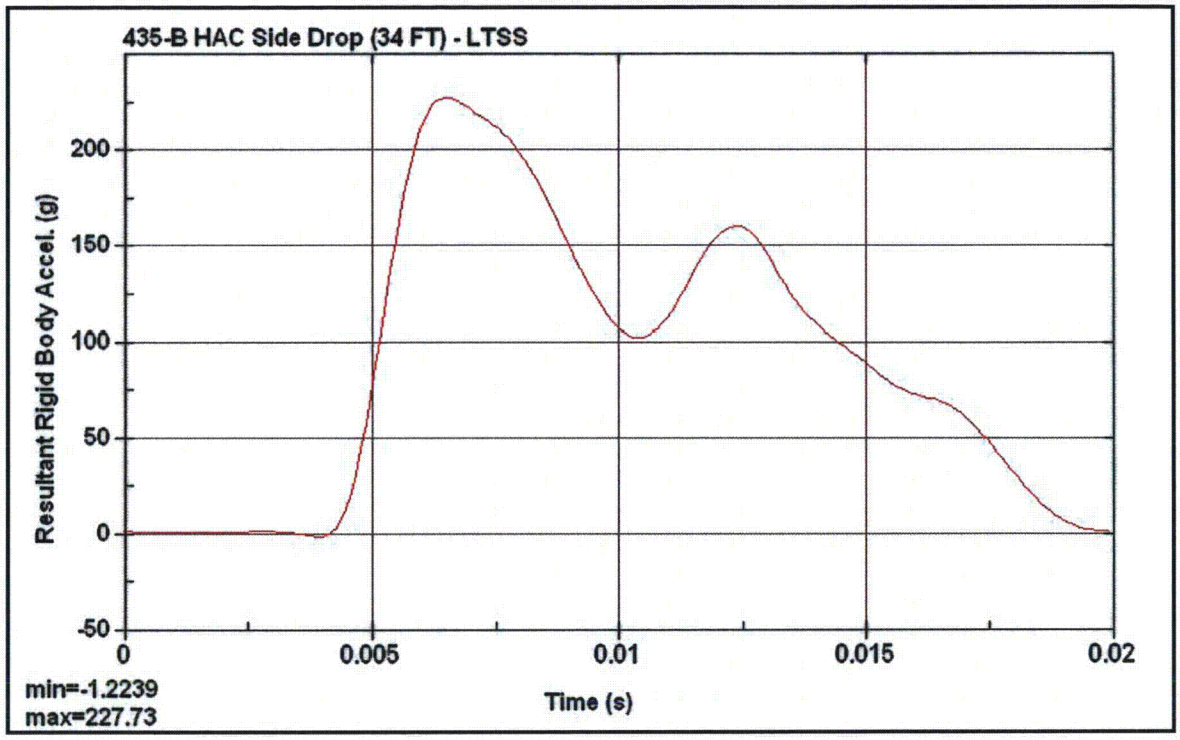

Figure 2.12.4-52 – Simultaneous Side Drop LTSS Acceleration

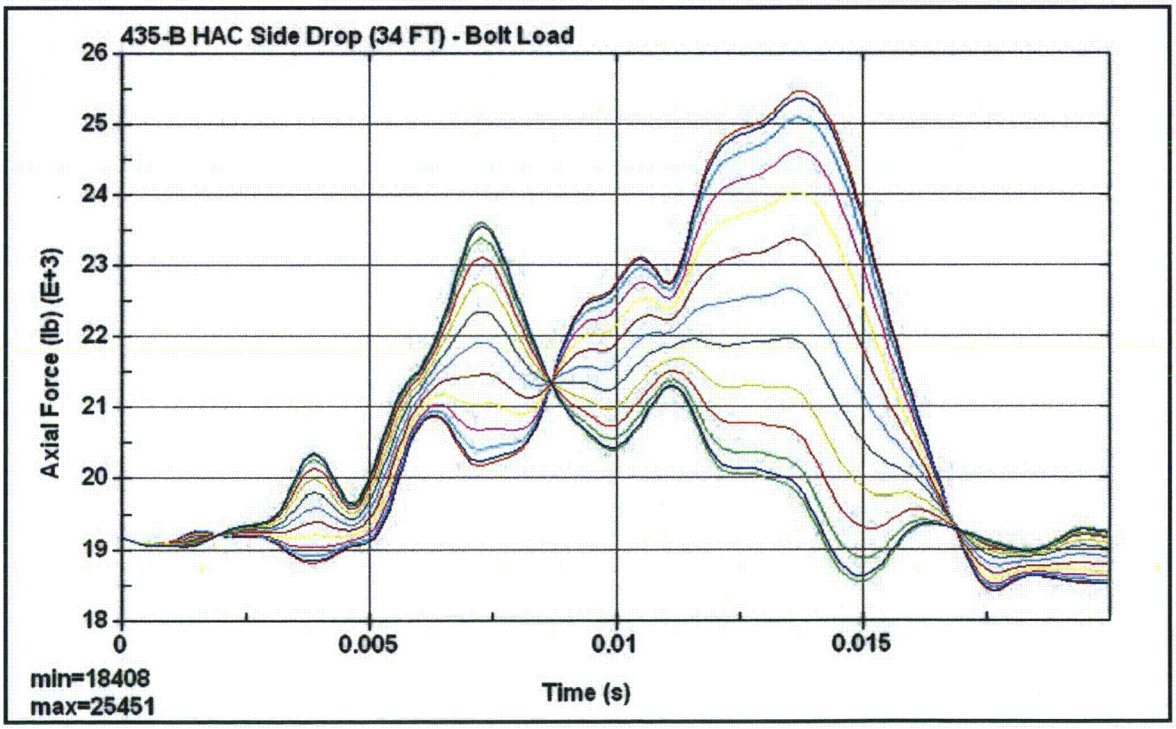

Figure 2.12.4-53 – Simultaneous Side Drop Axial Bolt Force

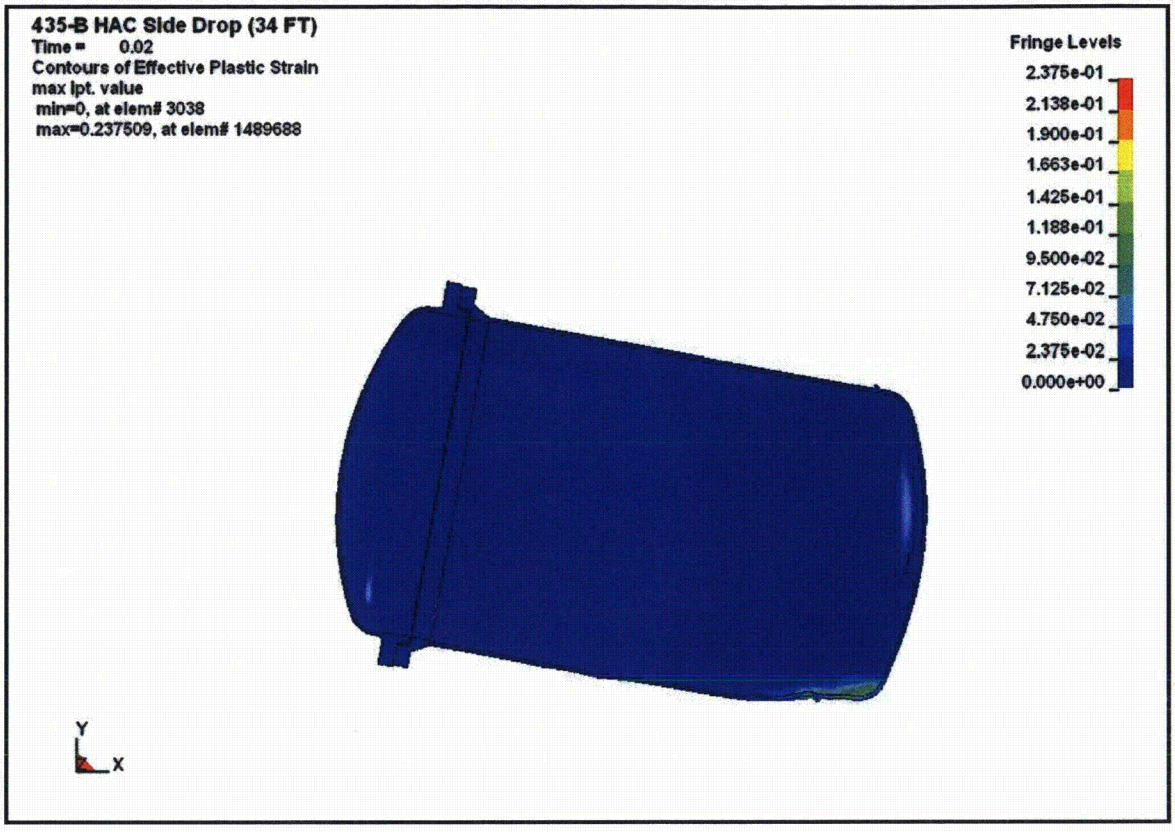

Figure 2.12.4-54 – Simultaneous Side Drop Containment Boundary Cumulative Effective Plastic Strain

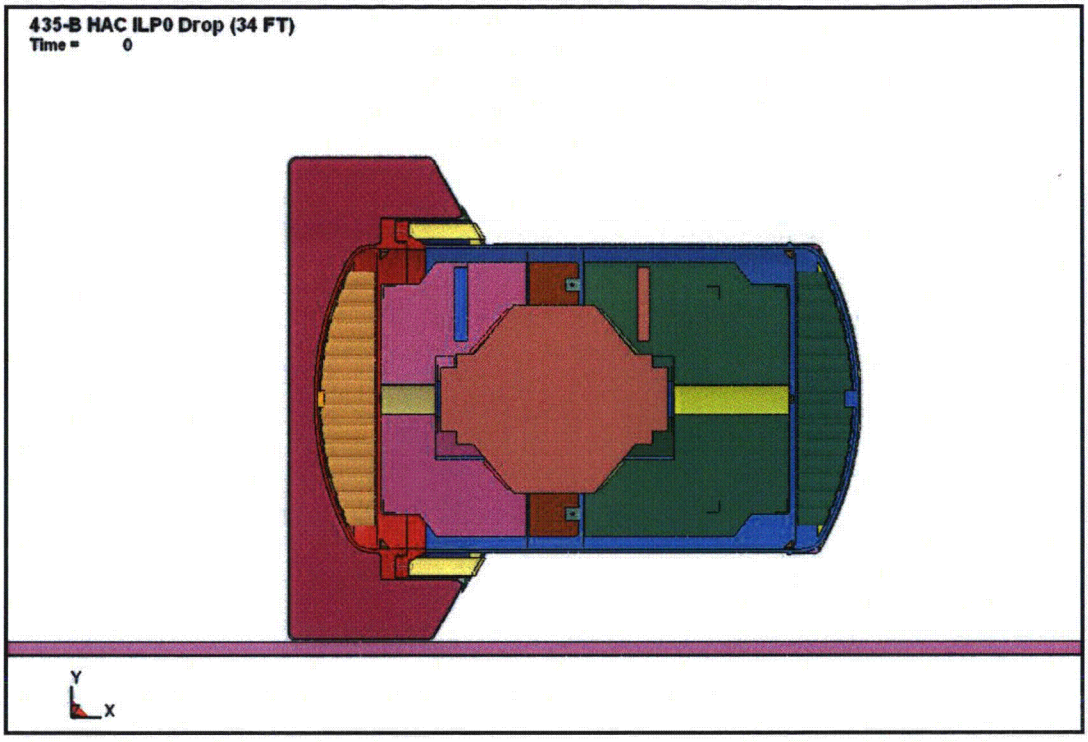

Figure 2.12.4-55 – ILP0 Initial State

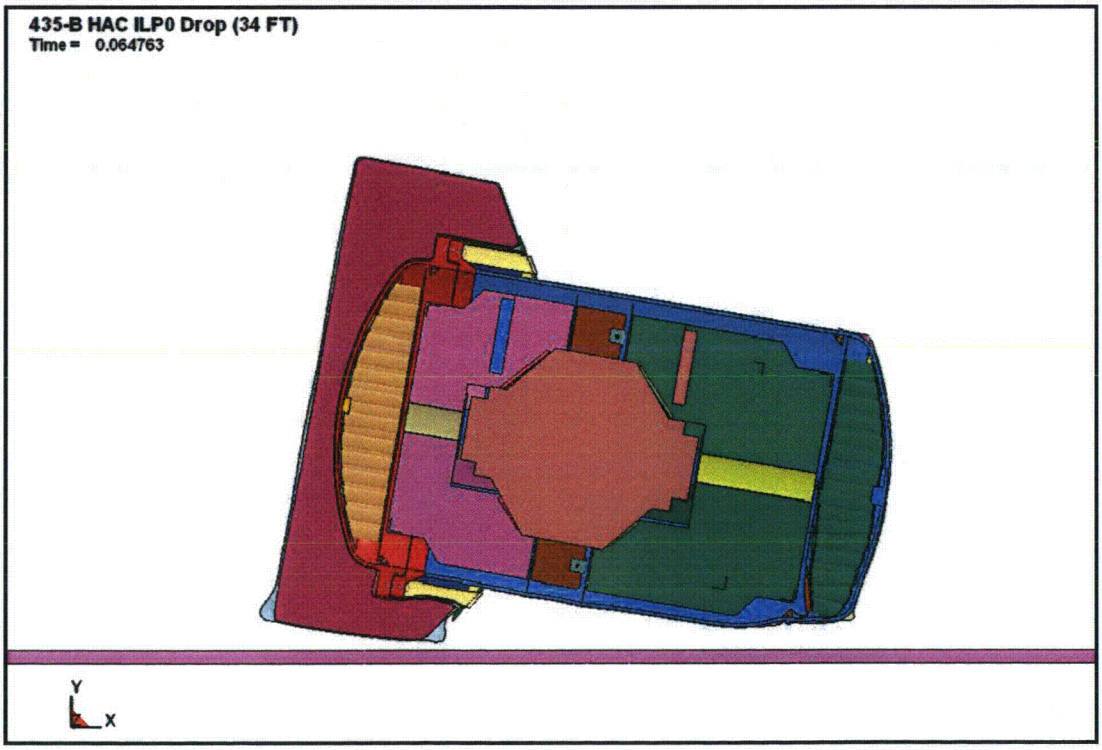

Figure 2.12.4-56 – ILP0 Final State

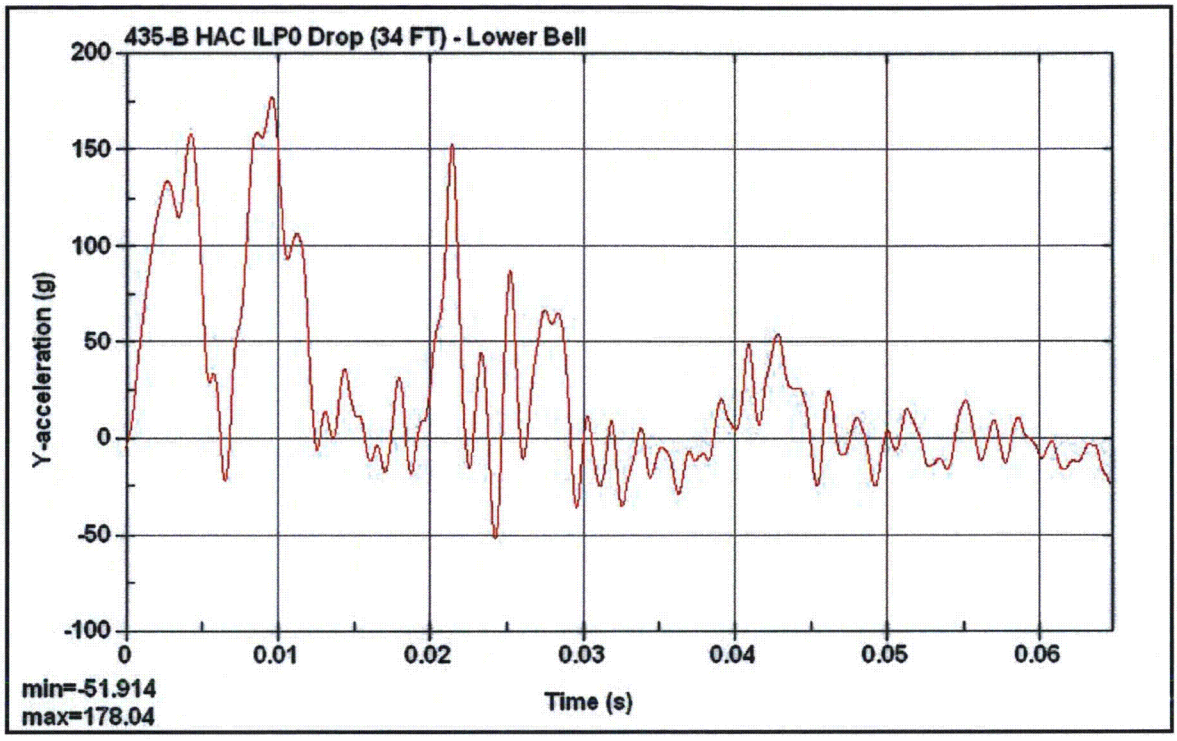

Figure 2.12.4-57 – ILP0 Lower Bell Acceleration

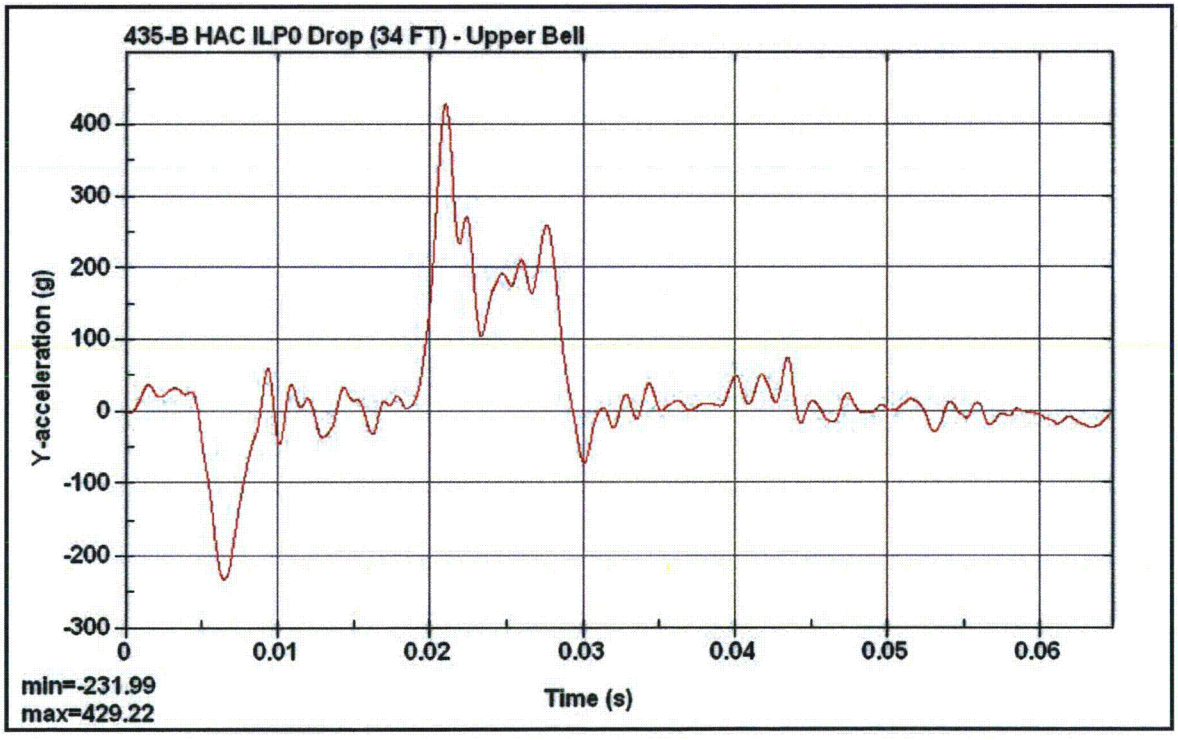

Figure 2.12.4-58 – ILP0 Upper Bell Acceleration

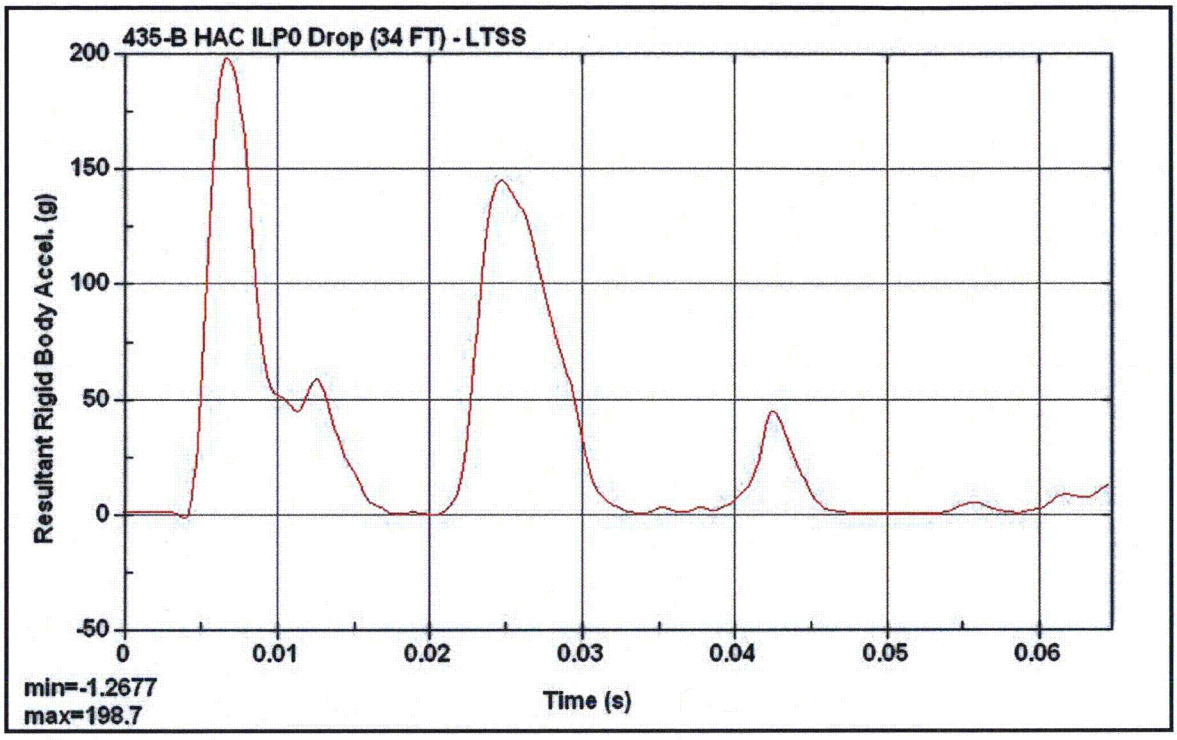

Figure 2.12.4-59 – ILP0 LTSS Acceleration

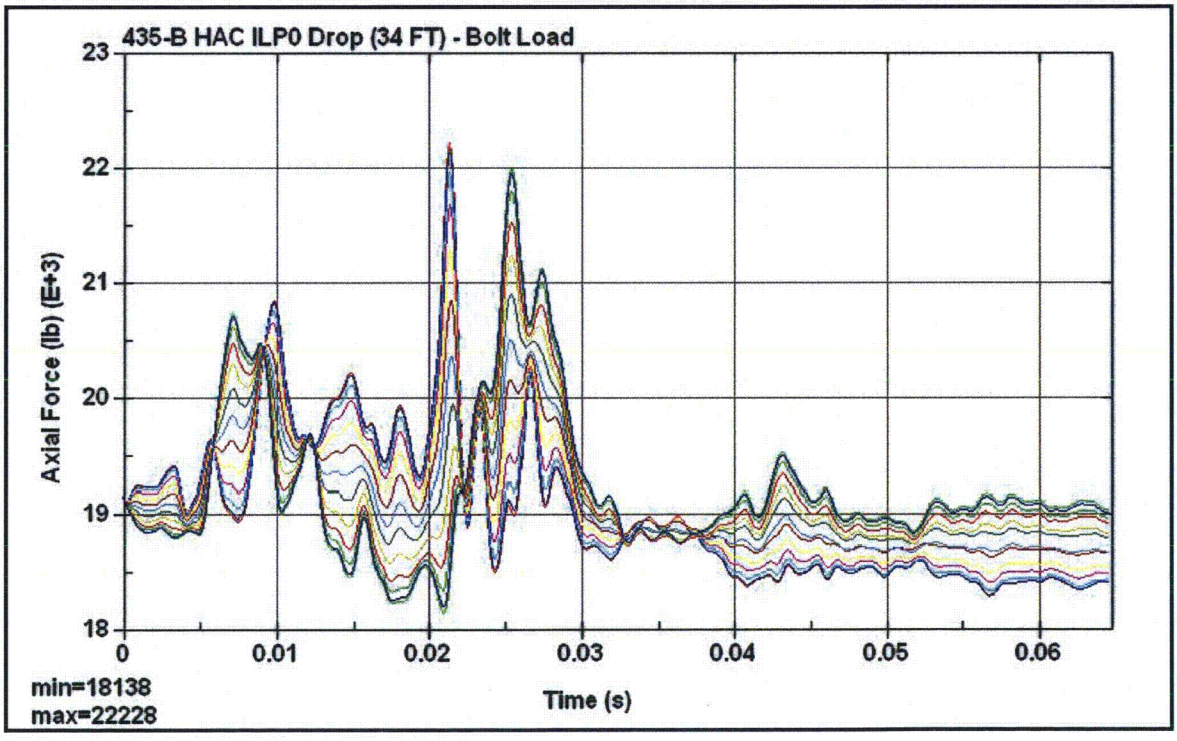

Figure 2.12.4-60 – ILP0 Axial Bolt Force

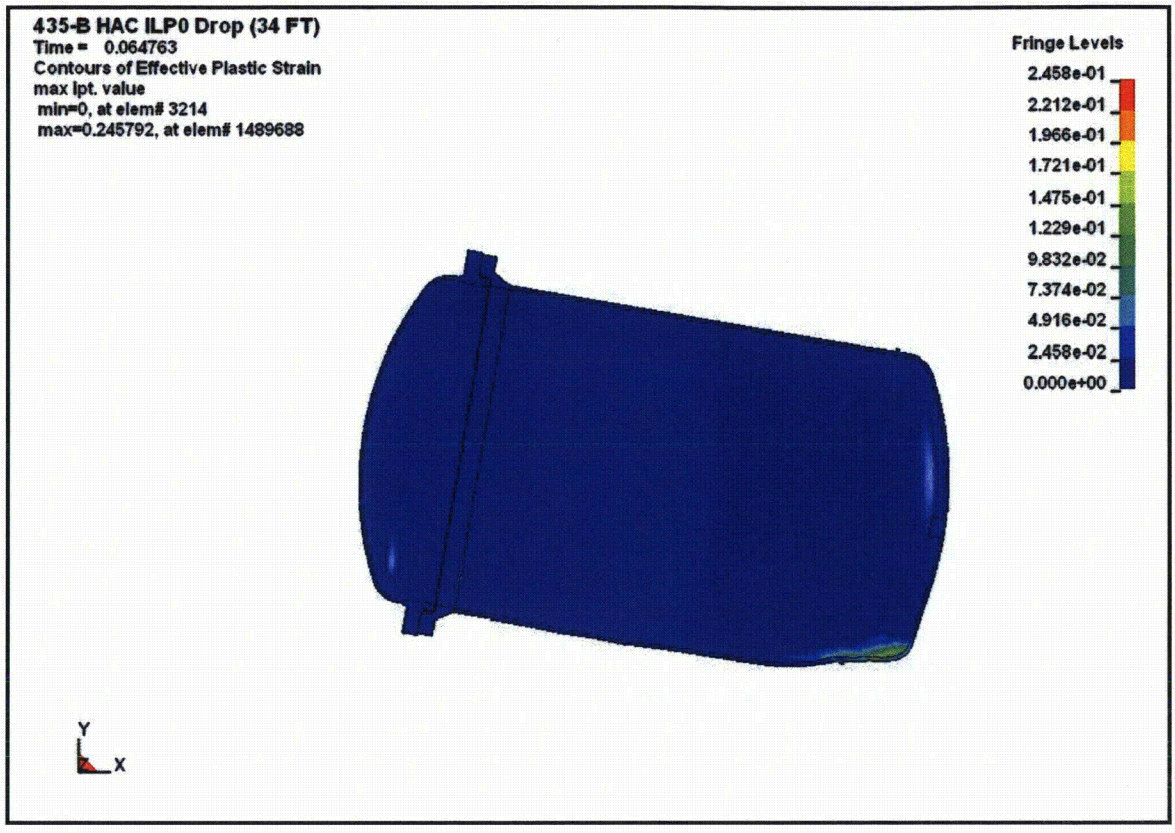

Figure 2.12.4-61 – ILP0 Containment Boundary Cumulative Effective Plastic Strain

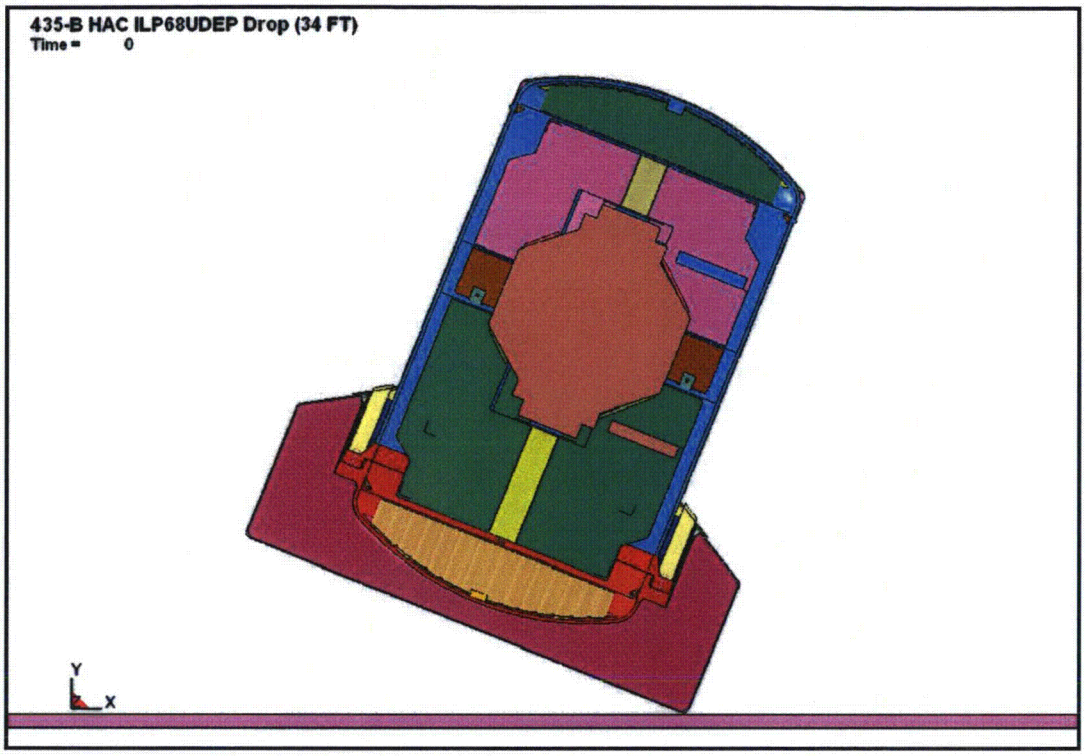

Figure 2.12.4-62 – ILP68UDEP Initial State

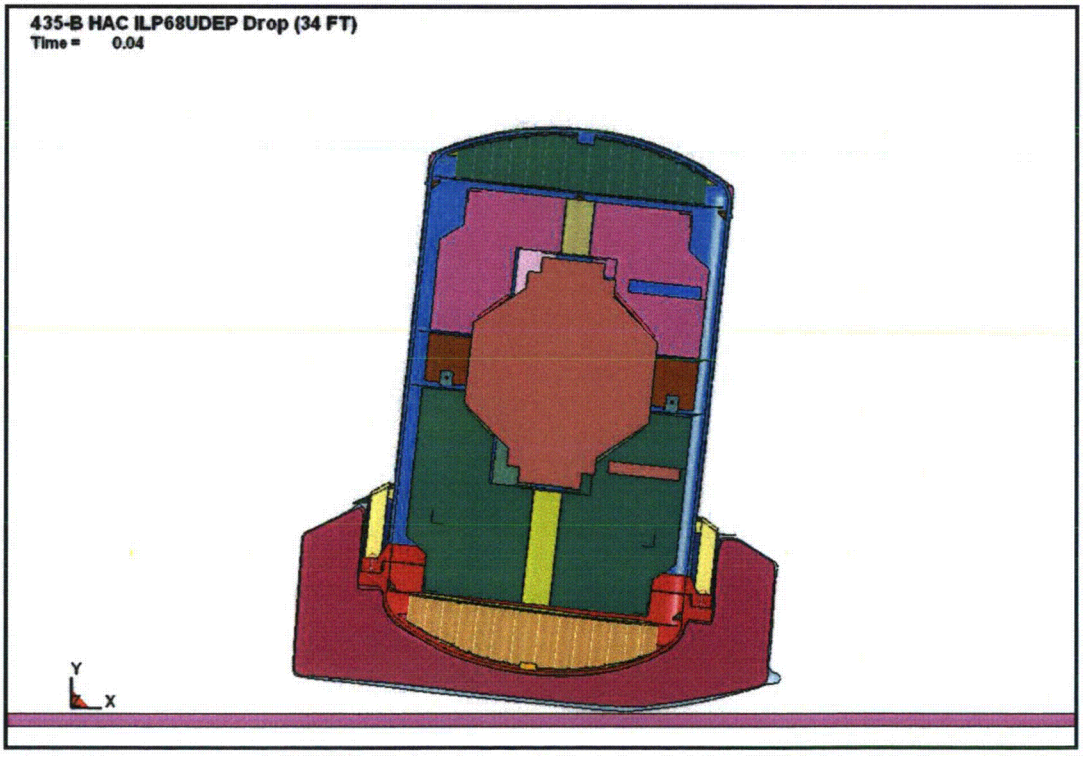

Figure 2.12.4-63 – ILP68UDEP Final State

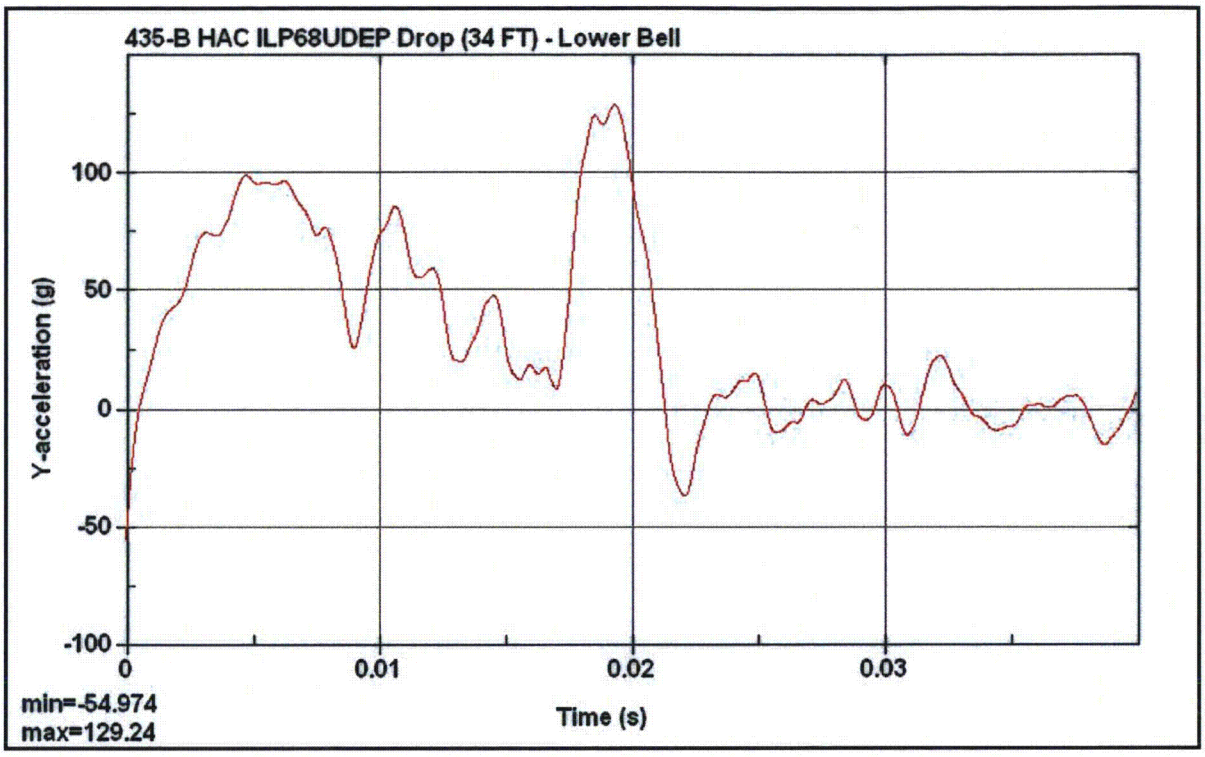

Figure 2.12.4-64 – ILP68UDEP Lower Bell Acceleration

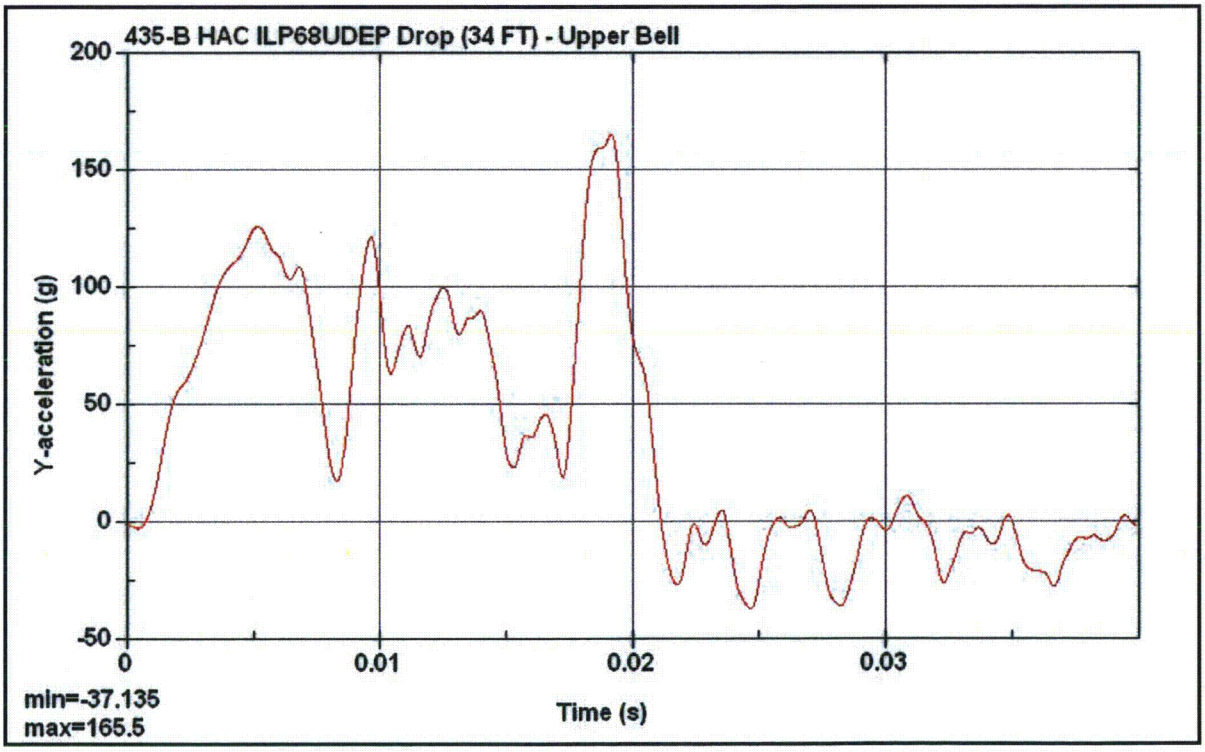

Figure 2.12.4-65 – ILP68UDEP Upper Bell Acceleration

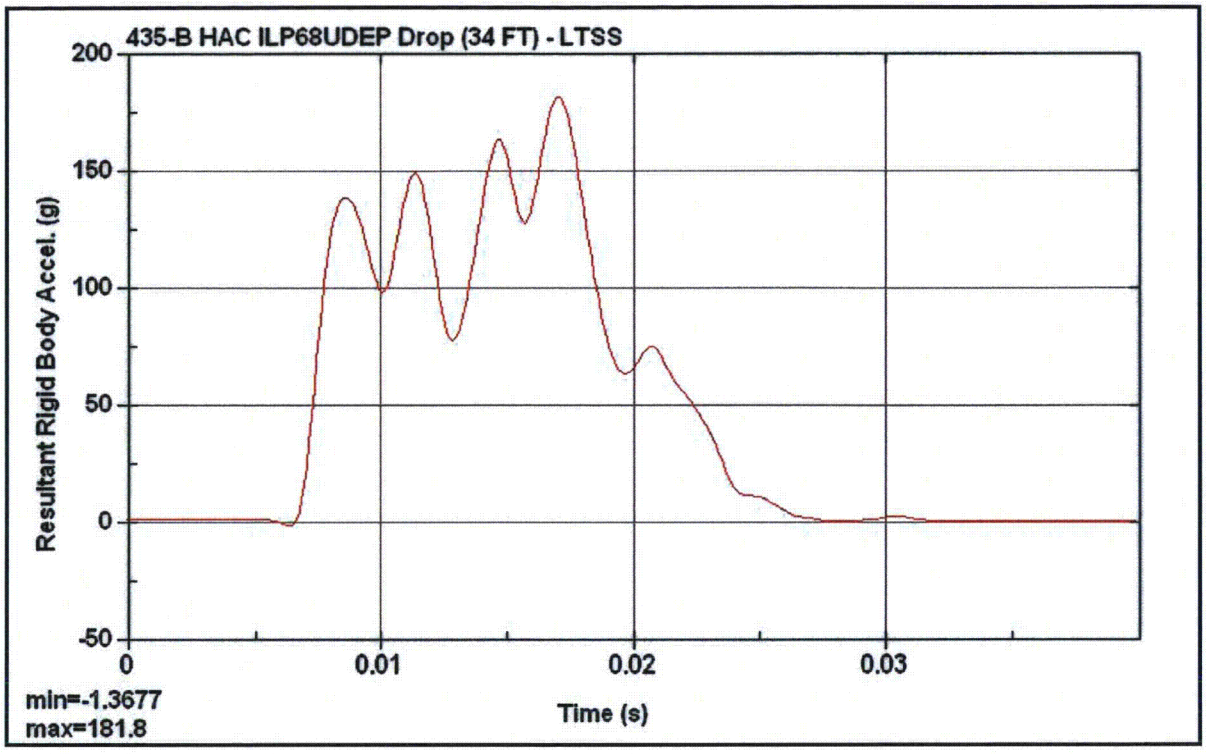

Figure 2.12.4-66 – ILP68UDEP LTSS Acceleration

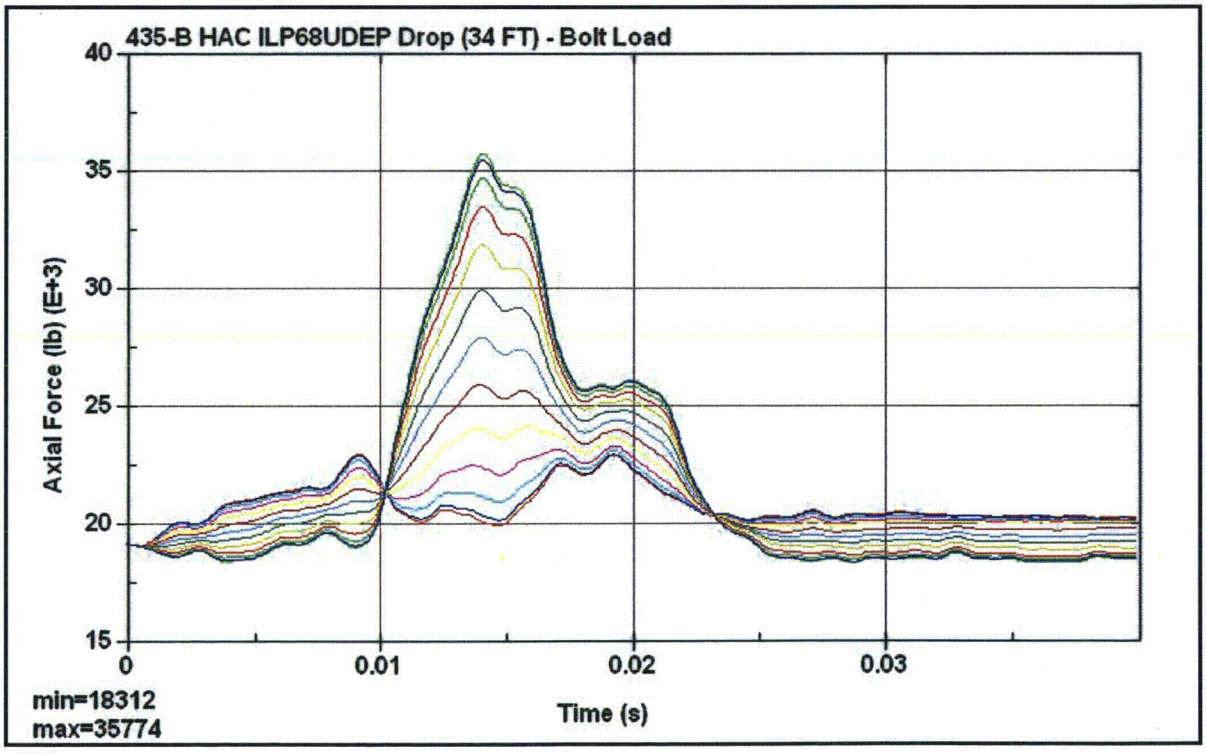

Figure 2.12.4-67 – ILP68UDEP Axial Bolt Force

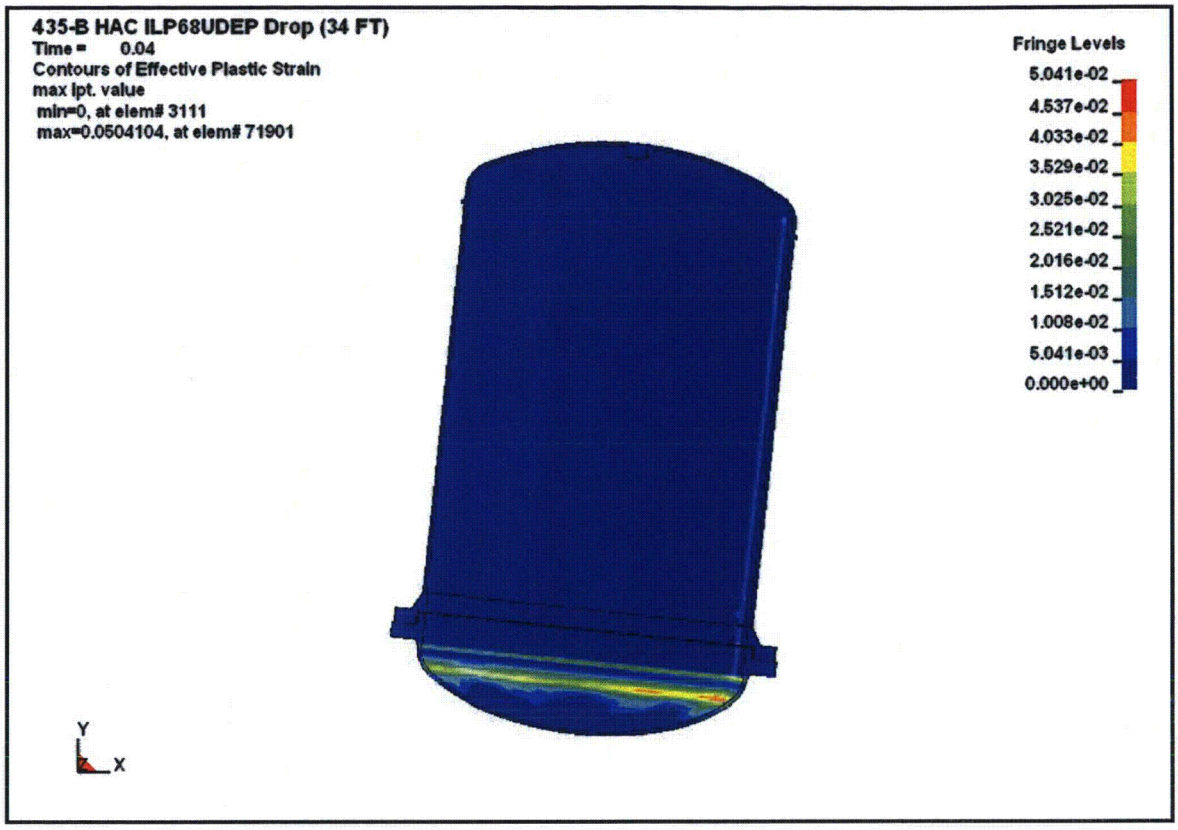

Figure 2.12.4-68 – ILP68UDEP Containment Boundary Cumulative Effective Plastic Strain

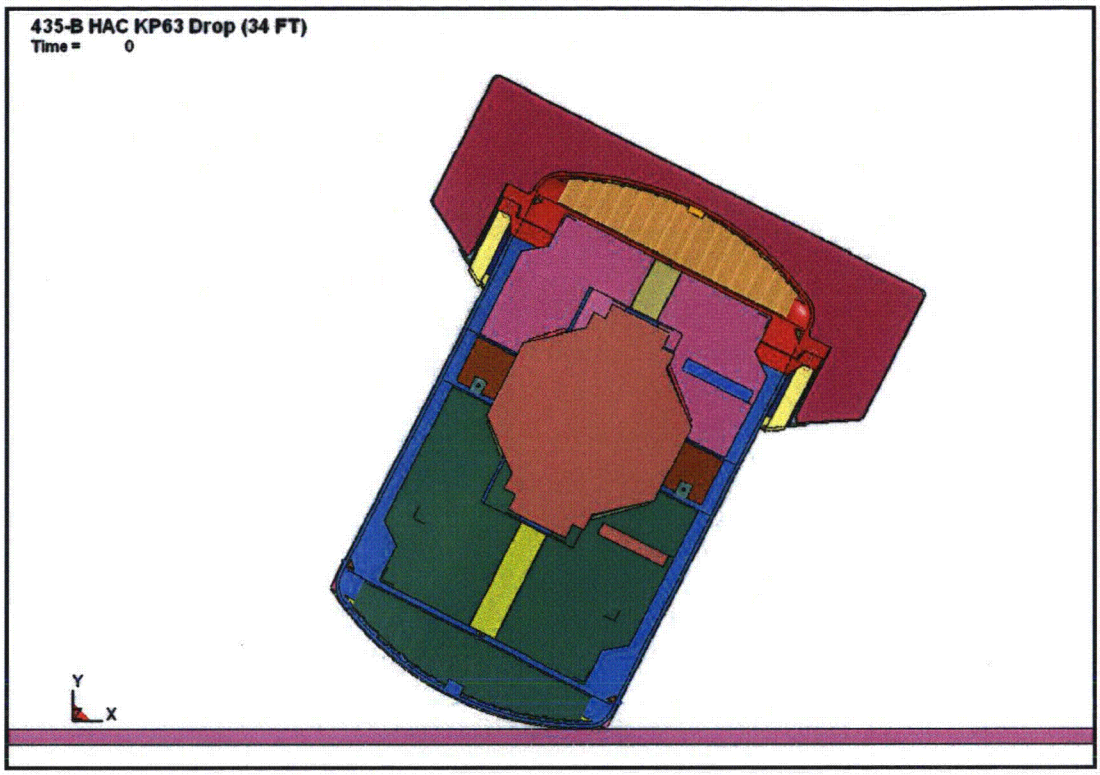

Figure 2.12.4-69 – KP63 (CG-over-Top Knuckle) Initial State

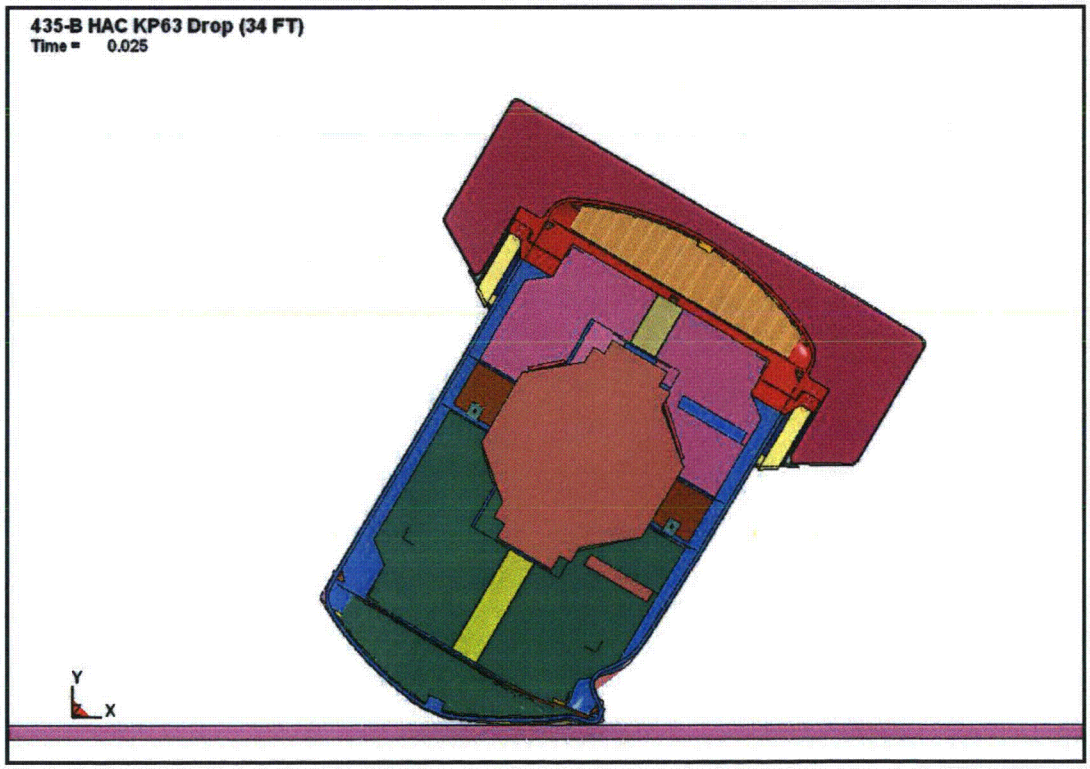

Figure 2.12.4-70 – KP63 (CG-over-Top Knuckle) Final State

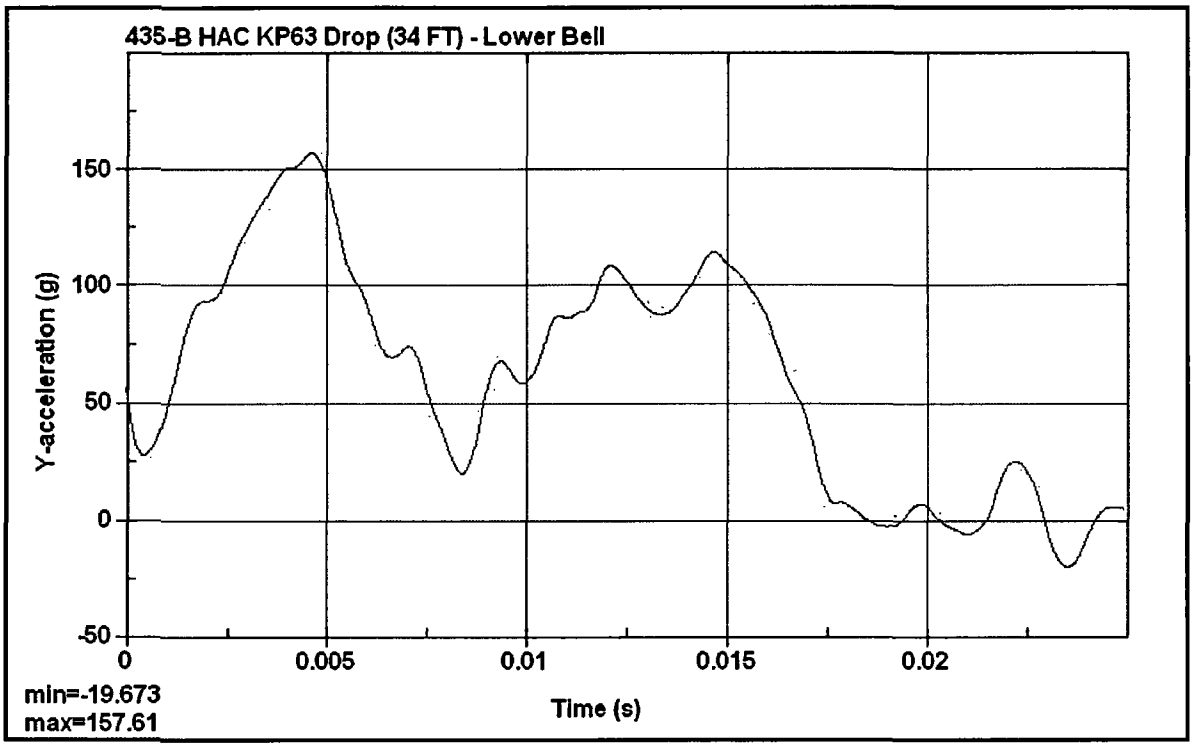

Figure 2.12.4-71 – KP63 Lower Bell Acceleration

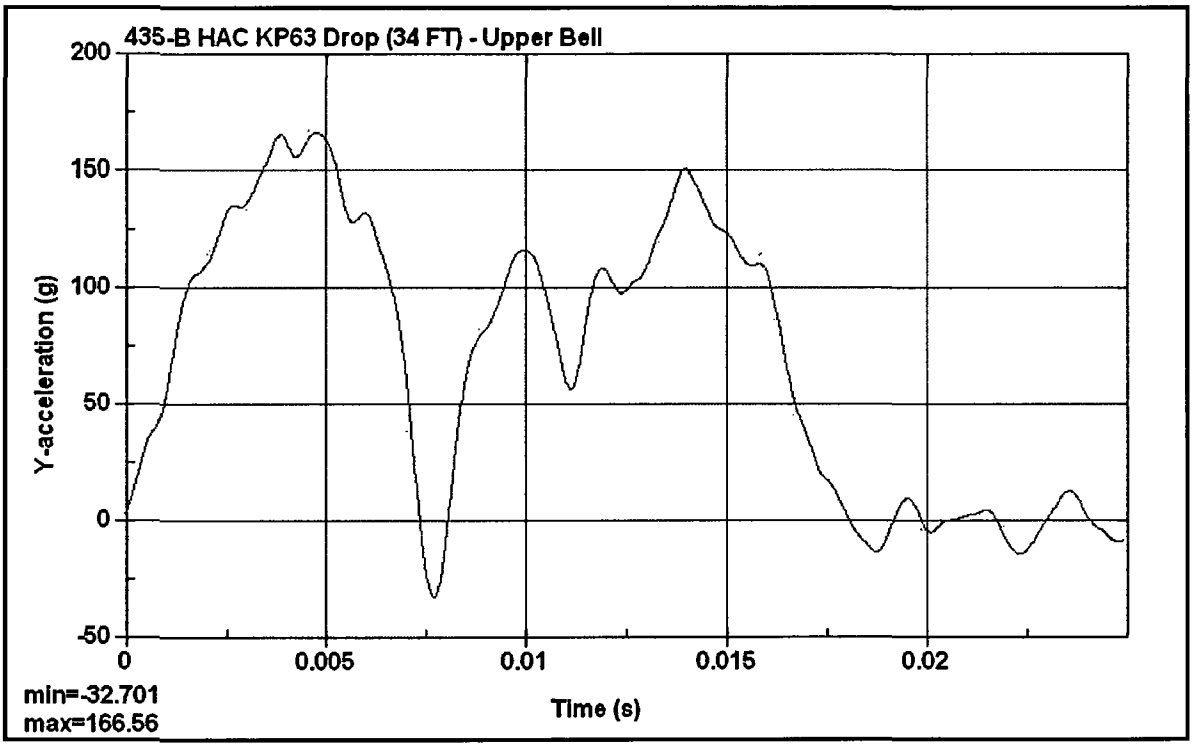

Figure 2.12.4-72 – KP63 Upper Bell Acceleration

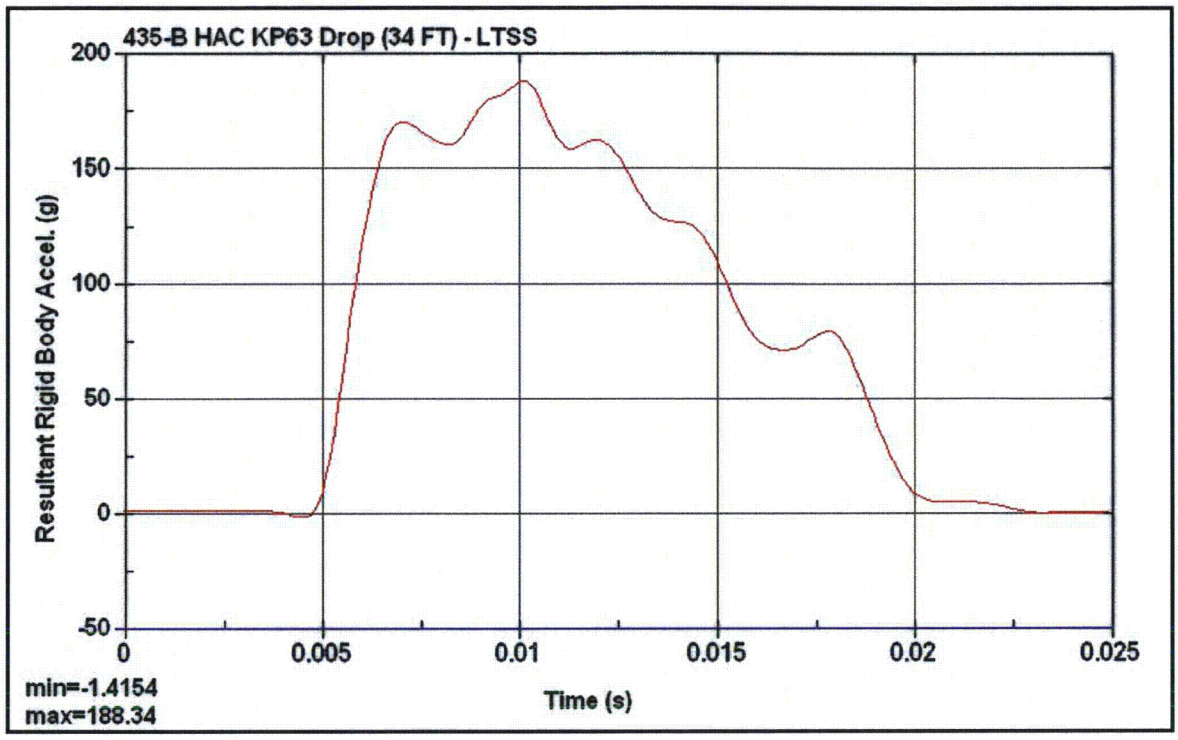

Figure 2.12.4-73 – KP63 LTSS Acceleration

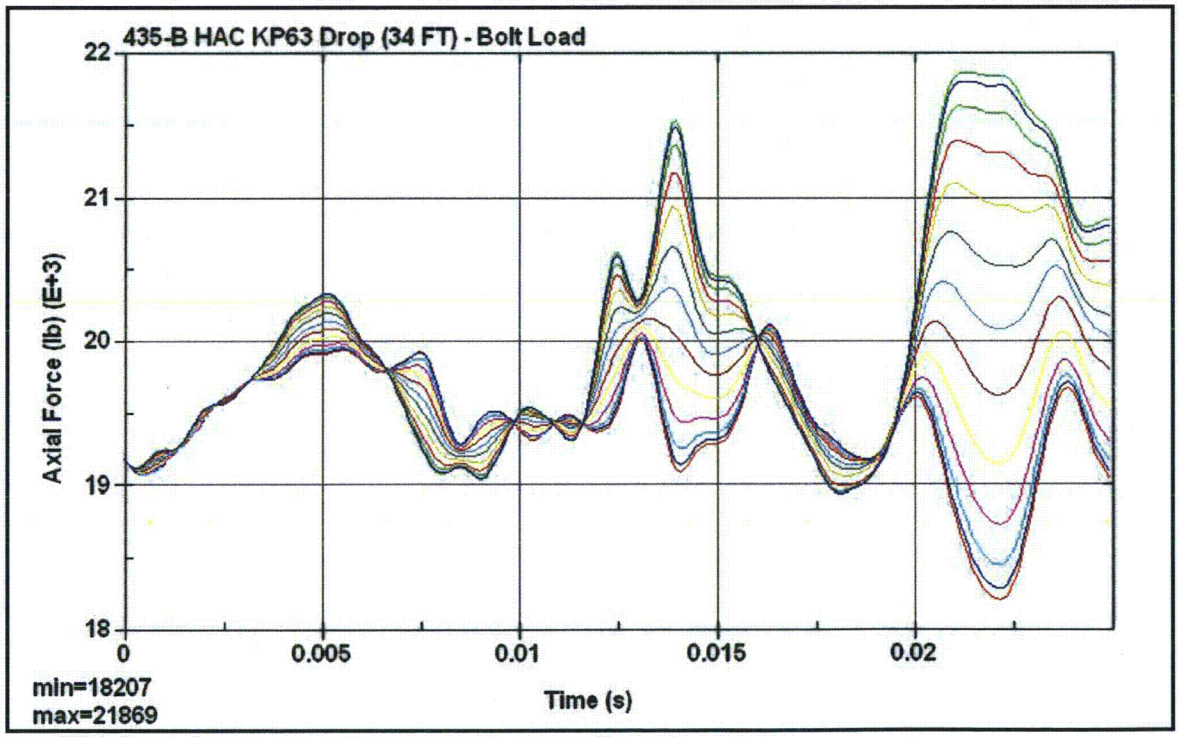

Figure 2.12.4-74 – KP63 Axial Bolt Force

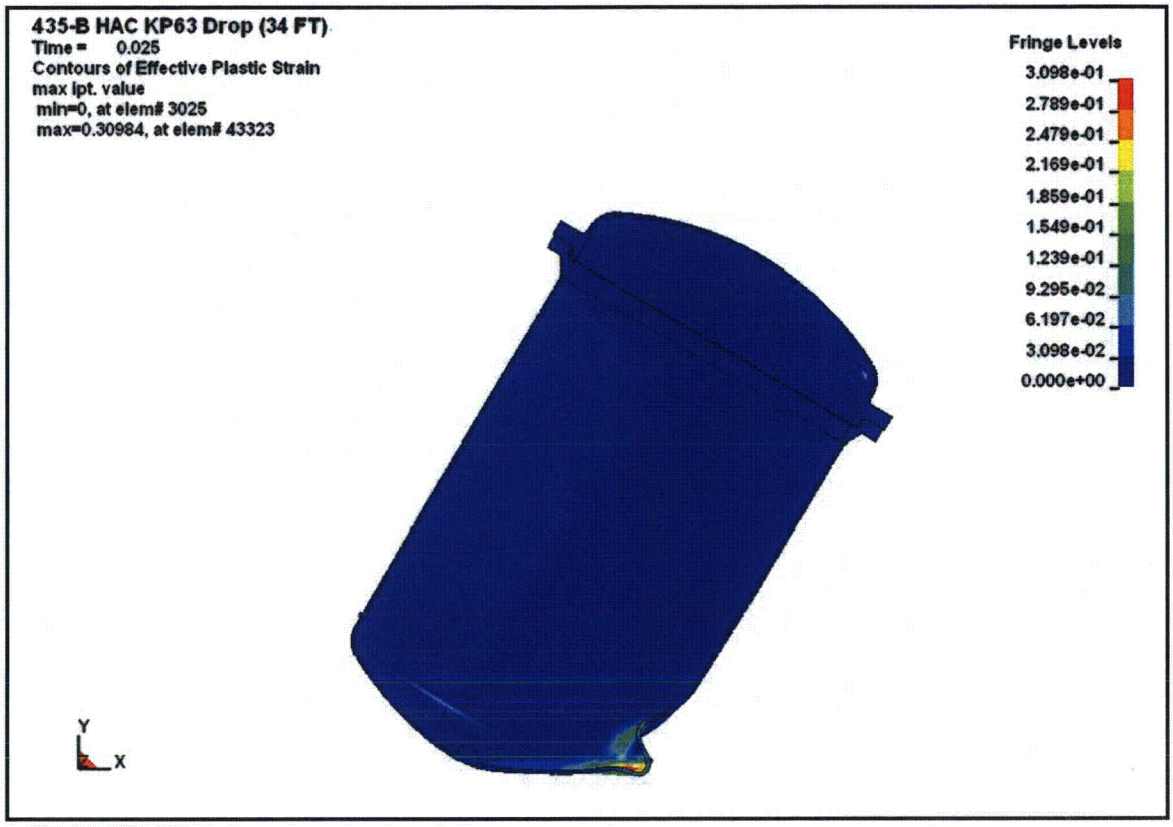

Figure 2.12.4-75 – KP63 Containment Boundary Cumulative Effective Plastic Strain

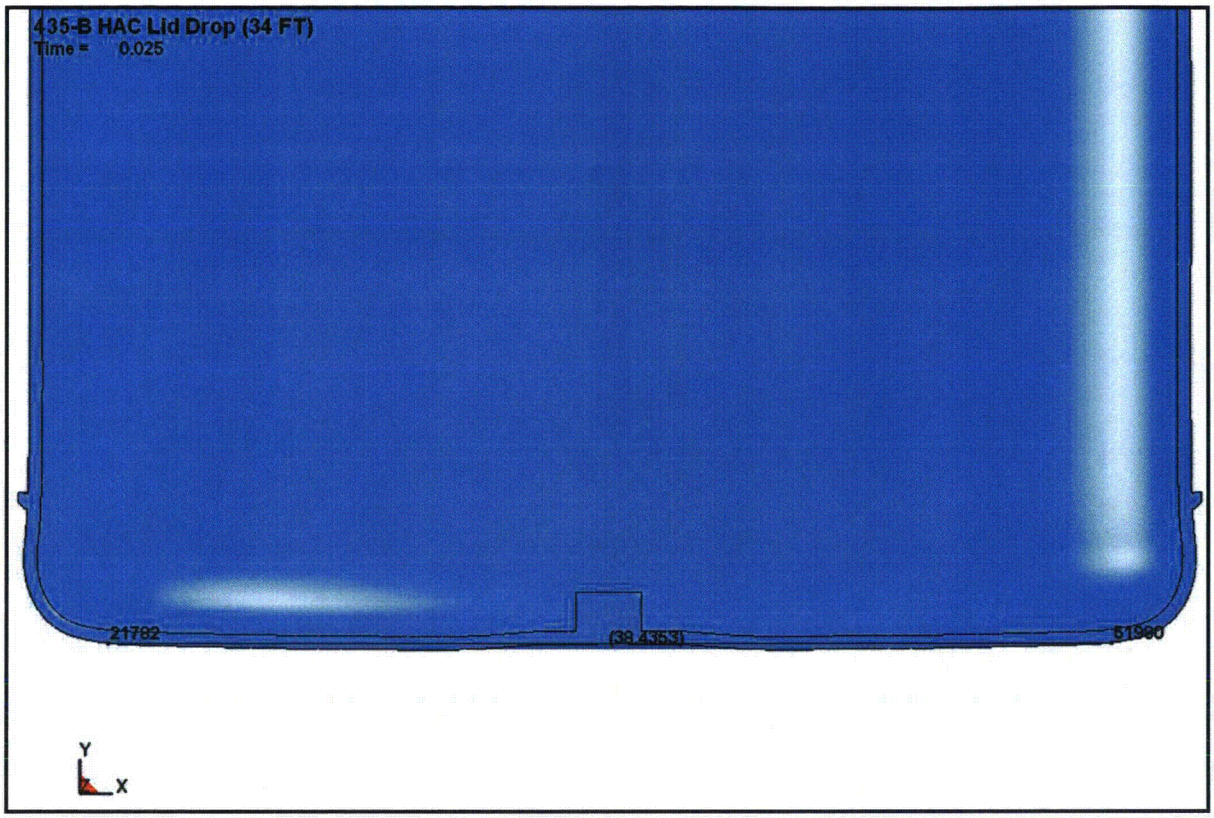

Figure 2.12.4-76 – Bell (Lid) Down Drop Flat Head Measurement

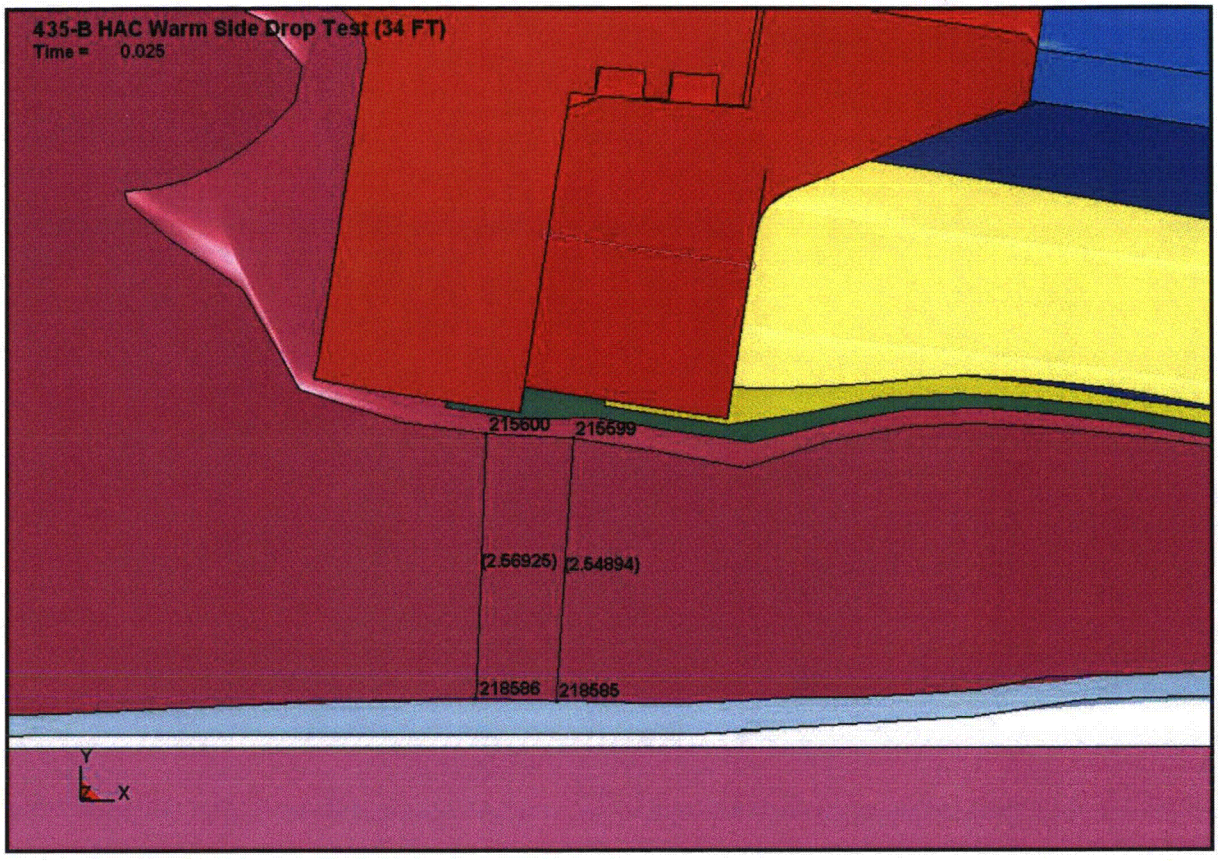

Figure 2.12.4-77 – Warm Side Drop Test Minimum Foam Thickness (14 pcf @ 117 °F)

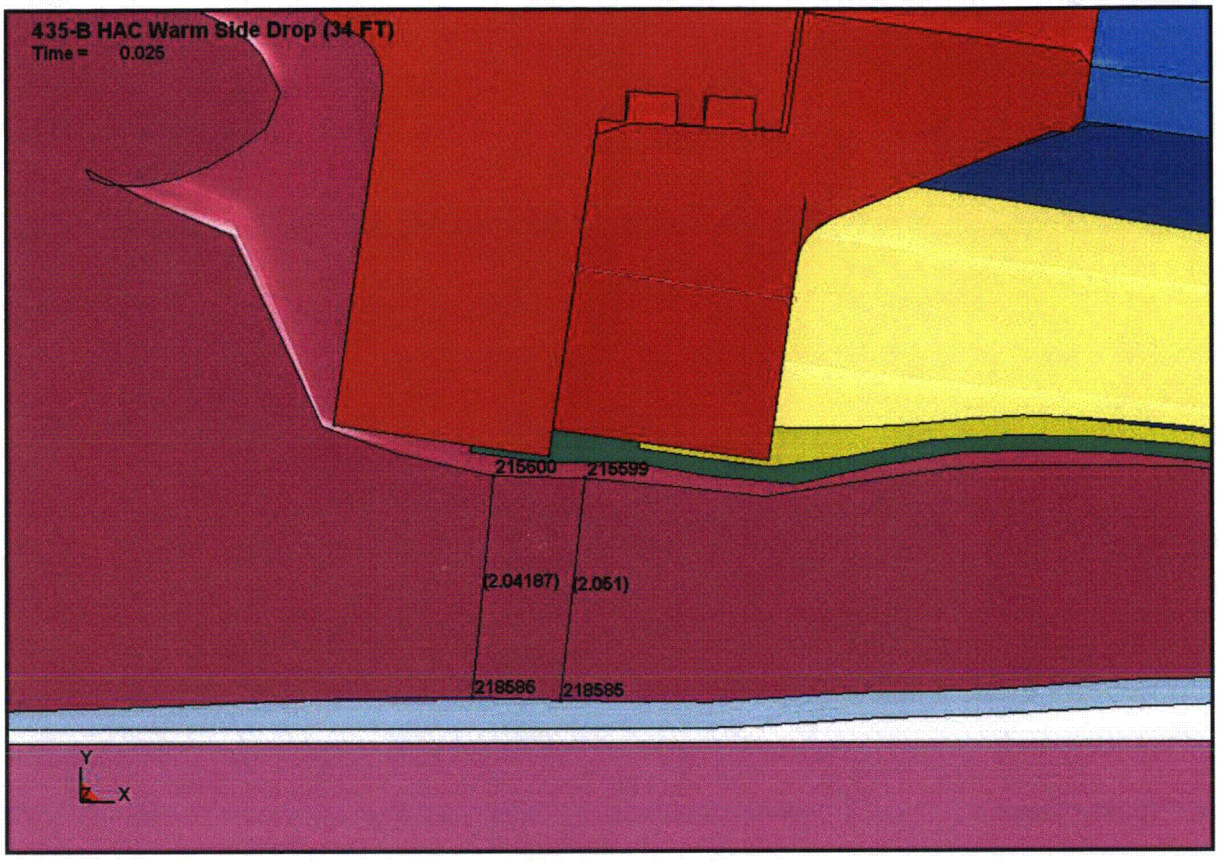

Figure 2.12.4-78 – Warm Side Drop Minimum Foam Thickness (15 pcf @ 150 °F)

2.12.4.7 References

1. Calculation 01916.01.C004.01-07, *435-B Drop Analysis*, Rev. 0, AFS.
2. Title 10, Code of Federal Regulations, Part 71 (10 CFR 71), *Packaging and Transportation of Radioactive Material*, 01-01-11 Edition.
3. International Atomic Energy Agency, *Regulations for the Safe Transport of Radioactive Material*, TS-R-1.
4. ANSI N14.5–1997 *American National Standard for Radioactive Materials – Leakage Tests on Packages for Shipment*, American National Standards Institute (ANSI), Inc.
5. Sandia National Laboratories, *Reexamination of Spent Fuel Shipment Risk Estimates,* Main Report, NUREG/CR-6672, Vol. 1, US Nuclear Regulatory Commission, March 2000.
6. *LS-DYNA Keyword User's Manual Version 971*, May 2007, Livermore Software Technology Corp., Livermore, CA.
7. *Design Guide for use of Last-A-Foam® FR-3700 for Crash & Fire Protection of Radioactive Material Shipping Containers*, Issue 005, General Plastics Manufacturing Company, Tacoma, WA.
8. International Atomic Energy Agency, *Advisory Material for the IAEA Regulations for the Safe Transport of Radioactive Material*, TS-G-1.1.
9. Avallone, E. A., and Baumeister, T, III., *Marks' Standard Handbook for Mechanical Engineers*, 10th Edition, 1996, McGraw-Hill, Inc.
10. Shigley, J.E., and Mischke, C.R., *Mechanical Engineering Design*, 5th Edition, 1989, McGraw-Hill, Inc.

2.12.5 Seal Performance Tests

This appendix contains descriptions of the performance tests which have been run on the butyl rubber compound used for the containment O-ring seal and sealing washers used in the 435-B package. The material is designated as Rainier Rubber R-0405-70. The performance tests which will be discussed have demonstrated the ability of this material to maintain a leaktight[1] containment boundary under minimum compression, minimum temperature, and maximum temperature conditions which are beyond those experienced in the 435-B package.

2.12.5.1 Performance Tests Associated with the TRUPACT-II Package

Two sets of butyl rubber performance tests have been done in support of the TRUPACT-II package certification (NRC Docket 71-9218). All relevant tests have used a bore-type fixture which is consistent with the configuration of the O-ring seals in the TRUPACT-II.

The test configuration and procedure was similar between the two tests and will now be briefly described. More details are available in Section 2.10.7.4 and Section 2.10.7.4A of [2]. Only the small test fixture is considered, since it was used in both sets of tests. The test fixture consists of an inner ring containing two O-ring grooves on its outer diameter and an outer ring which fits over the inner ring and provides compression of the two test O-rings. The cross-sectional diameter of the test O-rings was nominally 0.400 inches, which is essentially equivalent to the 0.375 nominal dimension of the 435-B package containment O-ring seal. To vary the O-ring compression in the test fixture, the radial position of the inner ring was controlled by jacking screws. When the inner ring was shifted to one side within the outer ring, a maximum compression was obtained on the side toward which the inner ring was shifted, and a minimum compression was obtained on the opposite side. The entire fixture could be placed in an environmental chamber and either cooled or heated for a set time. A helium leakage rate test was performed at various stages by testing the leakage rate between the outside of the fixture and the space between the two test O-rings.

The first set of tests was performed in 1989 and is documented in Section 2.10.7.4 of [2]. A typical test sequence consisted of the following steps:

1. Assemble the test fixture at ambient conditions.
2. Perform a leakage rate test with the inner ring centered in the outer ring.
3. Chill the fixture to -40 °F and perform a helium leakage rate test.
4. Allow the fixture to warm to -20 °F.
5. Shift the inner ring laterally within the outer ring to achieve maximum compression on one side and minimum compression on the other side.
6. Perform a helium leakage rate test with the fixture still at -20 °F.
7. Heat to an elevated temperature, maintaining the inner ring in the shifted position.

[1] Leaktight is defined as a maximum leakage rate of 1×10^{-7} ref-cc/sec, air, per [1].

8. Hold at temperature for 8 hours. Create a hard vacuum between the two test O-rings to confirm their integrity. A helium leakage rate test was not performed due to the tendency toward rapid saturation of the O-rings with helium at elevated temperature.
9. Chill the fixture to -20 °F, maintaining the inner ring in the shifted position.
10. Perform a final helium leakage rate test with the fixture still at -20 °F.

For each test, the maximum and minimum compressions were calculated using the dimensions of the fixture and of the test O-rings. The principal result of these tests was a demonstration that the subject rubber compound is capable of maintaining a leaktight condition at -20 °F with a minimum compression of 14.9% subsequent to an 8 hour soak at 400 °F. Details of the five small fixture tests are given in Table 2.12.5-1, adapted from Table 2.10.7-1 of [2]. Note that the term 'disk' in the table corresponds to the term 'inner ring' used in this description.

The second set of tests was performed in 1999, and are documented in Section 2.10.7.4A of [2]. These tests served to lower the minimum compression value at which a leaktight condition was demonstrated to be maintained. The tests used the same small test fixture, modified to allow it to achieve a lower minimum compression. The same test procedure was followed, except that all tests were run at a temperature of 400 °F. The principal result of these tests was a demonstration that the subject rubber compound is capable of maintaining a leaktight condition at -20 °F with a minimum compression of 11.9% subsequent to an 8 hour soak at 400 °F. Details of the three tests are given in Table 2.12.5-2, adapted from Table 2.10.7.4A-2 of [2].

2.12.5.2 Performance Tests Associated with the RTG Package

2.12.5.2.1 Face Seal Tests

O-ring tests were also performed in support of the Radioisotope Thermoelectric Generator (RTG) package certification (DOE Docket 94-6-9904). The results are reported in Section 2.10.6 of [3]. In these tests, a face-type fixture was used which permitted four different compressions to be tested at once. Unlike the TRUPACT-II testing, and consistent with the conditions in a face-type configuration, the O-rings were not mechanically moved or disturbed throughout the test. The fixture consisted of an inner plate having three concentric grooves on each side. Each groove had a different depth and contained an O-ring made from butyl compound R-0405-70 as described above. The inner and outer O-rings on each side were the test specimens; the center O-rings were used only to support leakage rate testing of the test specimens. The O-rings were compressed by outer plates which were set off from the inner plate by shims which, along with the groove depths, controlled the amount of compression of each test O-ring. The nominal test O-ring cross-sectional diameter was 0.275 inches. The minimum compression created by the fixture was 10%, which was uniform around the entire circumference of the fixture. Compressions of 12%, 14%, and 15.5% were tested at the same time. The dimensions of the fixture and of the test specimens, and the resulting compression values, are shown in Table 2.12.5-3.

The time/temperature sequence was as follows:

1. Assemble the test fixture at ambient conditions and perform a helium leakage rate test.
2. Chill the fixture to -40 °F and perform a helium leakage rate test.

3. Heat the fixture to 380 °F, and hold for 24 hours. Confirm integrity of the test O-rings by placing a hard vacuum on the test cavity (less than 0.2 mbar).
4. Allow the fixture to cool to 350 °F, and hold for 144 hours. The total time at elevated temperature is 168 hours, or one full week. Confirm integrity of the test O-rings by placing a hard vacuum on the test cavity (less than 0.2 mbar).
5. Cool the fixture to -20 °F and perform a final helium leakage rate test.

Each of the helium leakage rate tests demonstrated a leakage rate below the leaktight criterion of 1×10^{-7} ref-cc/sec, air, as defined by [1]. Of note, only the results from the outer O-ring tests (10% and 14% compression) were available at the time of publication of [3]. The successful completion of the inner O-ring tests (12% and 15.5% compression) was confirmed in [4].

2.12.5.2.2 Bore Seal Tests

Further O-ring tests were performed by Westinghouse Hanford Company in association with the RTG package, and documented in [5] and [6][2]. In these tests, the same bore-type fixture was used as that used for the TRUPACT-II tests described in Section 2.12.5.1, *Performance Tests Associated with the TRUPACT-II Package*. The procedure differed slightly in that a cold shift (step no. 5 from Section 2.12.5.1) was not performed. The test sequence was as follows:

1. Assemble the fixture at ambient conditions, and shift the inner ring fully to one side, generating minimum compression on one side and maximum on the other. Perform a helium leakage rate test.
2. Chill the fixture to -40 °F and perform a helium leakage rate test.
3. Heat to the specified elevated temperature and hold for the specified time. At the end of the hold time, perform a helium leakage rate test (saturation with helium at the high temperature was not reported to have had an effect on the helium leakage rate test).
4. Chill the fixture to -20 °F and perform the final helium leakage rate test.

For each test, the maximum and minimum compressions were calculated using the dimensions of the fixture and of the test O-rings. A number of different time/temperature tests were run, showing leaktight performance of the butyl material for 430 °F for one hour [6], 375 °F for 25 hours [6], and 350 °F for 168 hours [5]. Data is summarized in Table 2.12.5-4.

2.12.5.3 Long Term Performance of Butyl Rubber Seals

The tests of the Rainier Rubber R-0405-70 compound described in this appendix were performed at relatively high temperatures for relatively short times, consistent with the HAC fire event. Demonstration of the performance of the material at the lower temperature and longer duration associated with the NCT hot environment is made by extrapolation of this data.

Reference 7 uses thermogravimetric analysis to predict the relative lifetimes of some elastomers. One of the results of this study is to show that elastomer lifetime is linear when plotted on a log-lifetime (ordinate) vs. 1000/Temp (K) (abscissa) scales. This is shown in figure 3 of [7], which

[2] Note that some of the test reports refer to the material as 'RR-0405-70' while in some instances, 'R-0405-70' is used. Both refer to the same compound, where 'RR' is used for uncured material, and 'R' for a cured product form. All testing was performed on cured material.

is reproduced as Figure 2.12.5-1. The curve for butyl will not necessarily have the same slope or be placed in the same position relative to the scales as is shown in the figure. The position and slope for butyl will need to be established using the test data. Then, using linear extrapolation, its performance at longer lifetimes can be found. Note, since the abscissa is based on the inverse of temperature, temperature is actually decreasing along the abscissa towards the right, even though the values of 1000/Temp (K) are increasing. Consequently, the longest lifetimes correlate to the lowest temperature, as expected.

Figure 2.12.5-2 shows several time/temperature data points from the tests discussed above, along with the best-fit line through the data. For consistency, only data from the bore-type test fixture are considered. Note that this is not a locus of exact failure points (points defining the border between pass/fail), but of tests that passed (i.e., met the leaktight requirements of [1]). The possibility exists that some or all of these tests were "undertests", i.e., were not tested to the extreme limit of the material. Because the margin to failure may be different for each test, the actual locus of borderline results (zero-margin pass) may have a shallower slope than the best-fit curve to the data. If that curve were used to extrapolate upward to longer lifetimes, it might over predict the acceptable temperature (recall that temperature is decreasing to the right).

For the 435-B package, it is desired to determine the acceptable temperature for leaktight performance for a duration of one year (8,760 hours). The most conservative extrapolation (the lowest acceptable temperature) will be generated from the data curve fit having the shallowest (conservative) slope. To find the shallowest slope, a data point for a test failure (450 °F for 8 hours) is introduced, as shown in Figure 2.12.5-3. This is taken from the TRUPACT-II test results shown in Table 2.12.5-1. The straight line between this failure point and the longest-term successful data point (350 °F for 168 hours) has the shallowest slope which is consistent with the known data points. This can be concluded from the following observations:

1. The 450 °F/8 hour data point cannot be an undertest, since it is a known failure. Therefore, the actual zero-margin pass temperature must lie to the right of, but not to the left of, the test data point.
2. The 350 °F/168 hour data point is likely somewhat undertested. Therefore, the actual zero-margin pass temperature must lie to the left of, but not to the right of, the test data point.
3. Consequently, the actual locus of zero-margin performance could be steeper than, but could not be shallower than, the line formed by joining the 450 °F/8 hour and 350 °F/168 hour data points.

The equation of the line connecting these two data points is:

$$\mathrm{Log}_{10}(\mathrm{hrs}) = 5.396(1000/\mathrm{T(K)}) - 9.775$$

Using this expression, the maximum leak tight temperature for 8,760 hours (one year) is 249 °F. Therefore, the R-0405-70 butyl material can be held at at least 249 °F for one full year (constant temperature night/day) and is expected to be leak tight per ANSI N14.5. This is the most conservative extrapolation that can be made from the known data and is essentially equal to the long term limit for the butyl material of 250 °F which is stated in Section 3.2.2, *Technical Specification of Components*.

2.12.5.4 Summary

The butyl rubber compound used for the 435-B package containment seals was tested in both a bore-type and a face-type test fixture at low compression and elevated temperature. In the bore-type testing, the O-rings were demonstrated to be helium leaktight after a soak at 400 °F for 8 hours at a minimum compression of 11.9%. In the face-type testing, the O-rings were demonstrated to be helium leaktight after a soak at 380 °F for 24 hours followed by a soak at 350 °F for 144 hours at a minimum compression of 10%. In both types of test, the O-rings were shown to be helium leaktight at a temperature of -40 °F. These compression and temperature/time conditions exceed the severity of those experienced in the 435-B package. In addition, the seals are expected to be leaktight after one full year at a constant temperature of at least 249 °F. Because this value was conservatively obtained, the value of 250 °F used in Section 3.2.2, *Technical Specification of Components* is acceptable. The minimum compression of the 435-B package containment seal O-ring is calculated in Section 4.1.3, *Seals*, and the maximum temperature under NCT and HAC is discussed in Chapter 3, *Thermal Evaluation.*

Table 2.12.5-1 – TRUPACT–II O-ring Seal Performance Test Results (1989)⑦

Test Number	O-ring Seal Cross-Sectional Diameter (inches)				Stretch (%)		Maximum Gap (inches)		Minimum Compression (%)				Soak Temperature and Helium Leakage Rate Test Results ④				
	O-ring Seal No. 1		O-ring Seal No. 2				Disk Center	Disk Offset	Disk Centered		Disk Offset		Disk Centered		Disk Offset		
	Min	Max	Min	Max	Min	Max			Min	Max	Min	Max	Ambient	-40 °F	-20 °F	8 hrs⑤	-20 °F
1	0.387	0.397	0.387	0.396	2.0	4.1	0.026	③	22.1	25.6	14.9	20.0	Yes	Yes	Yes	350 °F	Yes
2	0.388	0.398	0.387	0.398	2.0	4.1	0.029	0.050	21.3	25.1	15.7	19.7	Yes	Yes	⑥	450 °F	No
3	0.387	0.397	0.387	0.399	2.0	4.1	0.027	0.052	21.9	25.8	15.2	19.4	Yes	Yes	Yes	400 °F	Yes
4	②	②	②	②	2.0	4.1	0.027	0.053	21.9	25.8	**14.9**	19.1	Yes	Yes	Yes	**400 °F**	**Yes**
5	②	②	②	②	2.0	4.1	0.026	0.050	22.1	26.0	15.7	19.9	Yes	Yes	Yes	400 °F	Yes

Notes:

① Material for all O-ring seal test specimens was butyl rubber compound R-0405-70, Rainier Rubber Co., Seattle, WA.

② Not measured; calculations assume the worst case range as taken from Tests Numbers 1 - 3 (i.e., Ø0.387 minimum to Ø0.399 maximum).

③ Range of values is 0.048 in. minimum to 0.053 in. maximum due to an indirect method of gap measurement (used for this test only).

④ A "Yes" response indicates that helium leakage rate testing demonstrated a leaktight condition as defined in [1], i.e., the leakage rate was less than or equal to 1×10^{-7} ref-cc/sec, air. In all cases, measured leak rates were less than or equal to 2.0×10^{-8} ref cc/s, helium, for tests with a "Yes" response.

⑤ No helium leakage rate tests were performed at elevated temperatures due to O-ring seal permeation and saturation by helium gas. The ability of the test fixture to establish a rapid, hard vacuum between the O-ring seals was used as the basis for leakage rate test acceptance at elevated temperatures. All tests rapidly developed a hard vacuum, with the exception of Test Number 2 at an elevated temperature of 450 °F, which slowly developed a vacuum.

⑥ Initial leakage rate of 1.0×10^{-5} ref cc/s, helium; became leaktight approximately one minute later.

⑦ Adapted from Table 2.10.7-1 of [2].

Table 2.12.5-2 – Supplementary TRUPACT–II O-ring Seal Performance Test Results (1999)④

Test No.	Disk Centered % Comp.		Disk Offset % Comp.		Helium Leak Tight②				
	O-ring #1	O-ring #2	O-ring #1	O-ring #2	Ambient Temp.	-40 °F	-20 °F (Disk Offset)	Hot Soak (Disk Offset)③	-20 °F (Disk Offset)
1	18.5	17.9	12.7	12.0	Yes	Yes	Yes	Held Vacuum	Yes
2	20.8	20.0	12.9	**11.9**	Yes	Yes	Yes	Held Vacuum	**Yes**
3	19.2	19.2	12.1	12.1	Yes	Yes	Yes	Held Vacuum	Yes

Notes:

① Material for all O-ring seal test specimens was butyl rubber compound R-0405-70, Rainier Rubber Co., Seattle, WA.

② Seal is considered to be leaktight if the actual leakage rate is less than or equal to 8×10^{-8} atm-cc/sec, He.

③ Hot soak was 8 hours at a uniform temperature of 400 °F.

④ Adapted from Table 2.10.7.4A-2 of [2].

Table 2.12.5-3 – RTG O-ring Face Seal Performance Test Parameters③

Fixture Side	Outer groove depth, in.	Inner groove depth, in.	Shim Thickness, in.	Outer O-ring X- section, in.	Inner O-ring X- section, in.	Outer O-ring compression, %	Inner O-ring compression, %
Side A	0.2053	0.2000	0.044	0.2770	0.2773	10	12
Side B	0.2075	0.2033	0.031	0.2776	0.2774	14	15.5

Notes:

① Material for all O-ring seal test specimens was butyl rubber compound R-0405-70, Rainier Rubber Co., Seattle, WA.

② Each of the four test O-ring seals were leaktight per [1] when tested at a temperature of -20 °F following the time/temperature sequence of 380 °F for 24 hours followed by 350 °F for 144 hours.

③ Adapted from Appendix 2.10.6, Table 4.1-1 and Table 4.1-2, of [3].

Table 2.12.5-4 – RTG O-ring Bore Seal Performance Test Parameters

Test No.	Min Compression, %	Max Compression, %	Max Temperature, °F	Hold Time, hours	Data Source
4	17.5	30.5	350	168	Table 3 of [5]
4B	17.8	31.3	375	25	Table 3 of [6]
3	19.2	32.3	430	1	Table 3 of [6]

Notes:

① Material for all O-ring seal test specimens was butyl rubber compound R-0405-70, Rainier Rubber Co., Seattle, WA.

② O-ring seals were leaktight per [1] when tested initially at room temperature, at a temperature of -40 °F, again at the stated maximum temperature at the end of the hold time, and finally when chilled to -20 °F.

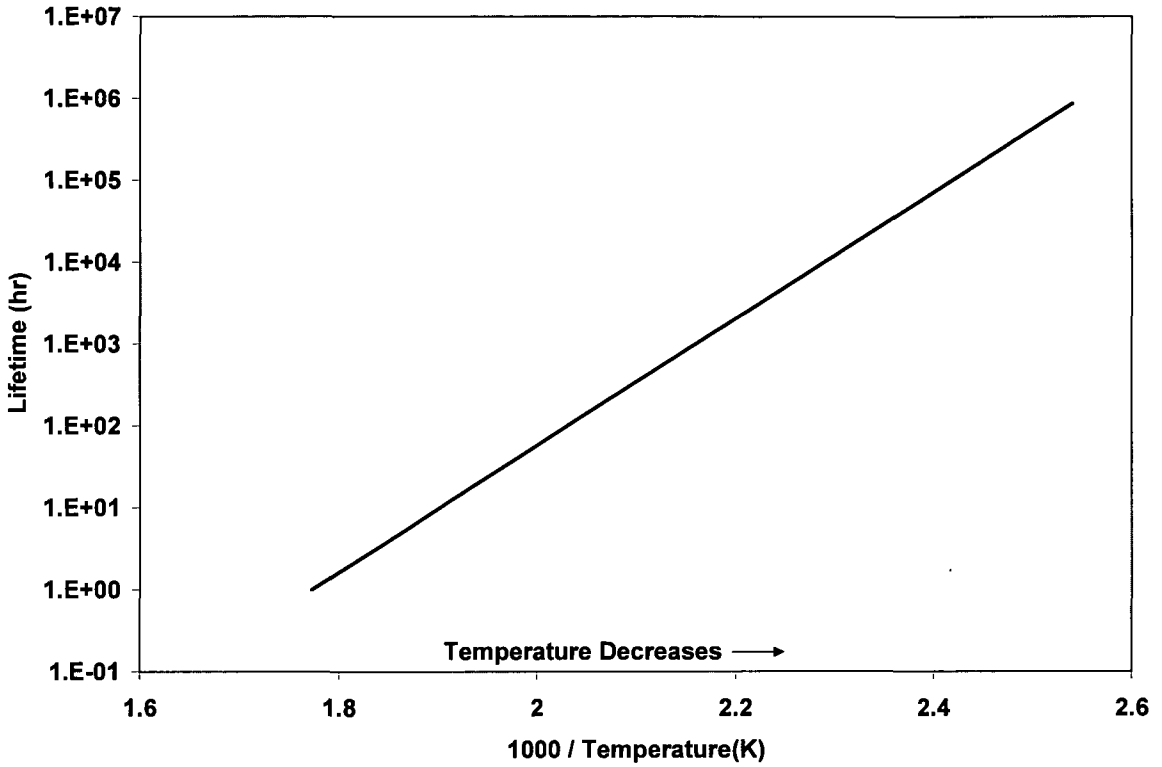

Figure 2.12.5-1 – Elastomer Time-Temperature Behavior (adapted from Figure 3 of [7])

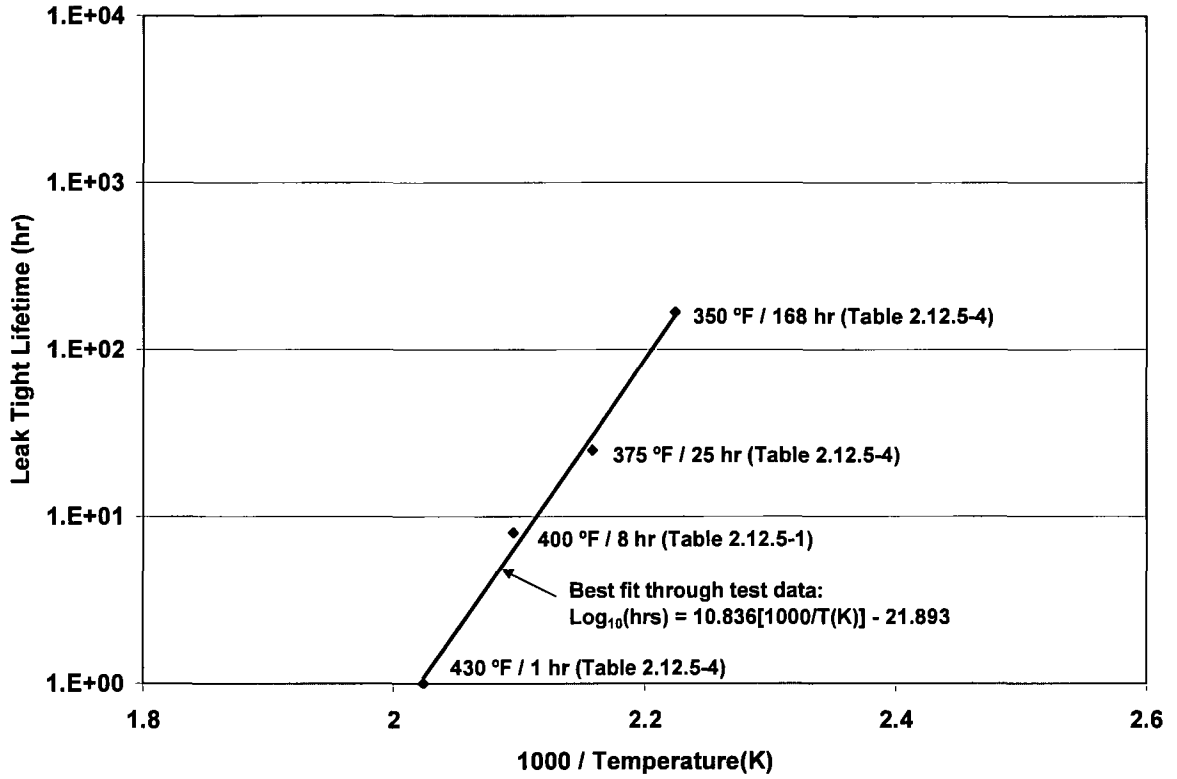

Figure 2.12.5-2 – R-0405-70 Test Data and Best Fit Curve

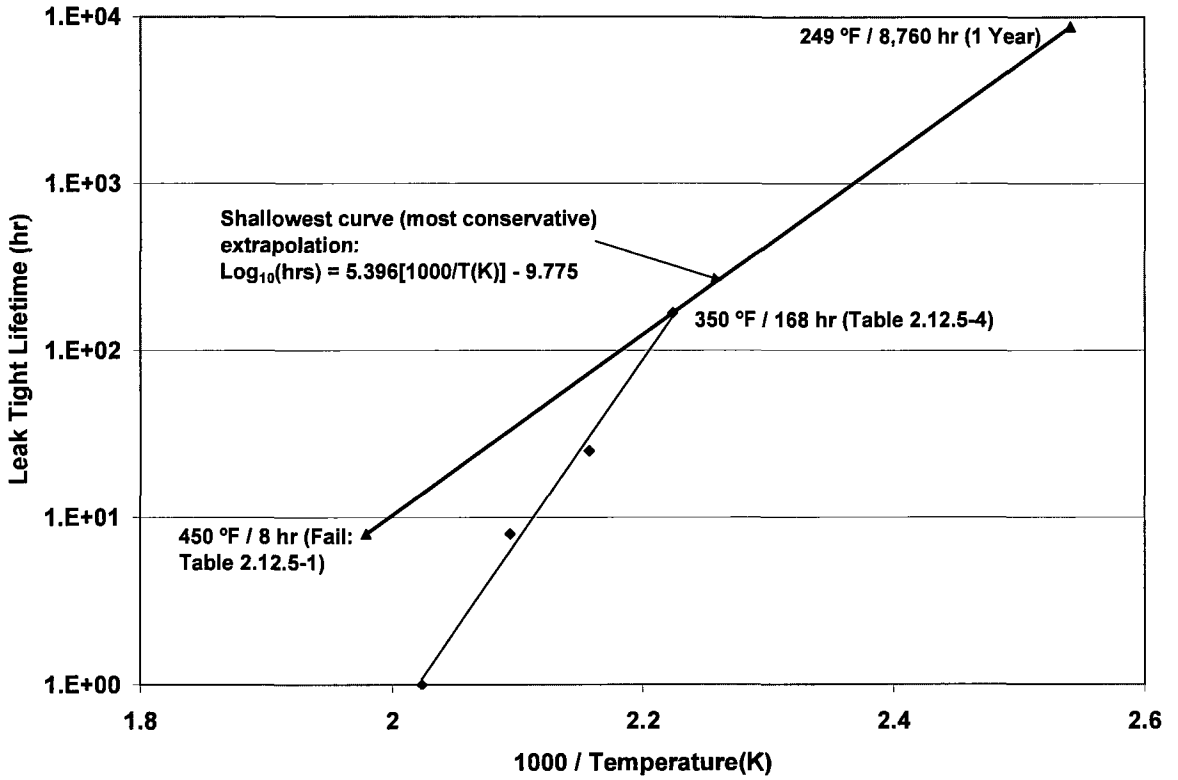

Figure 2.12.5-3 – Conservative Extrapolation to One Year

2.12.5.5 References

1. ANSI N14.5-1997, *American National Standard for Radioactive Materials – Leakage Tests on Packages for Shipment*, American National Standards Institute (ANSI), Inc.
2. USNRC Docket 71-9218, *Safety Analysis Report for the TRUPACT-II Shipping Package*, Revision 18, U.S. Department of Energy, Carlsbad Field Office, Carlsbad, New Mexico.
3. DOE Docket No. 94-6-9904, *Radioisotope Thermoelectric Generator Transportation System Safety Analysis Report for Packaging*, WHC-SD-RTG-SARP-001, prepared for the U.S. Department of Energy Office of Nuclear Energy under Contract No. DE-AC06-87RL10930 by Westinghouse Hanford Company, Richland, WA.
4. Westinghouse Hanford Company, *RTG Transportation System Packaging O-ring Material Thermal Validation Test Report for Face Seal Test Fixture*, WHC-SD-RTG-TRP-010, Rev 0.
5. Westinghouse Hanford Company, *Radioisotope Thermoelectric Generator (RTG) Transportation System Packaging O-ring Material Thermal Validation Test Report*, WHC-SD-RTG-TRP-001, Rev. 1.
6. Westinghouse Hanford Company, *Radioisotope Thermoelectric Generator (RTG) Transportation System Packaging O-ring Material Elevated Temperature Test Report*, WHC-SD-RTG-TRP-002, Rev. 0.
7. Nigrey, P. J., *Prediction of Packaging Seal Life Using Thermoanalytical Techniques*, Proceedings of the 12th International Conference on the Packaging and Transportation of Radioactive Materials, PATRAM 98, Vol. 4, p. 1730.